UNIVERSIDADE FEDERAL DO RIO GRANDE DO SUL
INSTITUTO DE GEOCIÊNCIAS
PROGRAMA DE PÓS-GRADUAÇÃO EM GEOCIÊNCIAS

IMPACTO DA TOPOGRAFIA RIFTE NA TECTÔNICA E SEDIMENTAÇÃO DOS ESTÁGIOS SAG E MARGEM PASSIVA – BACIAS DE CAMPOS E ESPÍRITO SANTO, SUDESTE DO BRASIL

FRANCYNE BOCHI DO AMARANTE

ORIENTADORES: Prof. Dr. Claiton Marlon dos Santos Scherer
Prof. Dr. Juliano Kuchle
Prof. Dr. Christopher Aiden-Lee Jackson (orientador no exterior)

Porto Alegre, 2021

UNIVERSIDADE FEDERAL DO RIO GRANDE DO SUL
INSTITUTO DE GEOCIÊNCIAS
PROGRAMA DE PÓS-GRADUAÇÃO EM GEOCIÊNCIAS

IMPACTO DA TOPOGRAFIA RIFTE NA TECTÔNICA E SEDIMENTAÇÃO DOS ESTÁGIOS SAG E MARGEM PASSIVA – BACIAS DE CAMPOS E ESPÍRITO SANTO, SUDESTE DO BRASIL

FRANCYNE BOCHI DO AMARANTE

ORIENTADORES: Prof. Dr. Claiton Marlon dos Santos Scherer
Prof. Dr. Juliano Kuchle
Prof. Dr. Christopher Aiden-Lee Jackson (orientador no exterior)

BANCA EXAMINADORA

Profa. Dra. Ariane Santos da Silveira – Universidade do Vale do Rio dos Sinos (Unisinos)

Prof. Dr. Fernando Farias Vesely – Universidade Federal do Paraná (UFPR)

Prof. Dr. Claudio Riccomini – Universidade de São Paulo (USP)

Tese de Doutorado apresentada como
requisito parcial para a obtenção do Título
de Doutor em Ciências.

Porto Alegre, 2021

CIP - Catalogação na Publicação

Amarante, Francyne Bochi do
Impacto da topografia rifte na tectônica e sedimentação dos estágios sag e margem passiva - bacias de Campos e Espírito Santo, sudeste do Brasil / Francyne Bochi do Amarante. -- 2021.
129 f.
Orientador: Claiton Marlon dos Santos Scherer.

Coorientador: Juliano Kuchle.

Tese (Doutorado) -- Universidade Federal do Rio Grande do Sul, Instituto de Geociências, Programa de Pós-Graduação em Geociências, Porto Alegre, BR-RS, 2021.

1. bacias marginais brasileiras. 2. bacia rifte. 3. bacia sag. 4. bacia de margem passiva. 5. tectônica do sal. I. Scherer, Claiton Marlon dos Santos, orient. II. Kuchle, Juliano, coorient. III. Título.

Elaborada pelo Sistema de Geração Automática de Ficha Catalográfica da UFRGS com os dados fornecidos pelo(a) autor(a).

Eu não quero ser grande
Apenas bom
Comigo e os demais
Que estão ao meu redor
Sofrendo e aprendendo
Perdidos como eu...
Cuscobayo

Eu dedico esse trabalho a todos que compõe a resistência ao descrédito na ciência e ao desmonte das universidades públicas.

AGRADECIMENTOS

Quem trabalha na academia sabe que nenhuma produção científica se faz com uma pessoa só. Meu doutorado não foi diferente: ele tem a mão de muita gente que me deu suporte – intelectual e/ou emocional. Certamente foi meu maior desafio profissional até hoje, e sem as pessoas que vou mencionar aqui eu não teria conseguido.

Primeiro, quero agradecer meus orientadores Claiton Scherer e Juliano Kuchle que me incentivaram e capacitaram ao longo desses 4 anos. Aprendi e sigo aprendendo um tanto com vocês! Além disso, vocês me deram espaço para crescer como profissional, tanto criando oportunidades valiosas como me questionando e ensinando. Os admiro muito e espero que sigamos trabalhando juntos no futuro.

I want to thank my supervisor abroad, Christopher Jackson. Chris, you have taught me so much – not only about salt tectonics, but also about how to face and fight the injustices within academia. Thank you for your ongoing support – especially during my time in London, in the middle of the covid pandemics. For that, I also want to thank Leonardo Pichel, my “co-supervisor” abroad. Our (almost) weekly meetings last year made me accomplish more than what I had planned for my time at Imperial College, with the Basins Research Group.

Não poderia deixar de mencionar meus colegas de pós-graduação da Estratigrafia, em especial os queridos do SeisLab: André, Vitor, Adler, Patrycia e Renata. A estes e a todos os colegas da Estrati, obrigada pelo convívio leve e produtivo. E um agradecimento especial para o Carlinhos e ao Rodrigo, que mantém tudo nos eixos e funcionando!

Agradeço minha família por todo o apoio, amor e compreensão ao longo do meu doutorado – e ao longo da vida. Vocês sabem bem que não foi fácil, e sou imensamente grata por tudo o que fizeram e deixaram de fazer por mim. Sem vocês eu com certeza não teria conseguido, vocês são meus pilares, minha sustentação. Mãe, obrigada.

Quero agradecer também meu namorado-noivo-marido-crush-companheiro, Maurício. Tu sabe que tu foi essencial para eu suceder nesse doutorado. Tu me apoia incondicionalmente, me incentiva a crescer sempre, e me coloca de volta no eixo quando

eu sinto que não vou conseguir. Obrigada, meu amor. Não só por isso, mas por um tanto mais.

Muitíssimo obrigada também aos meus amigos do coração, Cris e Laerte <3, e também Pacífico, Lipe, Nati, Rianne (que saudade!), amigas da mãe da Mari, Raissa, migos do IBA team... Amigos são a família que a gente escolhe, e eu escolhi os meus per-fei-ta-men-te. Gente, amo vocês. Vocês me levantam depois de uma queda, e me lembram quem eu sou e do que eu sou capaz (Cristine e Laércio em especial, meus chatos!). Essa tese também é de vocês. Obrigada.

Meu muito obrigada ao CNPq (Conselho Nacional de Desenvolvimento Científico e Tecnológico) pela bolsa de doutorado na UFRGS e também pela bolsa de doutorado no exterior (SWE) na Imperial College London. Agradeço à ANP (Agência Nacional de Petróleo, Gás Natural e Biocombustíveis) por me ceder os dados para pesquisa e permitir a publicação dos resultados.

RESUMO

As bacias marginais do sudeste brasileiro compreendem três estágios evolutivos: rifte, sag e margem passiva. Os modelos geológicos clássicos destas bacias abordam os estágios finais, sag e margem passiva, como isolados e independentes do estágio rifte inicial, onde tem-se subsidência mecânica expressiva controlada por falhas normais. Porém, essa abordagem simplifica a complexidade estratigráfica e estrutural onde as fases rifte e sag formam um contínuo evolutivo. O objetivo principal da presente tese é analisar o quanto a morfologia herdada do estágio rifte impacta a tectônica e sedimentação dos estágios posteriores nas bacias de Campos e Espírito Santo. A metodologia central é a interpretação sismoestratigráfica a partir de dados sísmicos 2D e 3D, e dados petrofísicos e litológicos de poços. A base de dados provém da BDEP-ANP. Na Bacia do Espírito Santo fez-se a análise interna do intervalo sag pré-sal, onde foram individualizadas quatro sequências genéticas. Unindo interpretações estratigráficas e tectônicas, observa-se que as duas unidades basais são fortemente controladas pelo paleorelevo herdado, de forma que a sedimentação é confinada às calhas rifte. As duas unidades superiores registram um gradual aumento na área deposional, à medida que a sedimentação transcende gradualmente as calhas rifte conforme há subida do nível de base lacustre. Na Bacia de Campos fez-se a caracterização dos estilos estruturais relacionados à tectônica do sal, bem como a identificação dos principais fatores controladores da deformação. A interpretação do estilo e distribuição das estruturas de sal e do sedimento sobrejacente (estágio margem passiva) relacionadas resultou na definição de três domínios de deformação halocinética: domínio extensional proximal, domínio contracional distal, e domínio multifásico intermediário. Rampas na superfície da base do sal relacionadas ao paleorelevo herdado, geram eixos locais de contração e extensão em resposta a variações na velocidade de fluxo do sal. Tais mudanças de tensão locais afetam os domínios regionais de deformação e influenciam os tipos de estruturas geradas no sal e sedimentos do estágio margem passiva, bem como sua evolução no tempo e espaço. A partir do estudo das bacias de Campos e Espírito Santo conclui-se, portanto, que a morfologia do estágio rifte influencia na tectônica e sedimentação dos estágios sag e margem passiva sobrejacentes.

Palavras-chave: bacias marginais brasileiras, bacia rifte, bacia sag, bacia de margem passiva, tectônica do sal.

ABSTRACT

The marginal basins of southeastern Brazil comprise three evolutionary stages: rift, sag and passive margin. Classic geological models of these basins address the final stages, sag and passive margin, as isolated and independent from the initial rift stage, where there is expressive mechanical subsidence controlled by normal faults. However, this approach oversimplifies the stratigraphic and structural complexity where the rift and sag phases form an evolutionary continuum. The main objective of the present thesis is to analyze how the morphology inherited from the rift stage impacts the tectonics and sedimentation of the later stages in the Campos and Espírito Santo basins. The central methodology is the seismostratigraphic interpretation using 2D and 3D seismic data, and petrophysical and lithological data from wells. The database comes from BDEP-ANP. In the Espírito Santo Basin, an analysis of the pre-salt sag interval was performed, and four genetic sequences were identified. From stratigraphic and tectonic interpretation, it is clear that the two basal units are strongly controlled by the inherited paleorelief, so that sedimentation is confined to the rift troughs. The two upper units record a gradual increase in the depositional area as sedimentation gradually transcends the rift troughs as the base lacustrine level rises. In the Campos Basin, the focus was the characterization of the structural styles related to salt tectonics, as well as the identification of the main factors controlling deformation. The interpretation of the style and distribution of the salt and overburden structures resulted in the definition of three halokinetic deformation domains: proximal extensional domain, distal contraction domain, and intermediate multiphase domain. Base-salt ramps, related to the inherited paleorelief, generate local hinges of contraction and extension in response to variations in the velocity of salt flux. Such local stress changes affect the regional domains of deformation and influence the types of structures generated in the salt and overburden sediments, as well as their evolution in time and space. From the study of the Campos and Espírito Santo basins, one can therefore conclude that the morphology of the rift stage influences the tectonics and sedimentation of the overlying sag and passive margin stages.

Keywords: Brazilian marginal basins, rift basin, sag basin, passive margin basin, salt tectonics.

LISTA DE FIGURAS

LISTA DE TABELAS

SUMÁRIO

ESTRUTURA DA TESE

Esta tese de doutoramento apresenta dois artigos científicos, acompanhados por um texto integrador. O artigo 1, intitulado "*Seismic tectono-stratigraphic analysis of the Aptian pre-salt marginal system of Espírito Santo Basin, Brazil*", foi publicado no periódico Journal of South American Earth Sciences (classificação Qualis Capes A3). O artigo 2, intitulado "*Pre-salt rift morphology controls salt tectonics in the Campos Basin, offshore SE Brazil*" foi publicado no periódico Basin Research (classificação Qualis Capes A1). O texto integrador é constituído pelos capítulos: 1) introdução; 2) estado da arte; 3) localização e contexto geológico; 4) dados e métodos; 5) síntese dos principais resultados e discussões; 6) considerações finais; 7) referências bibliográficas.

1 Introdução

As bacias marginais brasileiras são tipicamente subdivididas em três estágios tecno-estratigráficos: (sin-)rifte, sag e margem passiva. Os diferentes estágios evolutivos têm arquiteturas deposicionais distintas, que refletem contextos sedimentológicos e tectônicos particulares. Compreender a arquitetura deposicional característica de cada estágio, e o que os controla, é fundamental para avançar no conhecimento das bacias marginais - que além do interesse acadêmico, despertam interesse econômico visto que podem conter consideráveis reservatórios de hidrocarbonetos (como é o caso das bacias do sudeste brasileiro: bacias de Santos, Campos e Espírito Santo).

O estágio rifte é caracterizado por subsidência mecânica, marcada por uma alta taxa de subsidência em um curto intervalo de tempo. A subsidência mecânica ocorre pela movimentação de falhas normais, que criam subsidência diferencial na forma de meio-grábens por rotação de blocos, separados por regiões mais elevadas do embasamento, os horsts. Sabe-se que a taxa de criação de espaço de acomodação deste estágio é elevada quando comparada ao suprimento sedimentar (Prosser, 1993), gerando uma bacia assimétrica, com a maior espessura de sedimento acumulada junto a falha de borda do meio-graben. Conforme modelos evolutivos clássicos de bacias rifte (e.g. Prosser, 1993; Bosence, 1998; Kuchle e Scherer, 2010), o expressivo movimento das falhas cessa gradativamente, dando lugar a uma subsidência mais uniforme e regional, que marca o início do estágio tectono-estratigráfico sag e continua ao longo do estágio posterior, o margem passiva. Esse tipo de bacia apresenta uma geometria tabular, com uma taxa de criação de acomodação mais uniforme nas diferentes porções da bacia.

Entretanto, os modelos ideiais mostram-se demasiadamente simplificados dentro da complexidade estratigráfica e estrutural, onde as fases rifte e sag formam um contínuo evolutivo. Em decorrência dessa simplificação, existem algumas questões que permanecem em aberto. Primeiro, as falhas que delimitam os meio-grábens do rifte podem ser reativadas ao longo do sag, apesar do domínio da subsidência térmica? Segundo, se nem todo o espaço criado durante o estágio rifte por subsidência mecânica é preenchido (i.e. o aporte sedimentar não acompanha a taxa de susidência diferencial), há relevo residual estrutural ainda significativo no estágio sag? Caso haja, qual o controle que essa topografia herdada exerce sobre a sedimentação e tectônica durante estágio sag? Essa última questão se torna ainda

mais crítica nas bacias marginais do sudeste brasileiro, onde ao final do estágio sag tem-se a deposição de um espesso pacote evaporítico. Os evaporitos comportam-se no tempo geológico como fluidos altamente viscosos (Weijermars *et al.*, 1993); fluidos assim são sensíveis à geometria da superfície pela qual fluem. Assim, um potencial relevo herdado do estágio rifte pode inclusive controlar a tectônica adiastrófica causada por movimentos halocinéticos, que por sua vez exercerá um controle direto no estágio margem passiva das bacias.

Diante disso, a presente tese tem como objetivos específicos responder as questões acima citadas, a fim de atingir o objetivo central que dá título à tese. O objetivo central deste trabalho consiste em analisar o quanto a morfologia herdada do estágio rifte impacta a tectônica e sedimentação dos estágios posteriores nas bacias de Campos e Espírito Santo, mais especificamente:

- Estágio sag, pré-sal, proximal (onshore) na Bacia do Espírito Santo.
- Estágio sag, sal, e margem passiva, proximal a distal na Bacia de Campos.

2 Estado da Arte

Para melhor compreender o posicionamento dos estágios evolutivos sag e margem passiva dentro do contexto evolutivo do rifteamento, e individualizá-los em seções sísmicas ou litoestratigráficas, se faz necessária uma revisão bibliográfica abrangendo a evolução tectono-estratigráfica de bacias rifte, apresentada no item 2.1. Após este, o item 2.2 discorre sobre a evolução tectono-estratigráfica de bacias sag, essencial na construção do artigo 1 (apresentado no capítulo 8).

O final do estágio sag nas bacias do sudeste brasileiro – incluindo as bacias-alvo de estudos desta tese – é composto por uma espessa camada de sal. Suas movimentações (final do Aptiano – Recente) são influenciadas pela topografia herdada da fase rifte anterior, e impactam diretamente na sedimentação da fase margem passiva posterior. Assim é essencial, especialmente ao artigo 2 (apresentado no capítulo 9), uma revisão bibliográfica de tectônica do sal em margens passivas, apresentada no item 2.3 deste capítulo.

2.1 Evolução tectono-estratigráfica de bacias rifte

Riftes são áreas de afinamento crustal com falhamentos associados (Allen e Allen, 2005). Com o intuito de compreender a geração dessas bacias, Sengor e Burke (1978) propõem classificá-las em ativas e passivas. No rifteamento ativo, tem-se o estiramento litosférico em resposta a um processo termal ativo na astenosfera, como a colocação de uma pluma mantélica na base da litosfera. No rifteamento passivo, por outro lado, a extensão é gerada por movimentos de placas externos à bacia rifte e a entrada de material astenosférico é uma resposta passiva ao afinamento litosférico.

Para analisar a evolução tectono-estratigráfica de bacias rifte, serão apresentados três modelos evolutivos (Prosser, 1993; Bosence, 1998; Kuchle & Scherer, 2010) considerados os mais relevantes para os propósitos da presente monografia.

Prosser (1993), adaptando o conceito de tratos de sistemas de Posamentier e Vail (1988) – que os definem como sistemas deposicionais interligados desenvolvidos em resposta a mudanças cíclicas no nível relativo do mar, controladas por flutuações eustáticas, tectônicas e de taxa de sedimentação –, utiliza a nomenclatura tratos de sistemas tectônicos para definir quatro estágios tectono-estratigráficos de bacias rifte, já que a tectônica é o fator controlador dominante da sedimentação. Cada um dos

estágios detalhados a seguir apresenta um arranjo distinto de sistemas deposicionais, constituindo padrões de empilhamento, e uma expressão sísmica que permite seu reconhecimento em perfis de reflexão (Figura 2.1).

1- Trato de Sistemas Tectônico de Início de Rifte: caracterizado pela geração de pequenas sub-bacias isoladas como resposta ao primeiro incremento de movimento da falha normal. Formam-se novos altos topográficos nas cristas do hangingwall e do footwall, potenciais áreas-fonte de sedimento. Cursos de água circundantes são rapidamente redirecionados para o novo depocentro, dando início à sedimentação por canais fluviais e depósitos inter-canais nas novas bacias. Próximo às escarpas das falhas de pequeno rejeito encontram-se depósitos de sedimentação gravitacional de granulometria grossa. A assinatura sísmica externa deste trato de sistemas é a forma de cunha, e os refletores internos têm padrão hummocky e são descontínuos. Os pacotes de refletores são agradacionais mostrando que a taxa de sedimentação acompanha a de subsidência.

2- Trato de Sistemas Tectônico de Clímax de Rifte: estágio que representa a maior taxa criação de espaço, que ultrapassa o aporte sedimentar, e o padrão de empilhamento agradacional passa a ter um forte componente retrogradacional. A sedimentação na falha de borda é constituída por depósitos de talus e leques aluviais, com padrões de drenagem imaturos. No centro da bacia encontra-se um golfo lacustre ou marinho, alimentado por deltas e leques aluviais/deltaicos das margens. Ao longo da evolução desse trato de sistemas, o corpo de água estagnante se expande até que na fase final toda a calha rifte está submersa, e a sedimentação fina domina na bacia. Na sísmica têm-se refletores divergentes, com geometria interna caótica próximo à falha de borda.

3- Trato de Sistemas Tectônico de Pós-Rifte Imediato: caracterizado pelo fim do tectonismo ativo, o que significa o fim da subsidência diferencial ao longo da falha de borda. A subsidência mecânica dá lugar à subsidência térmica por resfriamento termal litosférico. O padrão de empilhamento neste estágio é agradacional com componente progradacional, com raseamento do lago ou mar em direção ao topo. A expressão sísmica é composta por refletores paralelos (em onlap contra a falha de borda remanescente) e relativamente contínuos.

4- Trato de Sistema Tectônico de Pós-Rifte Tardio: o final do rifte será marcado pela peneplanização gradual e lenta da topografia gerada por falhas, levando ao afinamento dos sedimentos em direção ao topo. Na sísmica, os refletores paralelos têm natureza mais contínua que no estágio anterior.

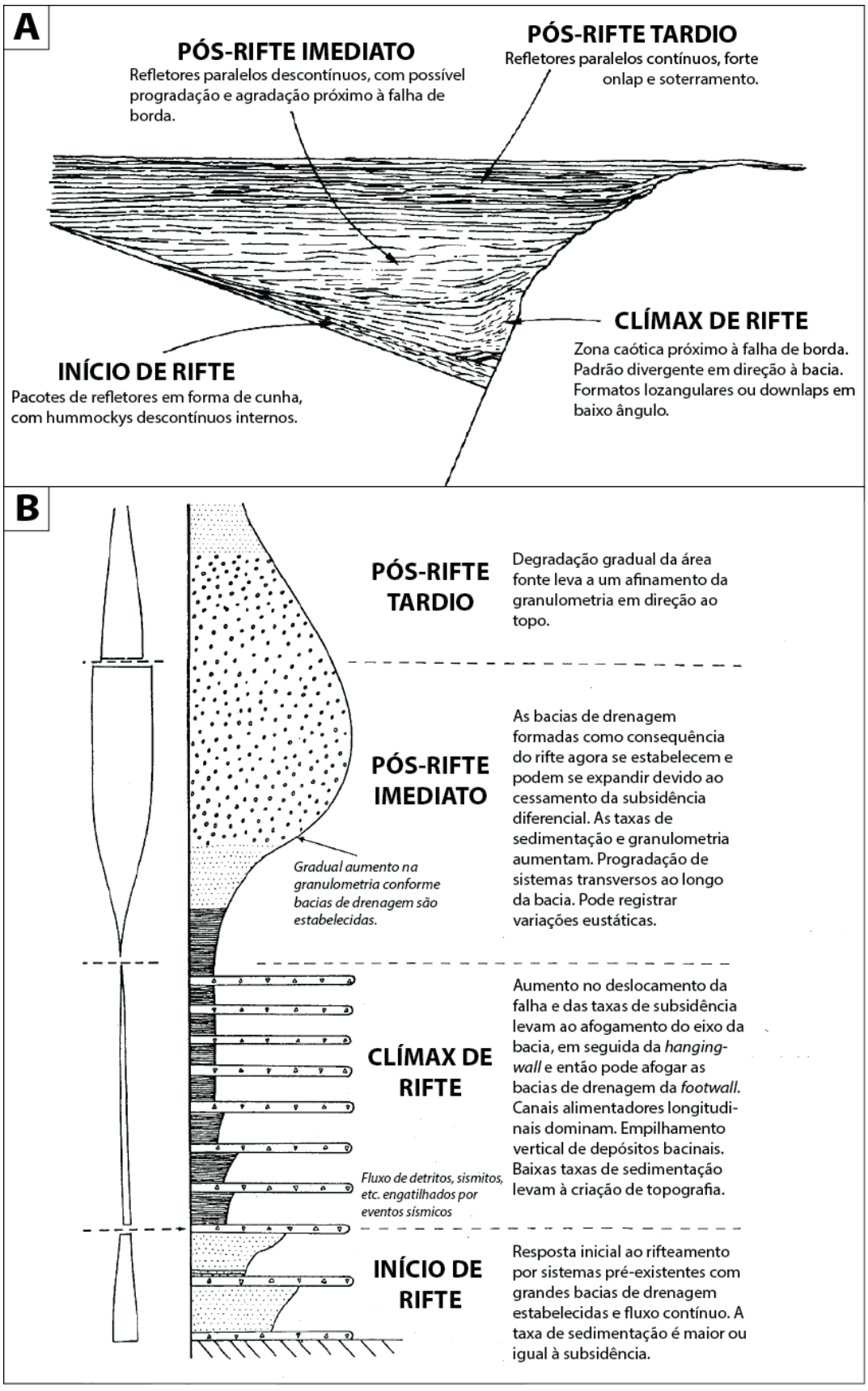

Figura 2.1. (A) Seção idealizada de uma seção sísmica de uma bacia rifte ideal, onde cada trato de sistemas tectônico pode ser identificado. (B) Seção vertical idealizada do centro da bacia, interpretada conforme a expressão de mudanças do controle tectônico no sistema deposicional. Modificado de Prosser (1993).

Bosence (1998) com base nos diferentes estágios estratigráficos e as discordâncias que os delimitam, estabeleceu critérios práticos e simples para o

mapeamento de uma seção rifte. O autor postula que o conjunto de estratos vinculados à fase rifte denomina-se sin-rifte, os estratos antecedentes são nominados de pré-rifte, e os posteriores de pós-rifte (Figura 2.2). O início da fase rifte é marcado pela Discordância Sin-Rifte, e no final forma-se a Discordância Pós-Rifte. É importante notar que as fases pré- e pós-rifte são assim denominadas para individualizar o evento sin-rifte dos demais, e o autor não faz menção ao contexto dinâmico e genético destas duas fases. Isso quer dizer que o pré-rifte pode ser uma bacia do tipo sinéclise, ou qualquer outro; a evolução do rifte na fase pós-rifte, por sua vez, pode ser para uma bacia do tipo margem passiva, rifte abortado, etc.

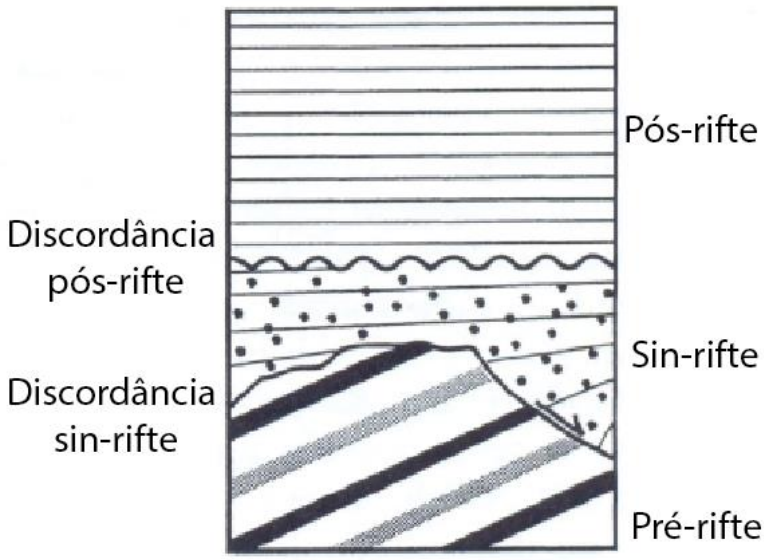

Figura 2.2. Estágios de uma bacia rifte de acordo com Bosence (1998).

1- Sin-Rifte: com o estabelecimento do rifte (Figura 2.3), a crosta estendida começa a sofrer subsidência mecânica no centro e soerguimento das cristas, que estarão sujeitas à erosão e irão registrar a discordância sin-rifte. É provável que essa discordância basal não seja rastreável por toda a extensão da bacia, já que em direção ao depocentro a mesma irá acumular sedimentos. Essa fase principal da evolução de bacias rifte resulta em um espaço de acomodação não totalmente preenchido, indicando que a taxa de subsidência ultrapassa a de suprimento sedimentar. A sedimentação é dominada por sistemas fluviais axiais, que originam pequenos lagos isolados, e estes tendem a se interconectar conforme o rifte evolui. Nas bordas do lago encontram-se depósitos de leques aluviais e deltas. Em determinado momento pode haver inundação marinha da bacia com início de produção de sedimentos carbonáticos, que irão preencher o espaço de acomodação ao nível do mar, enquanto os sedimentos clásticos serão transportados por canais submarinos através de baixos topográficos. O final da fase sin-rifte da bacia é marcado pela discordância pós-rifte a

qual, assim como a discordância sin-rifte, é do tipo desconformidade nas cristas do rifte e paraconformidade em direção ao depocentro.

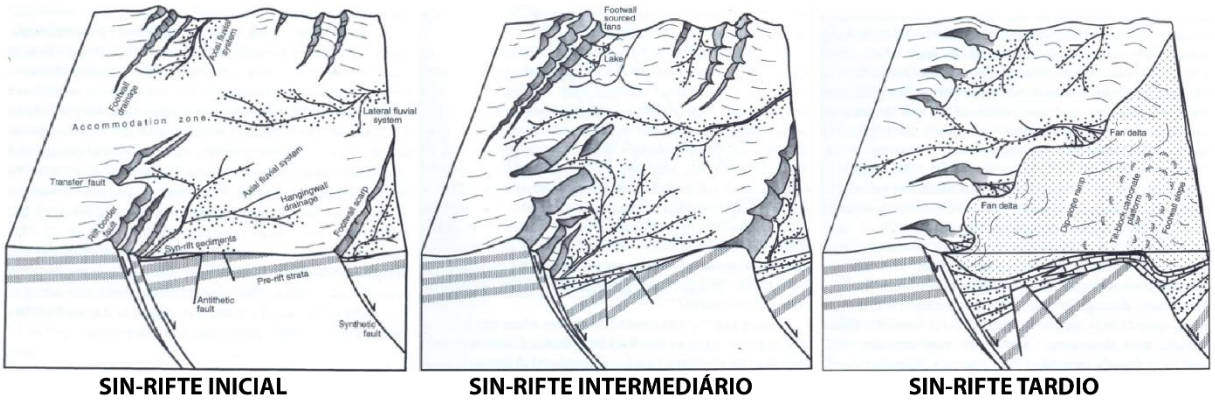

Figura 2.3. Diferentes estágios da fase sin-rifte. Modificado de Bosence (1998).

2- Pós-rifte: abrange os sedimentos depositados em contexto de subsidência termal, controlada por resfriamento e aumento da densidade da litosfera. Esse tipo de subsidência ocorre em uma área mais ampla do que a subsidência gerada por extensão mecânica. Na fase pós-rifte os estratos se acumulam em unidades paralelas que irão soterrar a topografia sin-rifte remanescente, ultrapassando os limites do meio-gráben. Fácies marinhas consistem em lamas pelágicas e hemipelágicas com fácies redepositadas adjacentes à topografia remanescente do meio-gráben. Em áreas tropicais onde se espera que a agradação de plataformas carbonáticas acompanhe a subsidência.

Na sísmica, a fase pré-rifte se caracteriza por estratos plano-paralelos e inclinados, retratando depósitos mais antigos que sofreram rotações estruturais associadas à tectônica do rifte. Os estratos sin-rifte apresentam geometria divergente, reflexo da intensa movimentação tectônica durante este período. Os estratos pós-rifte, por outro lado, são plano-paralelos e horizontais, refletindo um contexto deposicional de quiescência tectônica.

Kuchle e Scherer (2010) propõem a interpretação e mapeamento sistemático sismoestratigráfico de bacias do tipo rifte baseado em conceitos consagrados da estratigrafia de sequências. A compartimentação interna da seção fundamenta-se em tratos de sistemas tectônicos, utilizados inicialmente por Prosser (1993) e, levando em conta a classificação feita por Bosence (1998), abrange apenas o intervalo sin-rifte, desde a discordância sin-rifte até a pós-rifte (Figura 2.4).

1- Trato de Sistemas Tectônico de Início do Rifte: representado por uma ampla bacia rasa continental, formada em resposta aos pulsos iniciais de estiramento crustal em um contexto tectônico ativo, mas incipiente, de acordo com o modelo porposto por

Morley, (2002). Na base do pacote se encontra a discordância sin-rifte (DSR), um truncamento erosivo regional. O preenchimento deste estágio é composto por lagos rasos, comumente recobertos por depósitos fluviais e eólicos, resultando em um padrão de empilhamento agradacional. Na sísmica seus refletores apresentam um padrão plano-paralelo e continuidade comumente baixa.

2- Trato de Sistemas Tectônico de Desenvolvimento de Meio-Gráben: caracterizado pelo início da geração do meio-gráben e por um rearranjo do sistema de drenagem. A base desta unidade se dá pela Superfície de Desenvolvimento de Meio-Gráben, que corresponde a uma inundação na região central da bacia, correlata com uma discordância na borda da margem flexural. É preenchido por sistemas fluvio-lacustres rasos. Na sísmica, a geometria externa é uma seção suavemente em cunha (proto-calha), com padrão de reflexão interno plano-paralelo ou discretamente divergente, com refletores descontínuos

3- Trato de Sistemas Tectônico de Clímax do Rifte: reflete o momento de máxima atividade tectônica na bacia, com pleno desenvolvimento da falha de borda e alto relevo diferencial nas calhas do meio-gráben, resultando em alta taxa de criação de espaço e baixo aporte sedimentar. Como consequência, a margem flexural apresenta padrões fortemente retrogradacionais, enquanto os conglomerados de leques deltaicos associados à falha de borda progradam para dentro da bacia. Na base do Clímax encontra-se a Superfície de Clímax de Rifte, que constitui uma inundação regional mais intensa que a Superfície de Desenvolvimento de Meio-Gráben. O topo do Clímax é marcado pela Superfície de Máximo Rifteamento que representa a máxima inundação da bacia, o momento de maior expansão do sistema lacustre. Na sísmica, este estágio possui geometria externa em cunha e diversos truncamentos internos. Na falha de borda encontram-se refletores caóticos e sem continuidade, com amplitude extremamente variável, associados aos depósitos de leques deltaicos.

4- Trato de Sistemas Tectônico de Final do Rifte: marca uma diminuição da atividade tectônica, recuo do sistema lacustre e uma diminuição na taxa de criação de espaço de acomodação. As cristas do rifte são erodidas e servem de área-fonte para um alto aporte sedimentar que chega ao meio-gráben. Como consequência tem-se depósitos em um padrão progradante na margem flexural. Por outro lado, a falha de borda sofre um recuo devido à diminuição da sua movimentação por queda da atividade tectônica. Por fim, o rifte é totalmente preenchido e a fase rifte se encerra,

seja na forma de um rompimento crustal efetivo e geração de um oceano ou abortagem do processo, dando origem à discordância de pós-rifte.

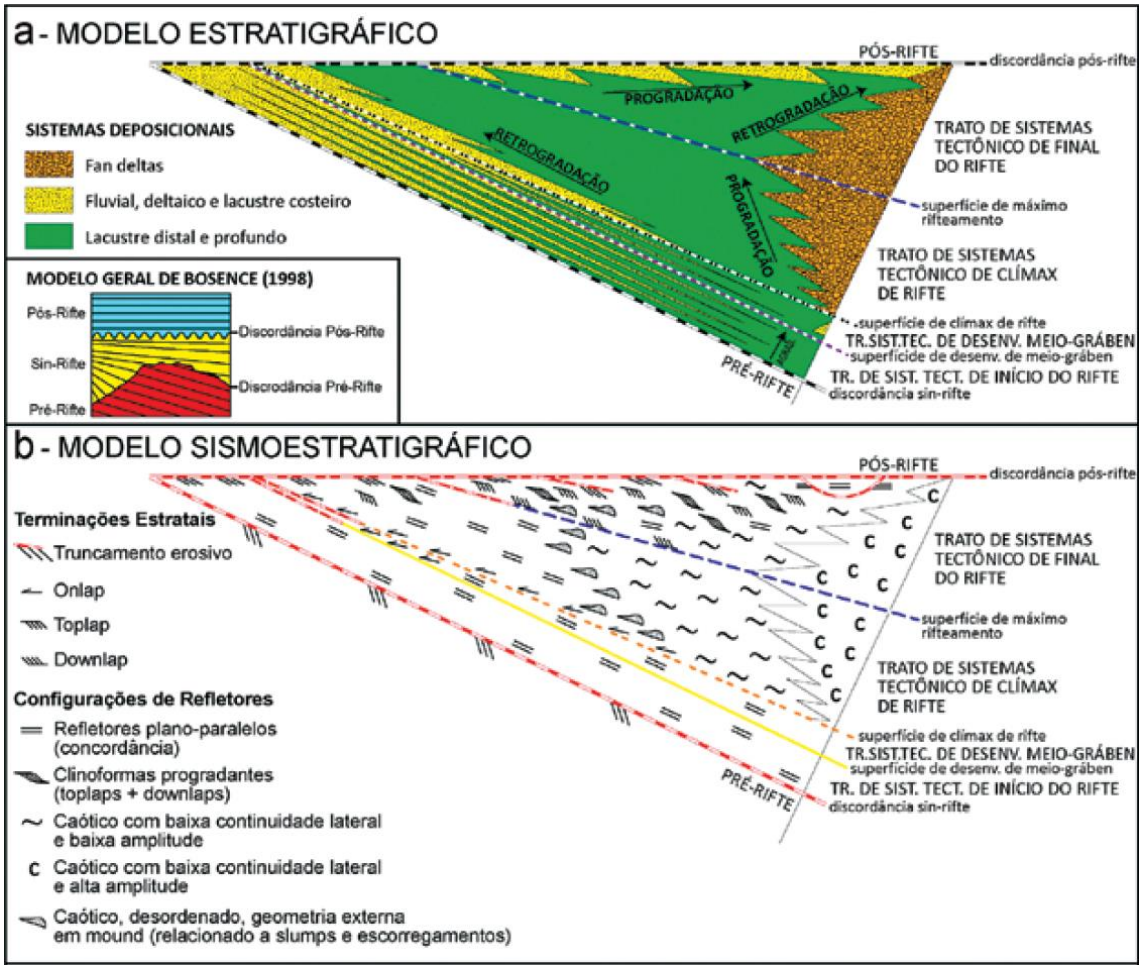

Figura 2.4. (A) Modelo estratigráfico idealizado de uma bacia rifte, incluindo os tratos de sistemas tectônicos, as tendências deposicionais e as superfícies limítrofes. (B) Expressão sísmica do modelo estratigráfico acima idealizada, ilustrando as terminações estratais e as configurações de refletores. Extraído de Kuchle e Scherer (2010).

2.2 Evolução tectono-estratigráfica de bacias sag

De acordo com Gabrielsen *et al.* (2001), a configuração da bacia sag é amplamente influenciada pelas principais características estruturais herdadas do rifteamento (cristas de blocos rotacionados, rampas de revezamento e sub-plataformas) pois as mesmas controlam a distribuição de sedimentos. No estágio mais precoce do desenvolvimento sag ocorre a amalgamação das sub-bacias geradas na fase sin-rifte e a suavização do assoalho da bacia. Conforme a bacia evolui, o efeito da contração termal diminui, enquanto a carga sedimentar continua a crescer fazendo com que a topografia gradualmente seja soterrada por sedimentos mostrando um contexto em que o suprimento sedimentar excede a taxa de criação de espaço de acomodação. O estágio sag maduro é alcançado quando o equilíbrio termal é obtido,

e a geometria final será uma bacia ampla em forma de pires, não mais influenciada pelas características herdadas do sin-rifte (Figura 2.5).

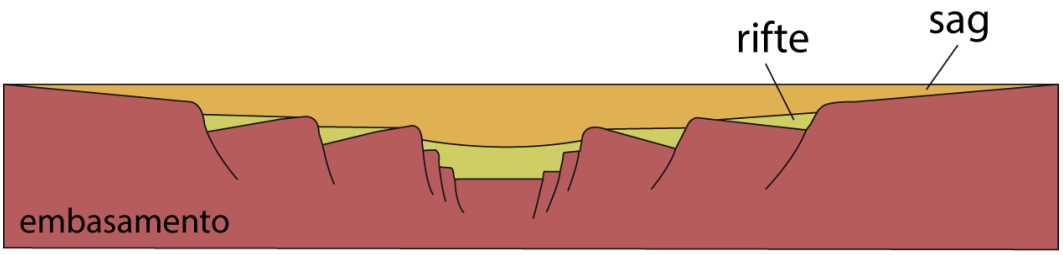

Figura 2.5. Desenho esquemático que dos estágios evolutivos rifte (sin-rifte) e sag. Nota-se que ainda há topografia residual da fase rifte nas etapas iniciais e intermediárias da fase sag. Elaborado pela autora a partir da descrição de Gabrielsen et al. (2001).

A geometria externa do sag é abordada pelos autores Loegering *et al.* (2013), com base em dados de sísmica de reflexão 2D e poços de exploração da Bacia do Colorado (leste da Argentina). A Bacia do Colorado é um rifte abortado que precedeu a quebra principal Supercontinente Gondwana, e que posteriormente sofreu duas fases de subsidência termal (sag I e sag II) (Figura 2.6). A primeira fase, em um primeiro momento, foi condicionada pela morfologia herdada da fase rifte. Ao preencher a topografia negativa gerada pelas calhas, a sedimentação extravasa os limites do meio-gráben. A segunda fase, já sem o controle do relevo gerado pelo rifte, é relacionada à abertura do Oceano Atlântico Sul, e registra uma mudança na orientação da bacia: de NW-SE para E-W.

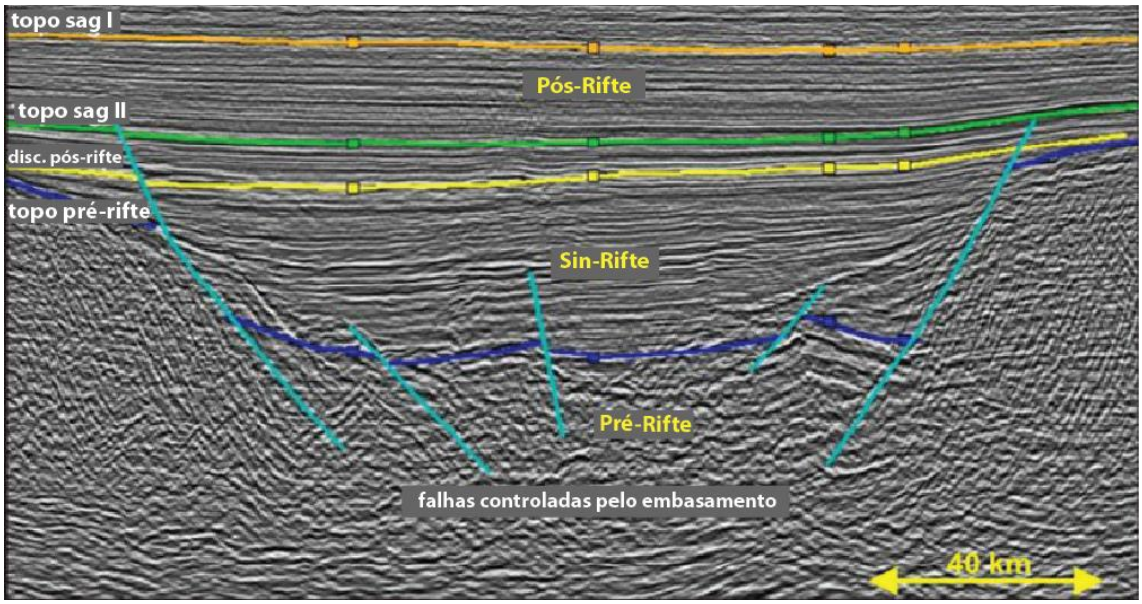

Figura 2.6. Linha sísmica 2D com as seções pré-, sin- e pós-rifte e as falhas relacionadas ao rifteamento. Nota-se que os refletores da seção sin-rifte têm geometria divergente, enquanto que os que compõe o estágio sag são plano-paralelos. Modificado de Loegering *et al.* (2013).

Karner e Gambôa (2007) descrevem as bacias sag pré-sal do Oceano Atlântico Sul. De acordo com os autores, a sucessão sag tem em média 200 a 300 m de espessura nas bacias de Campos e Santos, no SE brasileiro. Os refletores são sub-

paralelos e sub-horizontais ou com uma certa inclinação, e sobrepõe o pacote mais inclinado sin-rifte. A atividade das falhas normais diminui gradativamente da base para o topo da seção, desde os sedimentos sin-rifte até os sedimentos sag pré-sal. Na Bacia de Santos, observa-se, porém, que as falhas deslocam a superfície de base do sal, apontando que estavam ativas até o início de deposição evaporítica (Figura 2.7). O contato da sequência sag pré-sal com o sal é definido em ambas as margens por uma discordância, marcada por truncamentos erosivos (Figura 2.7). Os autores afirmam que essa discordância se deve a um rebaixamento no nível do lago desencadeado por uma mudança climática, que acabou em criação de espaço de acomodação (posteriormente preenchido pelos evaporitos).

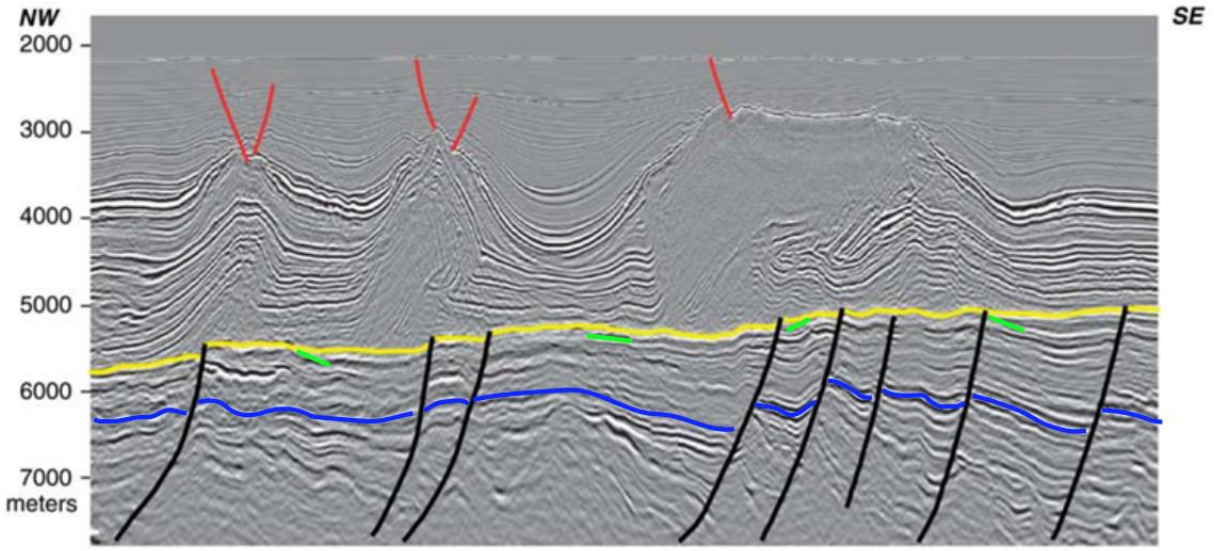

Figura 2.7. Linha sísmica interpretada da porção distal da Bacia de Santos. Nota-se que as falhas normais (em preto) se estendem até a base dos evaporitos, podendo causar deslocamentos no refletor de base do sal – marcado em amarelo. Em verde estão destacados truncamentos erosivos; em azul o contato entre o rifte e o sag. Modificado de Karner e Gambôa, 2007.

Kukla *et al.* (2018) também abordam as bacias marginais do Oceano Atlântico Sul. Os autores apresentam uma linha sísmica detalhada da Bacia de Santos, (Figura 2.8), onde é possível observar as bacias rifte (Neocomiano – Barremiano) delimitadas por falhas normais, com preenchimento caracterizado por refletores divergentes e inclinados. Sobrepondo o rifte, tem-se em azul claro o sag pré-sal (carbonatos Aptianos), de natureza mais contínua e com refletores sub-horizontais a levemente inclinados. Observa-se que o sag pré-sal é ausente acima do alto mais elevado (para E na linha), e este causa deslocamento na superfície de base do sal. Kukla *et al.* (2018) também mostram uma linha interpretada da Bacia de Campos, que indica que o sal é fino na porção proximal da bacia e sobrepõe uma bacia sag que é levemente afetada por falhas relacionadas ao rifte. Os autores afirmam que os evaporitos Aptianos têm espessura e distribuição altamente influenciada pela geometria,

localização e distribuição das unidades subjacentes, i.e. pela topografia rifte e sag pré-sal.

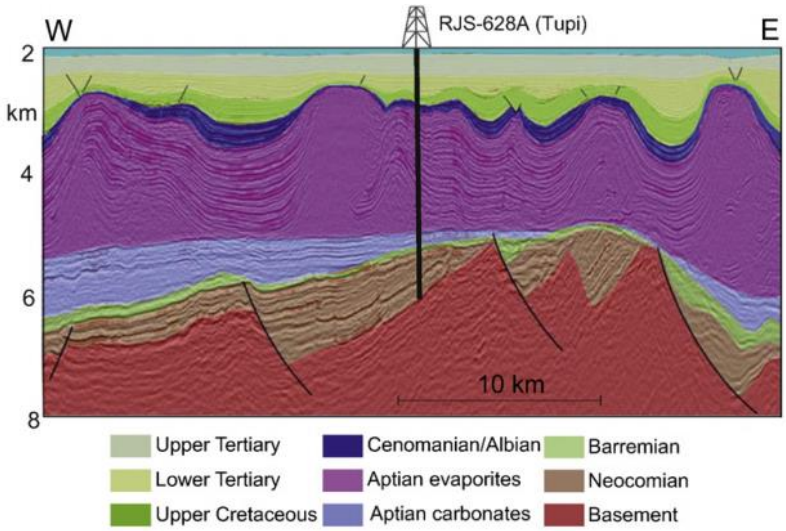

Figura 2.8. Linha sísmica interpretada da Bacia de Santos com a seção rifte (Neocomiano – Barremiano), sag (Aptiano) e margem passiva (Albiano – Terciário superior). Retirado de Kukla *et al.* (2018).

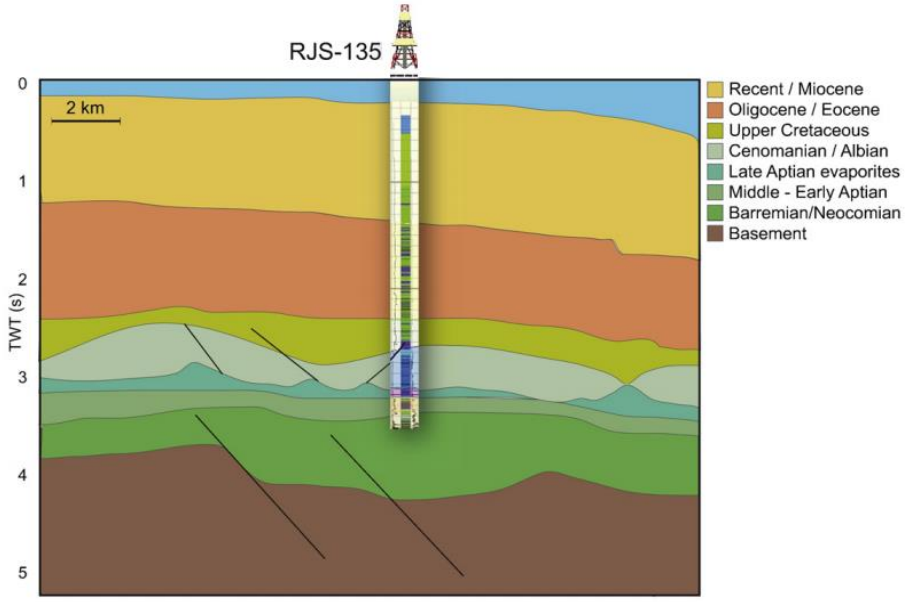

Figura 2.9. Sucessão de unidades da Bacia de Campos feita a partir de uma linha sísmica e um poço de exploração (RJS-135). Retirado de Kukla *et al.* (2018).

Ceraldi e Green (2016) subdividem o estágio sag pré-sal das bacias de Campos e Kwanza em duas unidades (sag 1 e sag 2), separadas por uma discordância (Figura 2.10). Os refletores sísmicos do sag pré-sal são sub-paralelos, sub-horizontais ou levemente inclinados próximo aos altos do embasamento. Os refletores basais da unidade sag 1 têm terminações em onlaps bilaterais contra falhas do estágio rifte. O topo da sag 1 e a unidade sag 2 tem natureza mais contínua, e são menos influenciados pelas falhas rifte, o que implica que os lagos começaram a coalescer e se tornaram mais profundos. A superfície de discordância entre as unidades aparenta ser erosional nos flancos da bacia (áreas onde vemos relações de *onlap*) e, no centro,

se torna uma paraconformidade. A discordância é sobreposta por uma reflexão de alta amplitude negativa, sismicamente relacionada a uma seção de folhelho com alto conteúdo orgânico total.

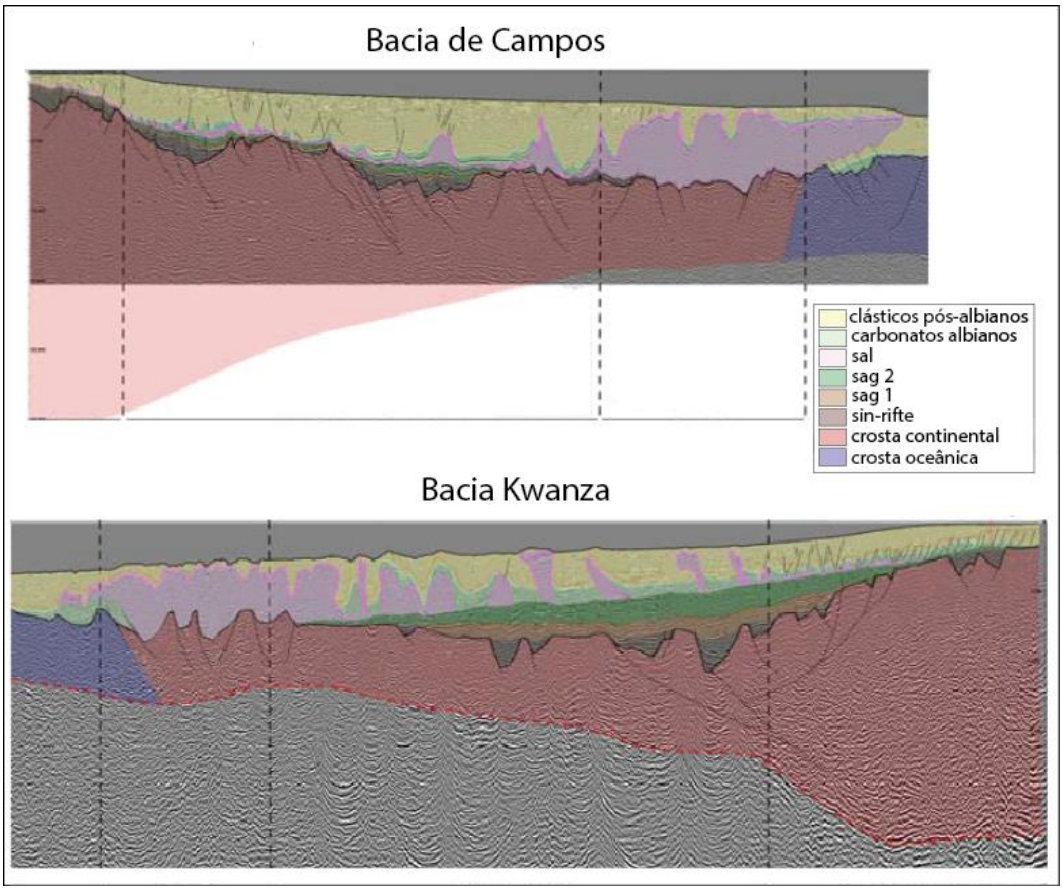

Figura 2.10. Linhas sísmica 2D da Bacia de Campos, acima, e da Bacia Kwanza, abaixo, com as principais unidades tectono-estratigráficas. Destaque para as duas unidads sag em laranja (sag 1) e em verde (sag 2). Modificado de Ceraldi e Green (2016).

Com base no que foi discutido até então, apontam-se as principais características tectono-estratigráfica do estágio sag:

- Na base, presença de uma não conformidade ou desconformidade nas margens das calhas rifte e uma paraconformidade interna às calhas rifte;
- Refletores internos (sub-)paralelos e (sub-)horizontais, podendo estar leve a moderadamente inclinados, especialmente caso haja falhamento ativo sin-deposicional;
- A sedimentação do estágio sag inicialmente preenche a topografia remanescente da calha rifte, e então extravasa os limites da mesma;
- Ao final do sag espera-se uma peneplanização da topografia gerada por falhas;
- Inicialmente um padrão de empilhamento agradacional com componente progradacional em direção ao topo, passando para retrogradacional conforme há degradação dos altos topográficos.

Conclui-se, portanto, que o estágio sag corresponde: (i) ao trato de sistema

tectônico de pós-rifte no modelo da Prosser (1993); (ii) ao sin-rifte tardio e pós-rifte de Bosence (1998); (iii) ao trato de sistema tectônico de final de rifte e pós-rifte de Kuchle e Scherer (2010) (Tabela 2.1). É importante ressaltar que o preenchimento sedimentar e a evolução tectono-estratigráfica do sag serão os mesmos em riftes abortados e em riftes que, após o sag, evoluirão para uma bacia de margem passiva com o estabelecimento de um centro de espalhamento de crosta oceânica, como é o caso das bacias de interesse desta tese.

Tabela 2.1. Tabela comparativa dos modelos de evolução tectono-estratigráfica de bacias rifte (Prosser, 1993; Bosence, 1998; Kuchle & Scherer, 2010), com análise da subsidência e início da fase sag.

<table>
<tr><th>PROSSER, 1993</th><th>BOSENCE, 1998</th><th>KUCHLE E SCHERER, 2010</th><th>subsidência</th><th></th></tr>
<tr><td>T.S.T. Pós-rifte Tardio</td><td rowspan="2">Pós-rifte</td><td rowspan="2">Pós-rifte
discordância</td><td rowspan="6">Térmica

Mecânica</td><td rowspan="6">S
A
G</td></tr>
<tr><td>T.S.T. Pós-rifte Imediato</td></tr>
<tr><td>T.S.T. Clímax de Rifte</td><td>Sin-rifte Intermediário</td><td>T.S.T. Clímax de Rifte</td></tr>
<tr><td rowspan="2">T.S.T. Início de Rifte</td><td rowspan="2">Sin-rifte Inicial</td><td>T.S.T. Desenvolvimento do Meio-Gráben</td></tr>
<tr><td>T.S.T. Início de Rifte</td></tr>
<tr><td>Pré-rifte</td><td>Pré-rifte</td><td>Pré-rifte</td></tr>
</table>

2.3 Tectônica do sal em bacias de margem passiva

A deformação em margens passivas controladas pela tectônica do sal, como é o caso das bacias do offshore sudeste brasileiro e das bacias conjugadas africanas, é impulsionada por forças gravitacionais. Os dois principais processos responsáveis por desencadear a deformação associada ao sal são denominados: deslizamento gravicational (*gravity gliding*) e espalhamento gravitacional (*gravity spreading*) (Hudec e Jackson, 2007). A diferença fundamental estre os dois processos está no modo de liberação da energia gracitacional. No deslizamento gravitacional, tem-se liberação de energia causada pela inclinação da margem à medida que a bacia subside. No espalhamento gravitacional, há liberação de energia com o rebaixamento do centro de gravidade relacionado ao afinamento do material dúctil, e ocorre essencialmente devido ao aumento da carga de sedimentos conforme a margem prograda (Peel, 2014).

Margens dominadas por deslizamento gravitacional são divididas em zonas cinematicamente ligadas que se formam conforme o sal flui para o centro da bacia;

são elas: zona de extensão (proximal) e zona de contração (distal), comumente separadas por uma zona de transição, (Figura 2.11; Fort *et al.*, 2004; Hudec e Jackson, 2004; Brun e Fort, 2011; Quirk *et al.*, 2012; Peel, 2014). As estruturas relacionadas à tectônica do sal se formam perpendiculares à direção de máxima tensão, o que significa que a maior parte se forma perpendicular à direção de mergulho da superfície de base do sal e paralelo à margem. Margens dominadas por espalhamento gravitacional são caracterizadas por zonas de contração na base e à frente da cunha sedimentar progradatne conforme o sal é empurrado para o centro da bacia (Figura 2.12; Brun e Fort, 2011; Peel, 2014). As estruturas relacionadas à tectônica do sal se formam subparalelas à margem, paralelas à e seguindo a geometria arqueada da frente deltaica.

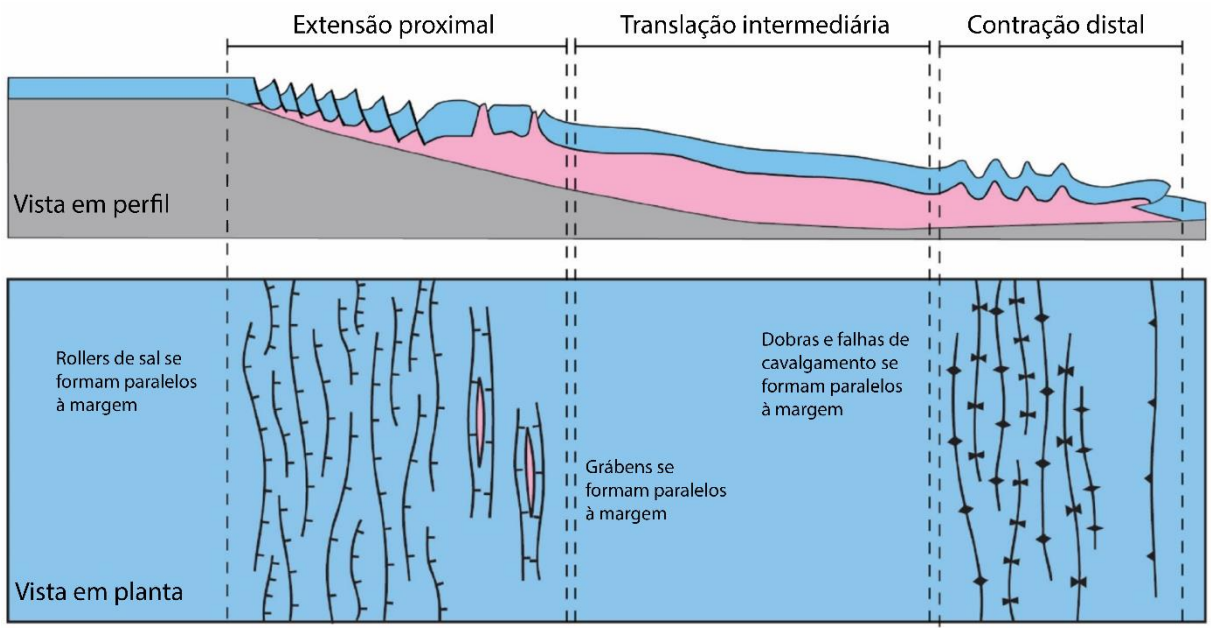

Figura 2.11. Vista em perfil e em planta de deformação de sal em margem passivas associada a deslizamento gravitacional (*gravity gliding*). Modificado (traduzido) de Evans *et al.*, 2019.

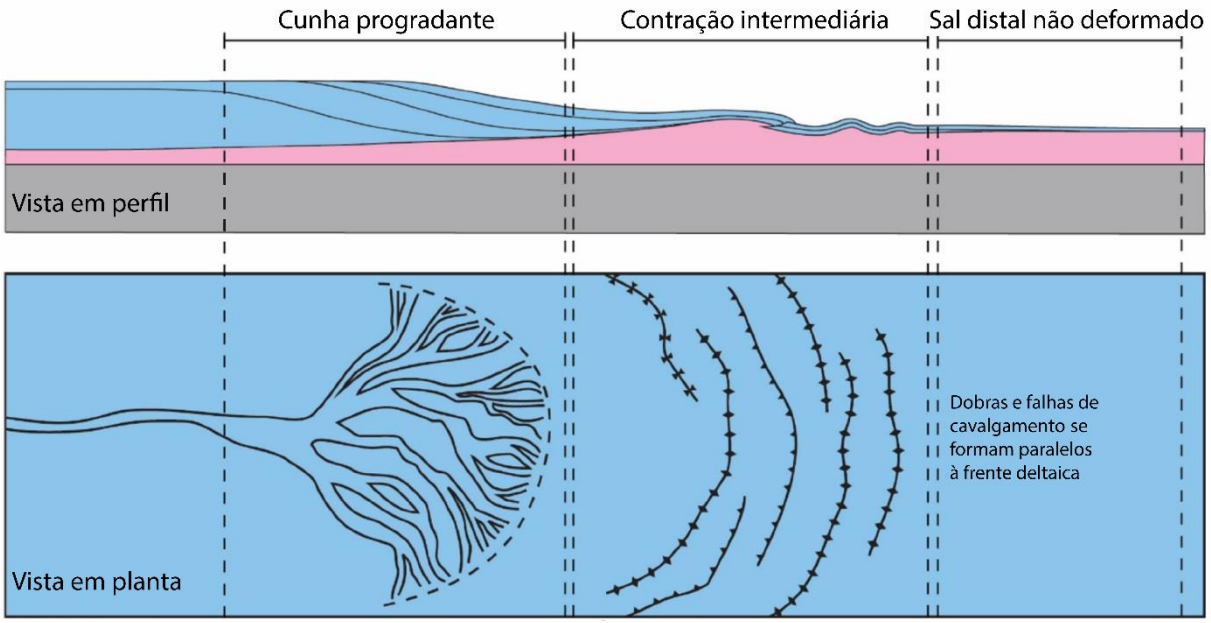

Figura 2.12. Vista em perfil e em planta de deformação de sal em margem passivas associada a espalhamento gravitacional (*gravity spreading*). Modificado (traduzido) de Evans *et al.*, 2019.

Na realidade, as margens passivas naturais são sistemas mistos, influenciados tanto por deslizamento como por espalhamento gravitacional ao longo do tempo e espaço (Rowan *et al.*, 2012). O deslizamento em geral inicia muito cedo conforme a subsidência termal faz com que a margem se incline, podendo inclusive começar simultaneamente à deposição da sequência evaporítica. O espalhamento torna-se importante mais tarde na evolução tectônica da margem, particularmente em regiões onde o fluxo sedimentar para dentro da bacia é alto, como é o caso com deltas progradantes. A interação entre os dois processos gravitacionais controla o estilo, o timing e a área de movimentação do sal.

Modelos clássicos de tectônica do sal em margens passivas as dividem em três domínios deformacionais cinemáticos, cada um associado a uma variedade distinta te estruturas de sal e do sedimento posterior (e.g. Rowan *et al.*, 2004, Brun e Fort, 2011, Peel, 2014). O domínio extensional proximal é associado com a formação de falhas lístricas, diápiros triangulares, jangadas (rafts) e rollers de sal (Figura 2.13). A extensão é acomodada por deformação contracional no domínio distal, caracterizado por dobras e anticlinais de sal, falhas de cavalgamentos e nappes de sal (Figura 2.13). Os dois domínios das extremidades são separados por um domínio de translação, onde a deformação é tipicamente descrita como relativamente suave (Brun e Fort, 2004; Davison *et al.*, 2012). Tais modelos consideram uma superfície de base do sal com mergulho suave, sem variações abruptas no relevo – o que não é o caso para muitas bacias de margem passiva.

O sal comporta-se reologicamente ao longo do tempo geológico como um fluido altamente viscoso (Weijermars *et al.*, 1993). Fluidos altamente viscosos são sensíveis à geometria da superfície pela qual fluem, e nos casos em que o sal é depositado logo após o rifteamento (como é o caso das bacias do Oceano Atlântico Sul), a superfície de base do sal é irregular. Diferentes trabalhos – discutidos a seguir – através de observações de margens passivas com dados sísmicos, modelos analógicos físicos e numéricos mostram que o fluxo do sal em direção ao centro da bacia pode ser complicado por topografia rifte residual basal (Figura 2.14). As dobras ou escarpas de falhas subjacentes podem criar uma superfície irregular na base do sal com a qual o sal interage à medida que flui para a bacia (Evans *et al.*, 2019).

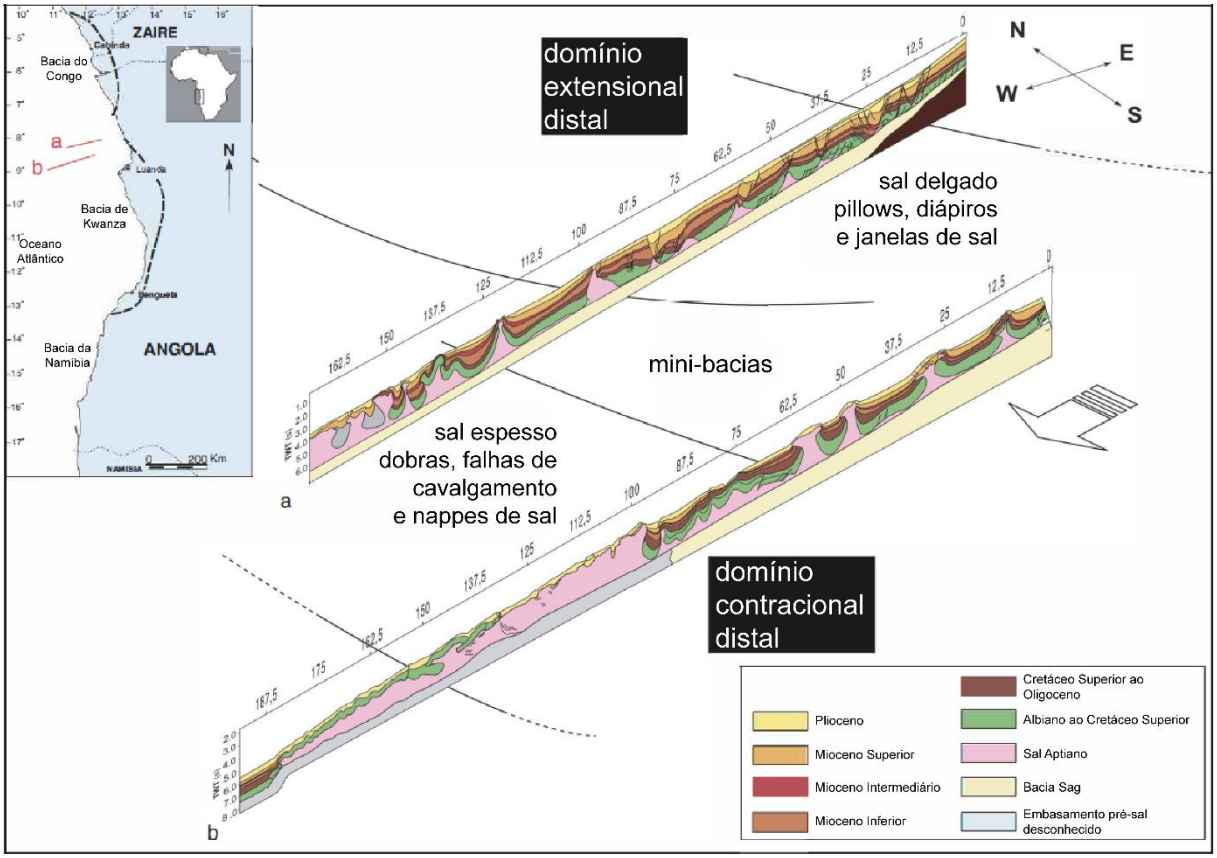

Figura 2.13. Estilos estruturais relacionados à tectônica de sal ao longo da Bacia de Kwanza, no offshore oeste da África. Modificado Rodriguez (2018) e Brun e Fort (2004).

Gaullier *et al.* (1993) investigaram os efeitos das estruturas herdadas da fase rifte na tectônica do sal utilizando modelos físicos. Os autores mostraram que degraus na superfície de base do sal, oblíquos à direção de translação do sal, iniciaram falhas também oblíquas no sedimento posterior. Os ‘degraus’ representam escarpas de falhas da fase sin-rifte que foi sobreposta por sal. Os modelos demonstram uma forte similaridade entre as direções estruturais abaixo da superfície de descolamento basal de sal e àquelas formadas no sedimento posterior.

Cobbold e Szatmari (1991) e Tadeu dos Reis *et al.* (2008) também utilizaram modelos físicos, neste último acompanhados de exemplos naturais do Mediterrâneo ocidental, para mostrar como mudanças locais na direção de mergulho na base do sal podem localmente redirecionar o fluxo de sal. Mais especificamente, eles mostram que locais côncavos ou convexos na superfície de base do sal podem geral padrões de deslizamento radiais ou bi-direcionais. Geometrias côncavas levam a um fluxo de sal convergente que pode gerar estruturas compressionais, enquanto geometrias convexas levam a um fluxo de sal divergente que pode gerar estruturas extensionais (Figura 2.14).

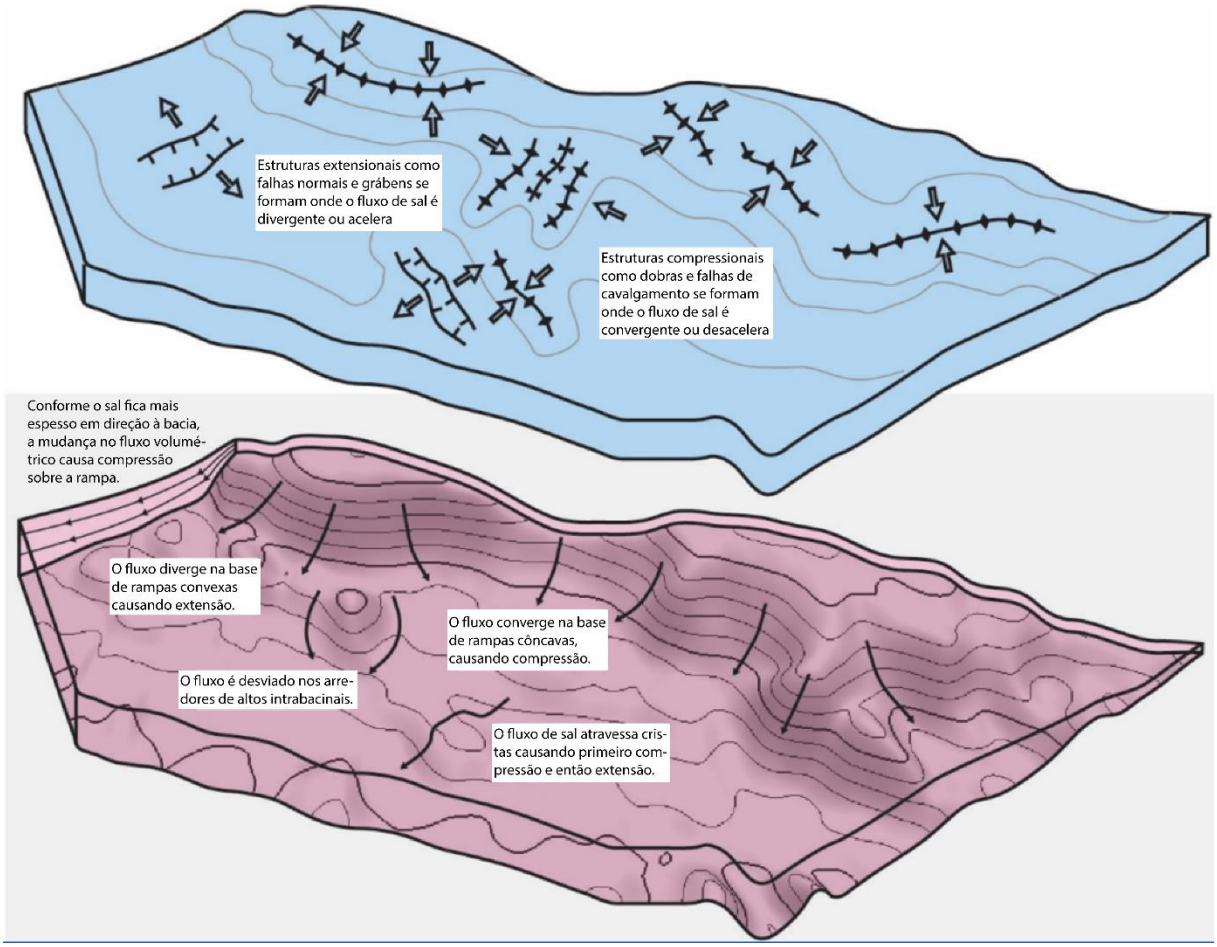

Figura 2.14. Ilustração esquemática dos efeitos da topografia residual herdada da fase rifte no fluxo de sal (figura de baixo) e na deformação associada no sedimento posterior (figura de cima). Ilustração feita por Sian Evans.

Conforme o sal é depositado ele preenche os baixos topográficos, drapeando altos topográficos. Variações na espessura do pacote evaporítico afetam o seu fluxo volumétrico conforme espessa e afina. Isso pode ocasionar zonas locais de extensão e compressão, conforme demonstrado por Dooley *et al.* (2017) com modelos numéricos e físicos, e com a interpretação de uma linha sísmica na Bacia de Campos. A Figura 2.15 demonstra as interações entre mudanças no relevo da superfície de base do sal e no fluxo de sal. Quando o sal se movimenta em direção a um bloco sub-

sal elevado, o fluxo causa contração conforme espessa no topo da rampa (Figura 5b). A desaceleração do fluxo de sal conforme o mesmo espessa em um baixo estrutural causa aceleração no topo da rampa e desaceleração na base (Fig. 2.15d). Tensões localizadas geram, portanto, um eixo extensional no topo e um compressional na base da rampa. Tais efeitos no fluxo de sal são atenuados a inexistentes quando o sal é espesso (Fig. 2.15a,c).

O impacto do relevo da superfície de base do sal no fluxo de sal aponta que contração e extensão podem ocorrer em qualquer lugar numa margem passiva, e estruturas podem se desenvolver oblíquas à margem e à direção de mergulho da superfície basasl. Conforme o sal movimenta o sedimento posterior, as estruturas acima do sal migrarão através de contração e extensão localizadas. Isso significa que estruturas podem passar por múltiplas fases de deformação. Por exemplo, estruturas extensioanis podem ser comprimidas, e estruturas contracionais podem, mais tarde, sofrer extensão.

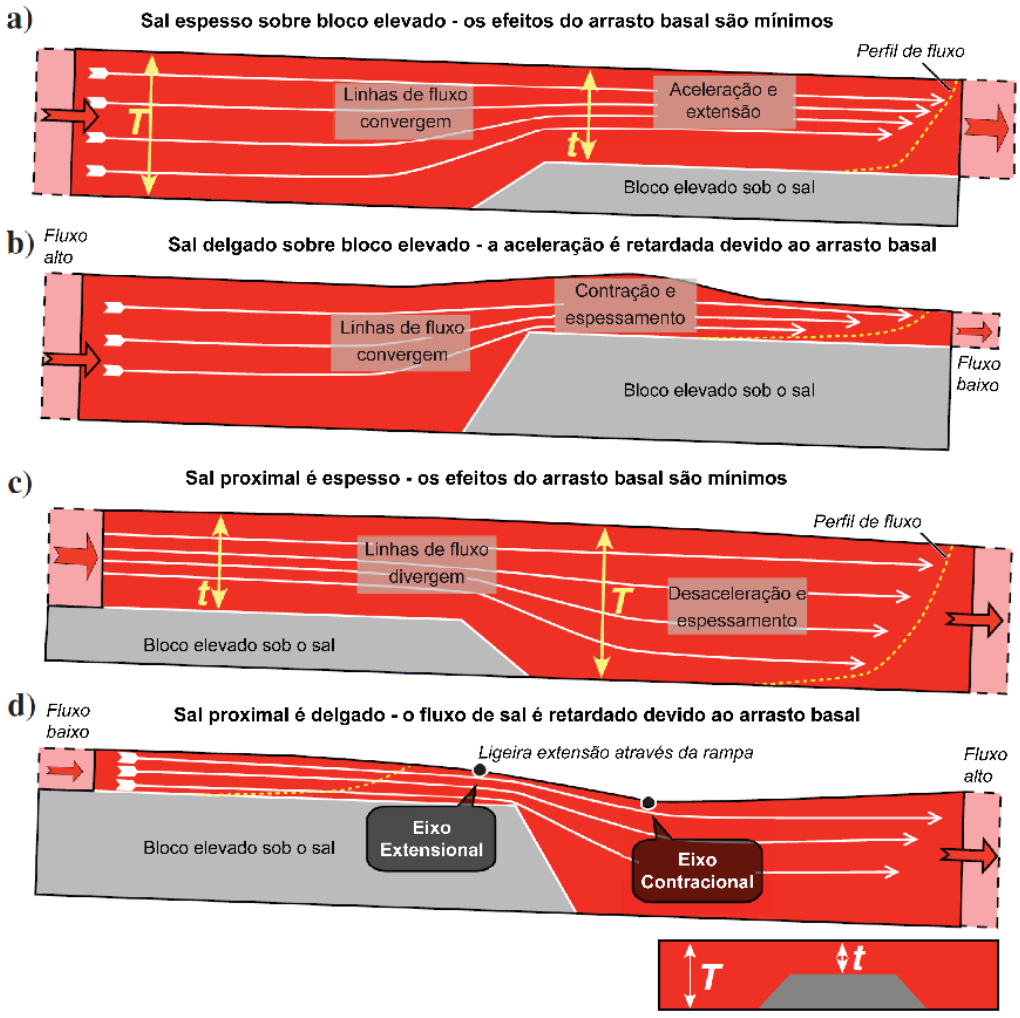

Figura 2.15. Interações entre mudanças no relevo da superfície de base do sal e no fluxo de sal, conforme determinado por modelos físicos. O relevo da superfície de base do sal causa desacelerações e acelerações locais no fluxo de sal e gerando locais com campos de tensão contracionais e extensionais, respectivamente. O efeito no fluxo de sal é atenuado a inexistente quando o sal é espesso (a) e (c). Modificado de Dooley *et al.*, 2017.

3 Localização e Contexto Geológico

As bacias de Campos e Espírito Santo fazem parte do sistema de bacias rifte originadas pela quebra do Supercontinente Gondwana por abertura o Oceano Atlânico Sul, no Jurássico tardio ao início do Cretáceo (Szatmari, 2000). A Bacia do Espírito Santo situa-se no Estado homônimo na margem continental brasileira (Figura 3.1). É delimitada ao sul pelo Alto de Vitória, que a separa da Bacia de Campos; e ao norte, pela Bacia de Mucuri, da qual foi dividida a partir de critérios geográficos (Figura 3.2a; Vieira, 1994). A fronteira leste da bacia coincide com o limite entre as crostas continental e oceânica. A presença do Complexo Vulcânico de Abrolhos a leste condiciona um alargamento da plataforma continental, que chega a uma largura de 240 km (França *et al.*, 2007). A Bacia de Campos é localizada na plataforma continental offshore nos estados de Rio de Janeiro e Espírito Santo (Figuras 3.1, 3.3a). Seu limite com a Bacia de Santos a sul se dá pelo Alto de Cabo Frio (Mohriak *et al.*, 1989); o limite leste da bacia é por sedimentos que se acunham na planície abissal oceânica, e a oeste por afloramentos de seu embasamento, rochas ígneas e metamórficas da Faixa Ribeira.

Figura 3.1. Mapa do Brasil com os estados e as bacias marginais brasileiras, com destaque para as bacias de Campos e do Espírito Santo.

A quebra da porção oeste do Supercontinente Gonduana teve início no Jurássico tardio/Eocretáceo (220-200 Ma). A configuração de um sistema rifte se confirma por elementos estruturais característicos de deformação rúptil que são claramente delineados na sísmica, incluindo horsts e grábens ligados por falhas

normais com continuidade direcional limitada (Karner, 2000). Em seguida houve uma fase tardia de afinamento plástico da crosta inferior e manto litosférico, que culminou com o início da expansão do fundo oceânico (Karner, 2000).

O magmatismo induzido pela pluma Tristão da Cunha teve um papel essencial na abertura do Atlântico Sul, pois enfraqueceu a litosfera continental expelindo derrames basálticos volumosos entre 145 e 129 Ma ao longo da Província Paraná-Etendeka na América do Sul e Oeste da África (Hawkesworth, 1992). A pluma Tristão da Cunha originou os lineamentos vulcânicos Walvis Ridge e do Alto de Rio Grande, localizados entre as bacias de Santos e Pelotas, no Brasil, e suas conjugadas Namibe e Walvis na África (Thompson *et al.*, 2015).

Durante o Aptiano, estas estruturas serviram como barreira separando a série de bacias de lagos interconectados geradas pelo rifteamento a norte do oceano aberto a sul. Tal isolamento permitiu o desenvolvimento de depósitos carbonáticos fluvio-deltaicos e lacustres com pouca ou nenhuma influência de água marinha nas bacias do Barremiano ao início do Aptiano (Moreira *et al.*, 2007).

Uma fase termal sag, pós-rifte, teve início no início do Aptiano, foi caracterizada por ampla subsidência regional associada com resfriamento da litosfera. Neste período, blocos de falha soerguidos foram erodidos em resposta à regressão regional, formando uma desconformidade conhecida como pré-Neo-Alagoas (Karner and Driscoll, 1999; Karner, 2000).

No Aptiano tardio os altos topográficos começaram a subsidir, o que promoveu o periódico ou episódico ingresso de água marinha. Os repetidos ciclos de entrada de água salgada e dissecação resultaram na deposição de amplas e espessas unidades evaporíticas (Ceraldi e Green, 2016). Condições plenamente marinhas se estabeleceram no Albiano, resultando na deposição de carbonatos marinhos de águas rasas gradando para deposição clástica de marinho raso a profundo (Séranne e Anka, 2005).

As evoluções tectono-estratigráficas das bacias do Espírito Santo e Campos até os intervalos de interesse em cada bacia, incluindo nomes e detalhamentos das formações constituintes, são abordadas a seguir.

3.1 Bacia do Espírito Santo

A sedimentação na Bacia do Espírito Santo tem início no Andar Valanginiano do Eocretáceo, e é representada pelo Grupo Nativo, constituído pelas formações

Cricaré e Mariricu (Figura 3.2b; Vieira, 1998). A Formação Cricaré (Valanginiano – Eoaptiano) é composta pelos membros Jaguaré e Sernambi e faz parte da megasequência rifte da bacia. O Membro Jaguaré engloba arenitos, conglomerados e rochas vulcânicas e vulcanoclásticas da Formação Cabiúnas, e o Membro Sernambi apresenta predominância de folhelhos, margas e carbonatos, com menor proporção de arenitos e conglomerados (Vieira, 1998; França *et al.*, 2007). Interpreta-se que o ambiente deposicional desta formação é aluvial/flúvio-lacustre com vulcanismo associado (França *et al.*, 2007). No Eoaptiano, durante o final da deposição da Formação Cricaré, as porções mais proximais das bacias da margem leste brasileira eram caracterizadas por grábens inativos sujeitos a processos erosionais, enquanto nas porções distais havia intensa sedimentação em um contexto tectônico de rifte (Dias, 2005). Tal quadro resultou na exposição subaéra de grande parte das porções proximais das bacias, originando uma discordância regional conhecida como “Discordância Pré-Alagoas”, que precedeu a deposição da Formação Mariricu.

A Formação Mariricu (Aptiano Superior), objeto de estudo deste projeto, compreende os membros Mucuri (inferior) e Itaúnas (superior) e representa a transição de um ambiente continental para deposição marinha restrita (Figura 3.2b; Vieira *et al.,* 1994), sendo parte da megasequência transicional. Tem contato inferior discordante com o embasamento ou com sedimentos da Formação Cricaré depositados nas calhas do rifte. O contato superior é concordante com o Grupo Barra Nova ou discordante com a Formação Urucutuca (Vieira, 1998). A deposição da Formação Mariricu se deu em um ambiente de quiescência tectônica, com falhamentos mais expressivos ocorrendo apenas localmente (Dias, 2005).

O Membro Mucuri, base da Formação Mariricu, é constituído por sedimentos clásticos areníticos e conglomeráticos arcóseos a líticos, intercalados com folhelhos, siltitos e delgados níveis evaporíticos de anidrita e halita contendo finas camadas de folhelho (Vieira et al*.,* 1994). A espessura da unidade atinge 2000 m com espessamento para o leste, em direção ao depocentro da bacia (França *et al.*, 2007), sendo altamente variável, pois está condicionada ao posicionamento das calhas da fase rifte (Vieira, 1998).

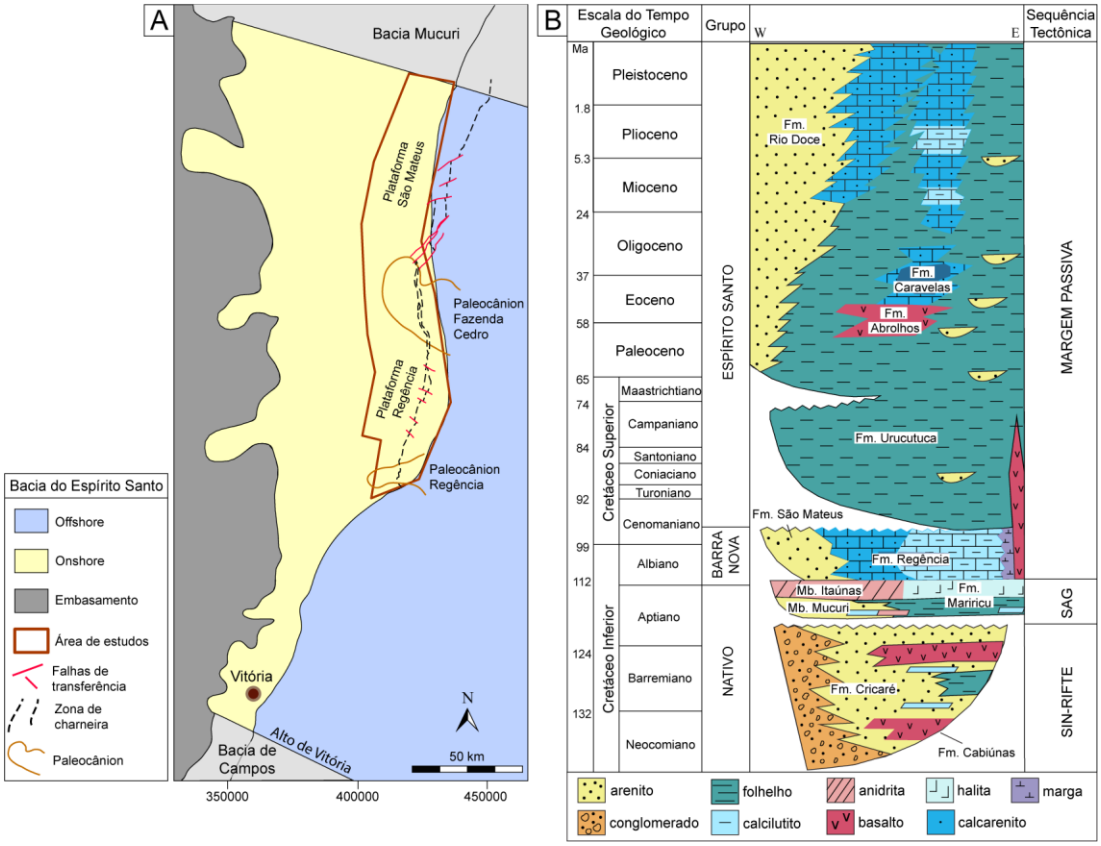

Figura 3.2. (A) Margem oeste da Bacia do Espírito Santo com o polígono da área de estudos; (B) Carta cronoestratigráfica da Bacia do Espírito Santo (modificada de Mohriak, 2003).

Vieira (1998), unindo dados de descrição macroscópica de testemunhos com perfis elétricos, dividiu o Membro Mucuri em três tectono-sequências delimitadas por discordâncias erosivas: a sequência basal (MUC-3), ainda sob tectonismo remanescente da fase rifte, contém fácies de leques aluviais e sistemas fluviais entrelaçados, apresentando gradação de conglomerados para arenitos arcoseanos grossos, arenitos finos, siltitos e níveis de anidrita ou carbonatos brechados; a sequência intermediária (MUC-2) registra o afogamento dos leques e sistemas fluviais, sendo constituída por arenitos muito finos a finos, com camadas de anidrita ou carbonato delimitando o topo; na sequência superior (MUC-1) os sedimentos areno-pelíticos com evaporitos associados foram interpretados como um sistema de lagunas com planícies lamosas que evolui para ambiente evaporítico do tipo *sabkha*. Segundo o autor, os sedimentos do Membro Mucuri se distribuem de forma que, a oeste, região proximal, predominam conglomerados e arenitos grossos mal selecionados, havendo diminuição da granulometria dos sedimentos siliciclásticos conforme o afastamento da área-fonte para o leste, além da presença de fácies evaporíticas. Vieira (1998) identificou uma tendência transgressiva para a unidade, com sedimentos aluviais sotopostos a sedimentos estuarinos e/ou lagunares retrabalhados por maré e ondas. A intercalação de evaporitos indica extremo

ressecamento gerado pela aridez climática, aliado à deficiência no aporte de água e sedimentos.

Dias (2005) definiu quatro sequências estratigráficas para o Membro Mucuri a partir da análise de perfis elétricos e cerca de 300 m de testemunhos contínuos. As sequências apresentam padrões de empilhamento bem definidos, iniciando com um pacote de associação de fácies fluvial seguida por associações de fácies relacionadas a ambientes marinho-marginais. Da sequência mais antiga para a mais nova tem-se uma progressiva diminuição da influência de marés nas fácies que seguem a deposição fluvial. De acordo com o autor, este quadro é característico de um vale preenchido por sistemas estuarinos, onde a influência de maré é mais ativa no início do preenchimento, quando as restrições topográficas são mais acentuadas e as velocidades de marés, maiores.

O Membro Itaúnas consiste em espessas camadas de evaporitos, com predominância de anidritas e carbonatos na porção oeste da bacia, e halitas na porção leste (Vieira, 1998). Sua espessura é altamente variável, de 50 a mais de 5000 m como diápiros e muralhas em direção a águas profundas e ultraprofundas (França e Tschiedel, 2006).

Interpreta-se que o Membro Itaúnas tenha sido depositado em um contexto de bacia restrita com alta evaporação em ambiente árido. É provável que as halitas se depositaram, preferencialmente, na parte central da bacia, enquanto que nas bordas, onde há mais erosão, predominavam anidritas, carbonatos e halitas subordinadas (França *et al.*, 2007). Vieira (1998) individualizou quatro sequências deposicionais correlacionáveis por toda a bacia compondo as sucessões de anidrita, separadas por níveis síltico-argilosos. As sequências são constituídas majoritariamente por anidritas e calcários subordinados nas porções proximais a oeste, e halita nas partes mais centrais da bacia, e representam o registro de pequenas transgressões marinhas.

3.1.1 Caracterização Estrutural e Geomorfológica

A porção proximal da Bacia do Espírito Santo contém as seguintes feições estruturais: Plataforma Regência, Plataforma São Mateus e Zona de Charneira (Figura 3.2; Vieira, 1998). As plataformas Regência e São Mateus são prolongamentos de altos estruturais do embasamento; ou seja, locais onde o embasamento encontra-se em profundidades relativamente pequenas (menores que 1200 m). Nestas feições, o embasamento é sobreposto diretamente por sedimentos dos estágios sag e margem passiva. As plataformas de embasamento raso são limitadas a leste pela zona de

charneira, definida por falhas normais de orientação N-S a NE-SW, que afetam o embasamento e tem grande rejeito vertical (Vieira, 1998). As falhas da zona de charneira delimitam os meio-grábens e a sucessão sedimentar do estágio rifte. A oeste desta zona, nos meio-grábens da porção offshore, o embasamento chega a 11000 m de profundidade (Costa, 1988). Para o norte da bacia, a zona de charneira é desviada para leste por uma zona de falhas de transferência, de orientação NE-SW (Figura 3.2; Vieira, 1998).

Na porção proximal da Bacia do Espírito Santo também encontram-se duas importantes feições geomorfológicas, os paleocânions Regência e Fazenda Cedro (Figura 3.2). As erosões que originaram os paleocânions ocorreram durante o final do Albiano – início do Cenomaniano, em resposta a: (i) contínua inclinação da bacia para leste em resposta à subsidência termal e flexura crustal, o que causou o aumento do gradiente de inclinação da rampa carbonática, juntamente com (ii) sucessivas variações no nível relativo do mar (Lindseth e Beraldo, 1985; Vieira, 1998; França et al., 2007). Os paleocânions escavaram sedimentos albianos a neocomianos e localmente, o topo do embasamento cristalino.

3.2 Bacia de Campos

O início da megasequência rifte na Bacia de Campos é caracterizado por intensa atividade vulcânica que originou as rochas basálticas e vulcanoclásticas da Formação Cabiúnas, com idades entre 122 e 134 Ma (Figura 3.3b; Mizusaki *et al.*, 1998). A sequência sedimentar da fase rifte (Neocomiano Superior – Aptiano) compreende os intervalos basal e intermediário do Grupo Lagoa Feia: formações Itabapoana, Atafona e Coqueiros (Winter *et al.*, 2007). A Formação Itabapoana é composta por conglomerados, arenitos e rochas pelíticas depositadas por fan deltas e sistemas fluviais ao longo da falha de borda da bacia (Winter *et al.*, 2007). As formações Coqueiros e Atafona registram sucessões de fácies lacustres, com folhelhos ricos em matéria orgânica que constituem importantes rochas fonte de hidrocarbonetos (Mello *et al.*, 1995). As fácies proximais da Formação Coqueiros incluem rudstones e grainstones, também conhecidos como “coquinas”, e são os principais reservatórios de hidrocarbonetos da megasequência rifte (Guardado *et al.*, 1989).

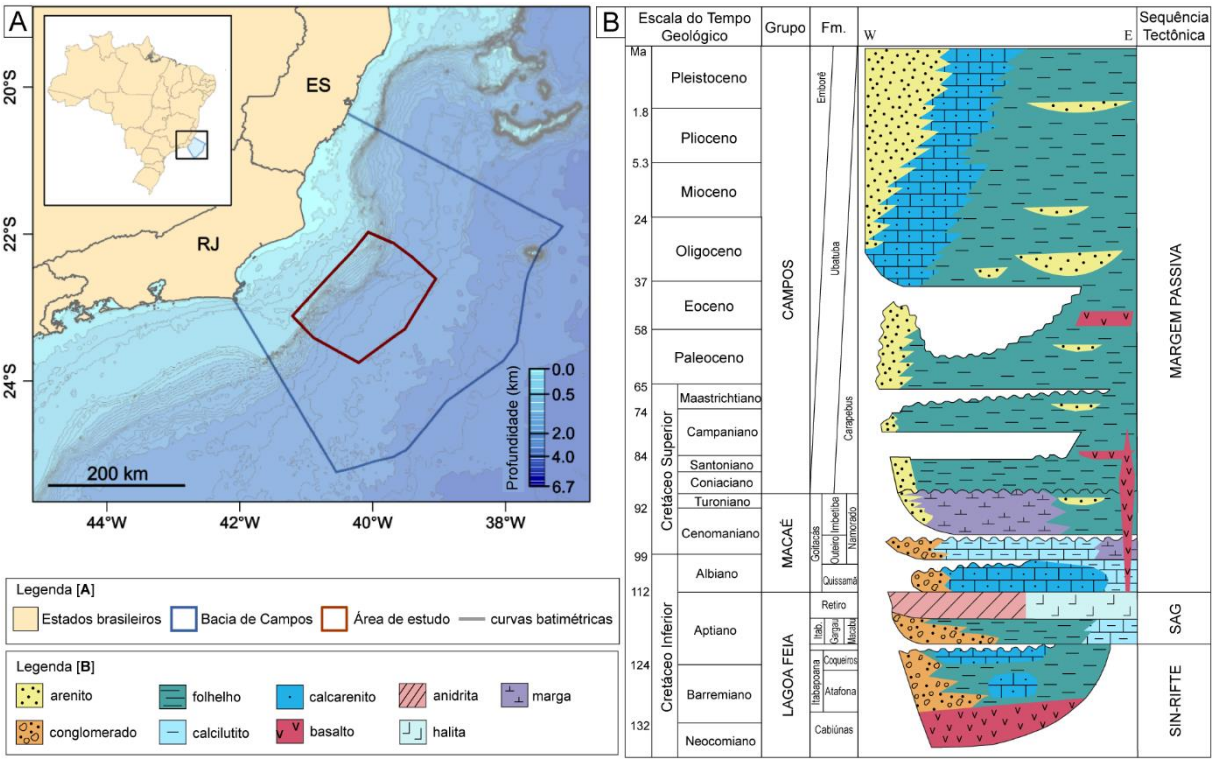

Figura 3.3. (A) Mapa regional mostrando a localização da Bacia de Campos, com o polígono da área de estudos. (B) Carta cronoestratigráfica da Bacia de Campos (redesenhado de Winter *et al.*, 2007).

A megasequência sag (Aptiano) marca a cessação de significativos falhamentos normais envolvendo o embasamento conforme a deformação rúptil foi substituída por deformação predominantemente dúctil, com extensão ativa concentrada na crosta inferior e litosférica mantélica (Karner, 2000; Karner e Gamboa, 2007). A mudança de subsidência diferencial relacionada a falhas para uma subsidência mais ampla e mais uniforme é registrada por uma discordância regional (i.e. a discordância Pré-Alagoas) e por um aumento na área deposicional conforme a sedimentação progressivamente transcendia as calhas rifte (Quirk *et al.*, 2013; Kukla *et al.*, 2018; Amarante *et al.*, 2019). A sucessão sedimentar da fase sag da Bacia de Campos compreende a porção superior do Grupo Lagoa Feia, composta, na base, pelas formações Itabapoana, Gargaú e Macabu, e, no topo, pela Formação Retiro (Figura 3.3b). A Formação Itabapoana representa os depósitos marginais de arenitos e conglomerados, também presentes na megasequência rifte. As formações Gargaú e Macabu são compostas por fácies de sistemas lacustres rasos; a primeira compreende rochas pelíticas, carbonatos, margas e arenitos, que lateralmente se interdigitam com estromatólitos e microbialitos da Formação Macabu (Winter *et al.*, 2007), importantes reservatórios da megasequência sag. A Formação Retiro é caracterizada por espessas sucessões evaporíticas que registram o influxo de água marinha sob clima árido (Winter *et al.*, 2007). O sal predominante nas sequências

evaporíticas é halita maciça, com intercalações com anidrita e sais ricos em potássio (carnalita, silvita e taquidrita) (Mohriak *et al.*, 2008). A Formação Retiro é parte da maior bacia evaporítica da província de sal brasileira, que se estende desde o norte de Santa Catarina até o sul da Bahia, limitada ao norte pela Bacia Jacuípe, um rifte profundo que não secou, e ao sul pelo Alto de Florianópolis (Davison, 2007). Esta extensa bacia de sal foi posteriormente dissecada por altos vulcânicos pós-sal (Sobreira e Szatmari, 2000).

A megasequência margem passiva marca o fim do rifteamento pelo desenvolvimento da dorsal meso-Atlântica e início do efetivo processo de abertura oceânica (Chang *et al.*, 1992). A sedimentação ocorreu em contexto marinho sob configurações de subsidência termal associada com tectonismo adiastrófico (Winter *et al.*, 2007). A megasequência margem passiva (Albiano – Presente) é subdividida em grupos Macaé e Campos (Figura 3.3b), separados por uma discordância regional erosiva de 93 Ma (Guardado *et al.*, 1989).

3.2.1 Caracterização estrutural

A Bacia de Campos apresenta dois contextos tectônicos contrastantes que originaram elementos estruturais distintos, um diastrófico envolvendo o embasamento, e outro adiastrófico relacionado com movimentações halocinéticas dos evaporitos Aptianos (Figura 3.4; Guardado *et al.*, 1989). Estruturas rifte do início do Cretáceo compreendem falhas normais sintéticas e antitéticas, com orientação predominante SW-NE, falhas transformantes e zonas de acomodação; tais estruturas controlam a ocorrência horsts e meio-grábens rifte (Dias *et al.*, 1988). A falha de Campos (Figura 3.4a), com orientação subparalela à margem da bacia, separa a porção oeste mais rasa, onde depósitos Terciários estão diretamente sobre o embasamento, da porção mais profunda a leste, com acumulações sedimentares espessas com idade a partir do início do Cretáceo (Guardado *et al.*, 1989). Dentre os altos e baixos estruturais da Bacia de Campos, as estruturas principais são o Alto de Badejo, o Baixo de Corvina-Parati, os altos Intermediário e Externo e o Baixo Externo (Figura 3.4a; Guardado *et al.*, 2000).

O segundo estilo tectônico é relacionado à halocinese de evaporitos Aptianos em direção ao oceano. Movimentos de sal começaram no Aptiano durante a sua deposição (Cobbold and Szatmari, 1991; Fiduk and Rowan, 2012; Davison *et al.*, 2012), com significativo fluxo de sal até o Maastrichiano (Quirk *et al.*, 2012). Com base nos tipos de estruturas de sal e das rochas sobrejacentes, a Bacia de Campos é

dividida em um domínio extensional proximal (de 70 a 200 km de largura) e um domínio contracional distal (de 70 a 300 km de largura); o último termina com um lençol de sal alóctone (de até 37 km de largura), localizado sobre o Alto Externo do embasamento (Figura 3.4b; Davison, 2007; Davison *et al.*, 2012).

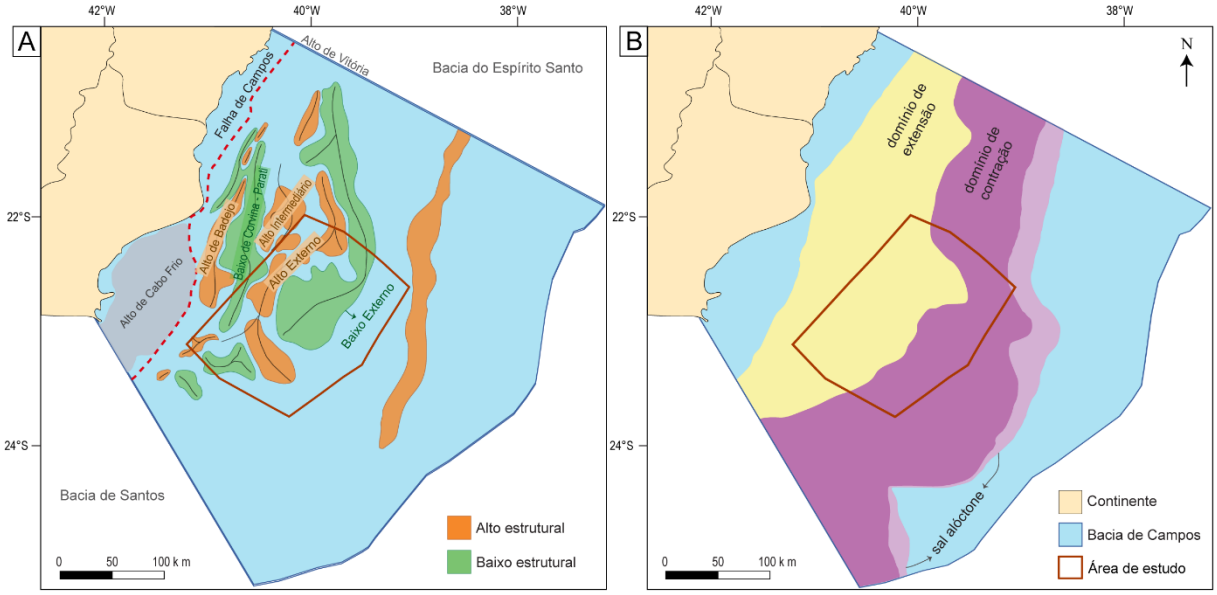

Figura 3.4. (A) Bacia de Campos com a delimitação das estruturas diastróficas relacionadas à fase rifte (modificado de Guardado *et al.*, 2000, com informações adicionais de Fetter, 2009). (B) Bacia de Campos com as províncias relacionadas à tectônica de sal (modificado de Davison *et al.*, 2012).

4 Dados e Métodos

Os dados para o desenvolvimento desta tese provêm da base de dados da ANP (Agência Nacional de Petróleo, Gás Natural e Biocombustíveis). Para o estudo da porção onshore da Bacia do Espírito Santo, foram utilizadas 220 linhas sísmicas 2D, 1 volume sísmico 3D e 103 poços com dados litológicos e geofísicos, cobrindo uma área de ~2300 km² (Figura 4.1). Para o estudo da porção offshore da Bacia de Campos, foram utilizadas 146 linhas sísmicas 2D, 1 volume sísmico 3D e 30 poços com dados litológicos e petrofísicos, cobrindo uma área de ~23500 km² (Figura 4.2). Os dados sísmicos de ambas as áreas de estudos estão em tempo sísmico (*two-way travel time*, TWT, milissegundos, ms), com processamento em fase zero (*zero-phase*), e polaridade segundo o padrão SEG “normal”.

Nos parágrafos seguintes segue-se uma breve descrição de cada etapa metodológica utilizada no desenvolvimento do projeto. Especificidades na metodologia de cada área de estudo (Bacia do Espírito Santo e Bacia de Campos) podem ser encontradas nos itens de Dados e Métodos nos respectivos artigos científicos (páginas 56–60 e 86–89).

Levantamento bibliográfico

Em um primeiro momento fez-se uma revisão bibliográfica voltada, principalmente, para estudos abordando as bacias de margem passiva conjugadas do Atlântico Sul, bem como para outras bacias em um contexto similar em outras localidades. Durante a interpretação dos dados sísmicos, o levantamento bibliográfico voltou-se para conceitos gerais de sísmica, estratigrafia e sedimentologia.

Interpretação sismoestratigráfica

A interpretação sismoestratigráfica iniciou com o carregamento e seleção dos dados (sísmicos e de poços), e delimitação das áreas de estudos. A partir daí fez-se a interpretação sísmica preliminar, onde foram definidos o topo e a base dos intervalos analisados. A interpretação começou nas proximidades dos poços de exploração que apresentam dados litológicos (provenientes da descrição de amostras de calha) e dados de checkshot – correspondência entre o tempo sísmico, ou seja, tempo gasto para a onda sísmica refletir em uma superfície e ser captada por um sensor terrestre, e a profundidade em metros de um poço. Uma vez finalizado o mapeamento regional de topo e base do intervalo de interesse com o auxílio dos poços e de atributos sísmicos, foram definidas unidades estratigráficas-chave com base nos padrões de terminação de refletores. Posteriormente, com o auxílio de atributos sísmicos,

determinaram-se as sismofácies. Para análise tectônica e estratigráfica foram gerados mapas das superfícies mapeadas e mapas de isócronas (mapas de espessura relativa, em tempo sísmico).

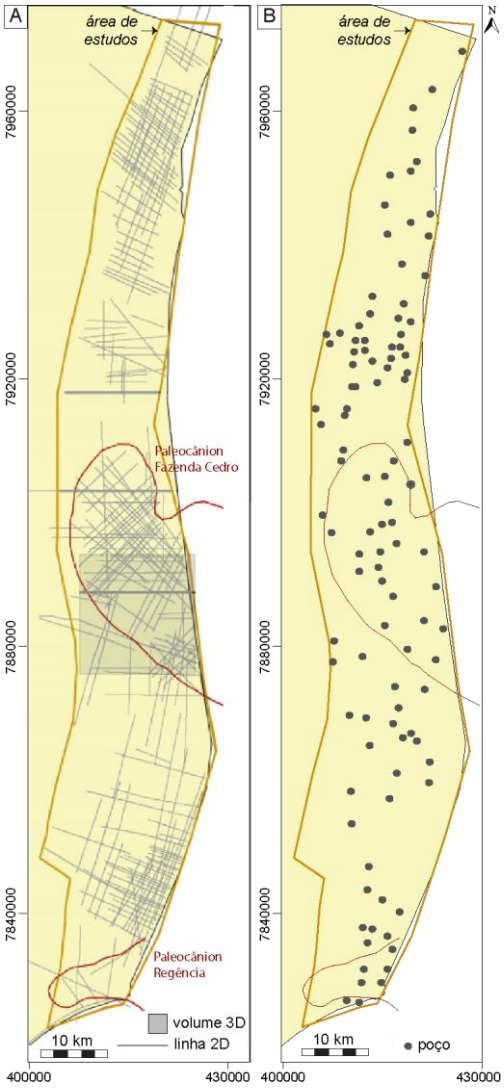

Figura 4.1. Base de dados do estudo da Bacia do Espírito Santo, porção onshore.

Levantamento estratigráfico

Na Bacia do Espírito Santo foi realizado o levantamento estratigráfico para dar suporte e conferir significado estratigráfico às unidades interpretadas na sísmica. A metodologia central envolveu a identificação de unidades estratigráficas genéticas (*sensu* Galloway, 1989) através da análise das curvas de raios-gama dos poços localizados próximos a linhas sísmicas. Adicionalmente, fez-se a análise faciológica de um testemunho, por meio do levantamento de perfis colunares de escala 1:50. Nos perfis colunares são representados o tamanho de grão, espessura e estruturas sedimentares de cada camada, e incluídos os códigos e descrições detalhadas das fácies. A análise faciológica segue os princípios de Walker e James (1992): primeiro são individualizadas as fácies, e estas são agrupadas em associações de fácies e

então em sucessões de fácies; posteriormente, faz-se uma comparação com modelos modernos e antigos para estabelecer sistemas deposicionais, que irão compor os tratos de sistemas deposicionais. A partir da integração das interpretações das curvas de raios-gama e litológicas, foi elaborada uma seção de correlação entre os poços, estabelecendo-se um arcabouço de estratigrafia de alta resolução a partir da correlação regional de superfícies limítrofes e unidades estratigráficas genéticas.

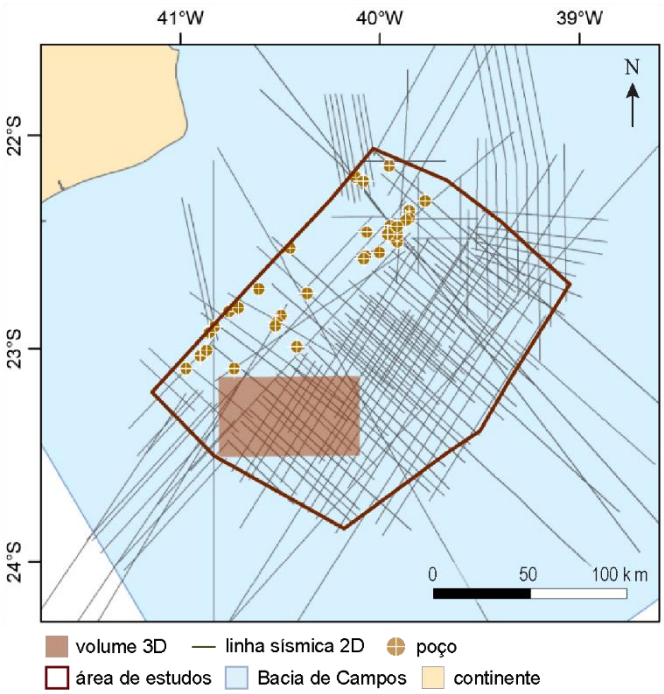

Figura 4.2. Base de dados do estudo da Bacia de Campos, porção centro-sul offshore.

5 Síntese dos principais resultados e discussões

O artigo 1 tem como objetivo principal auxiliar a suprir a prévia ausência de publicações científicas internacionais abordando a evolução geodinâmica do intervalo sag pré-sal da Bacia do Espírito Santo, e suas relações tectônicas e estratigráficas com a configuração rifte anterior. Para tal, desenvolvem-se diferentes questões, ou objetivos específicos. Primeiramente, o artigo 1 apresenta critérios claros para identificar a discordância Pré-Alagoas em dados sísmicos – utilizando o atributo de decomposição espectral de frequência – e, assim, distinguir o Membro Mucuri (fase sag) da Formação Cricaré (fase rifte). Tal distinção era incerta na porção proximal da bacia, tanto em publicações prévias como nos dados de poços adquiridos. Uma vez delimitados base e topo do intervalo, são reconhecidas por interpretação de dados sísmicos, curvas de raios-gama de poços e dados litológicos, quatro sequências estratigráficas genéticas (MUC1 a MUC4), delimitadas por superfícies de máxima inundação lacustres, então mapeadas em toda a área de estudos. O mapeamento das superfícies de máxima inundação revelam um progressivo aumento da área deposicional da base para o topo. A análise tectônica fez-se com o mapeamento das principais estruturas que afetam a sedimentação. Como resultado, foram identificados e caracterizados dois domínios estruturais: a norte, falhas menores e altos do embasamento, e a sul, falhas mais amplas e de maior rejeito, que definem meio-grábens na fase rifte. Em ambos os domínios o falhamento estava inativo durante a deposição do Membro Mucuri.

Unindo dados tectônicos e estratigráficos observamos que tanto o nível de base como o paleorelevo herdado da fase rifte controlaram a distribuição sedimentar do Membro Mucuri. Nas unidades basais, MUC1 e MUC2, o fator controlador dominante é o paleorelevo, e a sedimentação é confinada às calhas herdadas da fase rifte. Nas unidades superiores, MUC3 e MUC4, a sedimentação gradualmente transcende as calhas rifte, se espalhando por grande parte da área de estudos conforme tem-se subida do nível de base lacustre. A unidade de topo, MUC4, já foi depositada sobre uma superfície suave peneplanizada, indicando preenchimento da topografia sin-rifte. É importante ressaltar que não foram reconhecidas discordâncias internas no Membro Mucuri.

O artigo 2 tem como principal objetivo caracterizar os estilos estruturais relacionados à tectônica do sal, sua evolução ao longo do tempo e espaço, e os principais controladores da deformação. O artigo questiona a acuracidade dos

modelos clássicos de interpretação de tectônica do sal em margem passiva, os quais descrevem um domínio extensional proximal e um domínio contracional distal, separados por uma zona de translação, com pouca ou nenhuma deformação. A metodologia compreende mapeamento de 4 a 6 horizontes-chave por análise sismoestratigráfica (com o auxílio de poços): base e topo do sal, topo do Cretáceo e topo do Paleógeno em toda a área de estudos, e o topo do Albiano e o topo do substrato oceânico localmente em linhas-chave. A superfície de base do sal mergulha regionalmente ~2° para SE; mudanças na direção e ângulo de mergulho definem rampas do embasamento. Tais rampas representam o limite entre o Alto Externo e o Baixo Externo, estruturas do embasamento geradas pela tectônica rifte anterior. A interpretação do estilo e distribuição das estruturas de sal e do sedimento sobrejacente relacionadas resultou na definição de três domínios de deformação halocinética: domínio extensional proximal, subdividido em E1 e E2 de acordo com os tipos de estruturas extensionais, domínio contracional distal, e domínio multifásico intermediário. Este último contém estruturas com múltiplas fases de deformação, cinematicamente variáveis (extensional/ contracional).

Nas discussões, o artigo explora como o relevo da base do sal, relevo este herdado da fase rifte, causa variações locais na velocidade de fluxo do sal, afetando os domínios regionais de deformação e controlando/influenciando os tipos de estruturas geradas no sal e sedimento sobrejacente, bem como sua evolução no tempo e espaço. A principal consequência das variações locais na deformação, é que na Bacia de Campos o que separa os domínios extesional e contracional é um domínio com deformação intensa e complexa, com desenvolvimento híbrido extensional/ contracional. A morfologia do relevo herdado da fase rifte também influencia os tipos de estruturas geradas dentro de cada domínio, gerando subdomínios E1 e E2 dentro do domínio extensional, possibilitando o desenvolvimento de uma ampla *ramp syncline basin* a norte do domínio multifásico, e a presença de uma extensa estrutura anticlinal entre as paredes de sal no domínio contracional. Concluímos que os modelos clássicos de interpretação de tectônica do sal em margens passivas são muito simplificados e não representam a diversidade de estruturas interpretadas na Bacia de Campos. Isso porque tais modelos consideram um relevo de base do sal suave, o que não acontece em bacias de sal pós-rifte como na Bacia de Campos.

Ambos os artigos 1 e 2 demonstram a influência do morfologia da sequência tectono-estratigráfica rifte nas sequências posteriores – sag e margem passiva. No artigo 1 vemos como o relevo relicto controla a sedimentação das primeiras

sequências do estágio Sag em porções proximais da Bacia do Espírito Santo. O artigo 2 demonstra como as estruturas rifte herdadas impactam a tectônica do sal (sequência sag), e, consequentemente, a sedimentação e tectônica da sequência margem passiva posterior.

6 Considerações Finais

Através de dados sísmicos 2D e 3D, e dados petrofísicos e litológicos de poços, esta tese analisa o impacto da morfologia rifte nos estágios sag e margem passiva nas bacias de Campos e Espírito Santo. As principais conclusões são listadas a seguir.

- O estágio sag pré-sal proximal detalhado na porção onshore da Bacia do Espírito Santo é composto por quatro sequências estratigráficas genéticas (MUC 1 a MUC 4), delimitadas por três superfícies de inundação máxima lacustre. Da base para o topo, as unidades registram um aumento da área deposicional, de forma que as unidades MUC1 e MUC2 basais são controladas e confinadas às calhas rifte, e as unidades MUC3 e MUC4 de topo transcendem as calhas e ocupam áreas maiores. As falhas normais que originam e delimitam as calhas do estágio rifte estavam inativas durante a deposição do sag.
- O estudo da Bacia do Espírito Santo mostra que em porções proximais a morfologia rifte controla a área deposicional da sedimentação sag, que se dá sob um contexto de quiescência tectônica, i.e. sem movimentação de falhas.
- Na Bacia de Campos, foram identificados três domínios de deformação halocinética com base nas estruturas de sal e do sedimento sobrejacente relacionadas: extensional proximal (dividido em dois subdomínios, E1 e E2), multifásico intermediário e contracional distal. O domínio multifásico é composto por estruturas híbridas, que registram tanto extensão como contração durante seu desenvolvimento.
- O estudo da Bacia de Campos demonstra como rampas na superfície de base do sal, relacionadas ao estágio rifte, geram zonas locais de deformação contracional ou extensional, que sobrepõe a cinemática deformacional regional descrita para margens passivas. Em outras palavras, a topografia rifte influencia a tectônica do sal, que por sua vez deforma e controla a sedimentação posterior, do estágio margem passiva.

Claro que um projeto pensado para um doutorado raramente é concluído no fim deste doutorado. E é o caso do presente projeto, que compreende um tema de grande abrangência e complexidade, que exige mais do que dois artigos para sua conclusão. Por isso, está em andamento um terceiro manuscrito, que analisa a

interação entre a topografia rifte, a geometria do sag e erosões no contato pré-sal e sal na porção offshore distal da Bacia de Campos. Futuramente, pode-se pensar em um estudo que investigue a região offshore da Bacia do Espírito Santo, buscando as sequências estratigráficas genéticas identificadas no proximal, e observando se a sua relação com as falhas e topografia rifte se mantém. É possível que a relação sag/rifte seja mais complexa, pois pensa-se que as falhas rifte podem estar ativas durante a deposição sag pré-sal na porção distal (e.g. Karner e Gambôa, 2007). Outra proposta futura é um estudo de maior dimensão que integre os dados das bacias do sudeste brasileiro, observando similaridades e diferenças no impacto da topografia rifte nos estágios posteriores nas diferentes bacias.

7 Referências Bibliográficas

Allen, P.A. & Allen, J.R. 2005. *Basin analysis: Principles and application*. United States, Wiley-Blackwell, 562 p.

Amarante, F.B.d., Kuchle, J., Iacopini, D., Scherer, C.M.d.S., Alvarenga, R. dos S., Ene, P.L. & Schilling, A.B. 2020. Seismic tectono-stratigraphic analysis of the Aptian pre-salt marginal system of Espírito Santo Basin, Brazil. *Journal of South American Earth Sciences* 98: 102474.

Bohacs, K.M., Carroll, A.R., Nede, J.E. & Mankirowicz, P.J. 2000. Lake-basin type, source potential, and hydrocarbon character: an integrated sequence-stratigraphic-geochemical framework. *In*: Gierlowski-Kordesch, E.H., Kelts, K.R. (Ed.) *Lake Basins through Space and Time*. AAPG Studies in Geology, 46: 3-33.

Bosence, D.W.J. 1998. Stratigraphic and sedimentological models of rift basins. *In*: Purser, B.H.; Bosence, D.W.J (Ed.). *Sedimentation and Tectonics of Rift Basins: Red Sea, Gulf of Aden*. London, Chapman and Hall, 9-25.

Brun, J.-P. & Fort, X. 2004. Compressional salt tectonics (Angolan margin). *Tectonophysics,* 382: 129-150.

Brun, J.-P. & Fort, X. 2011. Salt tectonics at passive margins: Geology versus models. *Marine and Petroleum Geology,* 28: 1123-1145.

Ceraldi, T.S. & Green, D. 2016. Evolution of the South Atlantic lacustrine deposits in response to Early Cretaceous rifting, subsidence and lake hydrology. *In*: Ceraldi, T.S., Hodgkinson, R.A., Backe, G. (Ed.). *Petroleum Geoscience of the West Africa Margin*. Geological Society, London, Special Publications, 438.

Chang, H.K., Kowsmann, R.O., Figueiredo, A.M.F. & Bender, A. 1992. Tectonics and stratigraphy of the East Brazil rift system: an overview. *Tectonophysics,* 213: 97-138.

Cobbold, P.R. & Szatmari, P. 1991. Radial gravitational gliding on passive margins. *Tectonophysics,* 188: 249-289.

Costa, L.A.R. 1988. *Evolução Termomecânica da Bacia do Espírito Santo*. Ouro Preto, 144p. Dissertação de Mestrado. Universidade Federal de Ouro Preto.

Davison, I., Anderson, L. & Nuttall, P. 2012. Salt deposition, loading and gravity drainage in the Campos and Santos salt basins. *Geological Society*, London, Special Publications, 363: 159-174.

Dias, J.L., Oliveira, J.Q. & Vieira, J.C. 1988. Sedimentological and stratigraphyc analysis of the Lagoa Feia Formation, rift phase of Campos Basin, offshore Brazil. *Revista Brasileira de Geociências,* 18(3): 252-260.

Dias, J.L. 2005. Tectônica, estratigrafia e sedimentação no Andar Aptiano da margem leste brasileira. *Boletim de Geociências da Petrobras*, 13: 7-25.

Dooley, T.P., Hudec, M.R., Carruthers, D., Jackson, M.P.A. & Luo, G. 2017. The effects of base-salt relief on salt flow and suprasalt deformation patterns — Part 1: Flow across simple steps in the base of salt. *Interpretation* 5: SD1-SD23.

Evans, S.L. & Jackson, C.A.L. 2019. Base-salt relief controls salt-related deformation in the Outer Kwanza Basin, offshore Angola. *Basin Research,* 32: 668-687.

Fetter, M. 2009. The role of basement tectonic reactivation on the structural evolution of Campos Basin, offshore Brazil: Evidence from 3D seismic analysis and section restoration. *Marine and Petroleum Geology,* 26: 873-886.

Fiduk, J.C. & Rowan, M.G. 2012. Analysis of folding and deformation within layered evaporites in Blocks BM-S-8 & -9, Santos Basin, Brazil. *Geological Society*, London, Special Publications, 363: 471-487.

Fort, X., Brun, J.-P. & Chauvel, F. 2004. Salt tectonics on the Angolan margin, synsedimentary deformation processes. *AAPG Bulletin,* 88: 1523-1544.

França, R.L., Del Rey, A.C., Tagliari, C.V., Brandão, J.R. & Fontanelli, P.R. 2007. Bacia do Espírito Santo. *Boletim de Geociências da Petrobras,* 15(2): 501-509.

Gabrielsen, R.H., Kyrkjebø, R., Faleide, J.I., Fjeldskaar, W. & Kjennerud, T. 2001. The Cretaceous post-rift basin configuration of the norther North Sea. *Petroleum Geoscience,* 7: 137-154.

Galloway, W.E. 1989. Genetic stratigraphic sequences in basin analysi I: Architecture and genesis of flooding-surface bounded depositional units. *AAPG Bulletin*, 73: 125-142.

Gaullier V., Brun J.P., Guerin, G. & Lacanu, H. 1993. Raft tectonics: the effects of residual topography below a salt decollement. *Tectonophysics,* 228: 363-381.

Guardado, L.R., Gamboa, L.A.P. & Lucchesi, C.F. 1989. Petroleum geology of Campos Basin, Brazil: a model for producing Atlantic type basin. *In*: Edwards, J.D., Santagrossi, P.A. (Ed.). *Divergent/Passive Margins Basins*. AAPG Memoir, 48: 3-36.

Guardado, L.R., Spadini, A.R., Brandão, J.S.L. & Mello, M.R. 2000. Petroleum system of the Campos Basin, Brazil. *In*: Mello, M.R., Katz, B.J. (Ed.). *Petroleum Systems of South Atlantic Margins*. AAPG Memoir, 73: 317-324.

Hawkesworth, C.J. 1992. Paraná magmatism and the opening of the South Atlantic. *In*: Storey, B.C. (Ed.). *Magmatism and the Causes of Continental Break-up*. Geological Society, London, Special Publications, 68: 293-302.

Hudec, M.R. & Jackson, M.P. 2004. Regional restoration across the Kwanza Basin, Angola: Salt tectonics triggered by repeated uplift of a metastable passive margin. *AAPG bulletin,* 88(7): 971-990.

Hudec, M. & Jackson, M. 2007. Terra Infirma: understanding Salt Tectonics. *Earth-Science Reviews,* 82: 1-28.

Jackson, C.A.-L., Jackson, M.P.A. & Hudec, M.R. 2015. Understanding the kinematics of salt-bearing passive margins: A critical test of competing hypotheses for the origin of the Albian Gap, Santos Basin, offshore Brazil. *Geological Society of America Bulletin*, 127: 1730-1751.

Karner, G.D. 2000. Rifts of the Campos and Santos basins, southeastern Brazil: distribution and timing. *In*: Mello, M.R., Katz, B.J. (Ed.). *Petroleum Systems of South Atlantic Margins*. AAPG Memoir 73. AAPG, Tulsa, Oklahoma, USA: 301-316.

Karner, G.D. & Driscoll, N.W. 1999. Tectonic and stratigraphic development of the West African and eastern Brazilian margins; insights from quantitative basin modelling. *In*: Cameron, N.R., Bate, R.H. & Clure, V.S. (Ed.). *The Oil and Gas Habitats of the South Atlantic*. Geological Society, London, Special Publications, 153: 11-40.

Karner, G.D. & Gamboa, L.A.P. 2007. Timing and origin of the South Atlantic pre-salt sag basins and their capping evaporates. *In*: Schreiber, B.C., Lugli, S. & Bac¸bel, M. (Ed.). *Evaporites Through Space and Time*. Geological Society, London, Special Publications, 285: 15-35.

Kuchle, J. & Scherer, C.M.S. 2010. Sismoestratigrafia de bacias rifte: técnicas, métodos e sua aplicação na Bacia do Recôncavo. *Boletim de Geociências da Petrobrás,* 18(2): 179-206.

Kukla, P.A., Strozyk, F. & Mohriak, W.U. 2018. South Atlantic salt basins – Witnesses of complex passive margin evolution. *Gondwana Research,* 53: 41-57.

Lindseth, R.O., Beraldo, V.L. 1985. A Late Cretaceous Submarine Canyon in Brazil. *In*: Berg, O.R., Woolverton, D.G. (Ed.). *Seismic Stratigraphy II: An Integrated Approach to Hydrocarbon Exploration*. AAPG Memoir, 39p.

Lögering, M., Anka, Z., Autin, J., di Primio, R., Marchal, D., Rodriguez, J. F., Franke, D. & Vallejo, E. 2013. Tectonic evolution of the Colorado Basin, offshore Argentina, inferred from seismo-stratigraphy and depositional rates analysis. *Tectonophysics,* 604: 245-263.

Mello, M.R., Telnaes, N. & Maxwell, J.R. 1995. The hydrocarbon source potential in the Brazilian marginal basins: a geochemical and paleoenvironmental assessment. *In*: Huc, A.Y. (Ed.). *Paleogeography, Paleoclimate and Source Rocks*. Tulsa, AAPG: 233-272.

Mizusaki, A.M.P., Thomaz-Filho, A. & Cesero, P. 1998. Ages of the magmatism and the opening of the South Atlantic Ocean. *Pesquisas,* 25(2): 47-57

Mohriak, W.U., Mello, M.R., Karner, G.D., Dewey, J.F. & Maxwell, J.R. 1989. Structural and stratigraphic evolution of the Campos Basin, offshore Brazil. *In*: Tankard, A.J., Balkwill, H.R. (Ed.). *Extensional Tectonics and Stratigraphy of the North Atlantic Margins*. AAPG Memoir, 46: 577-598.

Mohriak, W.U. 2003. Bacias sedimentares da margem continental Brasileira. *In*: Bizzi, L.A., Schobbenhaus, C., Vidotti, R.M., Gonçalves, J.H. (Ed.). *Geologia, Tectônica e Recursos Minerais do Brasil: textos, mapas & SIG*. Brasilia, Companhia de Pesquisa de Recursos Minerais: 87-165.

Mohriak, W., Nemčok, M. & Enciso, G. 2008. South Atlantic divergent margin evolution: rift-border uplift and salt tectonics in the basins of SE Brazil. *Geological Society*, London, Special Publications, 294: 365-398.

Moreira, J.L.P., Madeira, C.V., Gil, J.A. & Machado, M.A.P. 2007. Bacia de Santos. *Boletim de Geociências da Petrobras*, 15: 531–549.

Morley, C.K. 2002. Evolution of large normal faults: Evidence from sesmic refletion data. *AAPG Bulletin*, 86(6): 961-978.

Peel, F.J. 2014. How do salt withdrawal minibasins form? Insights from forward modelling, and implications for hydrocarbon migration. *Tectonophysics,* 630: 222-235.

Posamentier, H.W. & Vail, P.R. 1988. Eustatic controls on clastic deposition. II - sequence and systems tract models. *In*: Wilgus, C.K., Hastings, B.S., Posamentier, H., Van Wagoner, J., Ross, C.A., Kendall, C.G.St.C. (Ed.). *Sea-level changes - An integrated approach. Society of Economic Paleontologists and Mineralogists*, SEPM Special Publication, 42: 125-154.

Prosser, S. 1993. Rift-related linked depositional systems and their seismic expression. *In*: Williams, G. D.; Dobb, A. (Ed.) *Tectonics and Seismic Sequence Stratigraphy*. Geological Society of London, London, Special Publication, 71: p. 35-66.

Quirk, D.G., Hertle, M., Jeppesen, J.W., Raven, M., Mohriak, W.U., Kann, D.J., Nørgaard, M., Howe, M.J., Hsu, D., Coffey, B. & Mendes, M.P. 2013. Rifting, subsidence and continental break-up above a mantle plume in the central South Atlantic. *Geological Society*, London, Special Publications, 369: 185-214.

Quirk, D.G., Schødt, N., Lassen, B., Ings, S.J., Hsu, D., Hirsch, K.K. & Von Nicolai, C. 2012. Salt tectonics on passive margins: examples from Santos, Campos and Kwanza basins. *Geological Society*, London, Special Publications, 363: 207-244.

Rodriguez, C.R. 2018. *Tectonostratigraphic evolution of a salt giant during passive margin development: Santos Basin, offshore Brazil*. Londres, 316p. Tese de Doutorado, Imperial College London, Londres, Reino Unido.

Rowan, M.G., Peel, F.J. & Vendeville B.C. 2004, Gravity-driven fold belts on passive margins. *In*: McClay, K.K. (Ed.). *Thrust tectonics and hydrocarbon systems.* AAPG Memoir, 82: 157-182.

Rowan, M.G. & Ratliff, R.A. 2012. Cross-section restoration of salt-related deformation: Best practices and potential pitfalls. *Journal of Structural Geology*, 41: 24-37.

Sengor, A.M.C. & Burke, K. 1978. Relative timing of rifting and volcanism on earth and its tectonic implications*. Geophysical Research Letters,* 5: 419-421.

Séranne, M. & Anka, Z. 2005. South Atlantic continental margins of Africa: a comparison of the tectonic vs climate interplay on the evolution of Equatorial West Africa and SW Africa margins. *Journal of African Earth Sciences,* 43: 283-300.

Sobreira, J.F.F. & Szatmari, P. 2000. New Ar-Ar ages for the Abrolhos volcanic rocks, East Brazilian margin. *In*: INTERNATIONAL GEOLOGICAL CONGRESS, 31., 2000, Rio de Janeiro, 31. *Anais*. Rio de Janeiro, IUGS.

Strozyk F., Back, S. & Kukla, P.A. 2016. Comparison of the rift and post-rift architecture of conjugated salt and salt-free basins offshore Brazil and Angola/Namibia, South Atlantic. *Tectonophysics,* 716: 204-224.

Szatmari, P. 2000. Habitat of petroleum along the South Atlantic margins. *In*: Mello, M.R., Katz, B.J. (Ed.). *Petroleum Systems of South Atlantic Margins*. Tulsa, AAPG Memoir, 73: 69-75.

Tadeu dos Reis, A., Gorini, C., Weibull, W., Perovano, R., Mepen, M. & Ferreira, É. 2008. Radial gravitational gliding indicated by subsalt relief and salt-related structures: the example of the Gulf of Lions, western Mediterranean. *Revista Brasileira de Geofísica,* 26(3): 347-365.

Thompson, D.L., Stilwell, J.D. & Hall, M. 2015. Lacustrine carbonate reservoirs from Early Cretaceous rift lakes of Western Gondwana: Pre-Salt coquinas of Brazil and West Africa. *Gondwana Research* 28, 26-51.

Vieira, R.A.B., Mendes, M.P., Vieira, P.E., Costa, L.A.R., Tagliari, C.V., Barcelar, L.A.P. & Feijó, F.J. 1994. Bacia do Espírito Santo e Mucuri. *Boletim de Geociências da Petrobras,* 8(1): 191-202.

Vieira, R.A.B. 1998*. Análise estratigráfica e evolução paleogeográfica da seção Neoaptiana na Porção Sul da Plataforma de São Mateus, Bacia do Espírito*

Santo, Brasil. Porto Alegre, 158p. Dissertação de Mestrado, Programa de Pós-Graduação em Geociências, Universidade Federal do Rio Grande do Sul.

Walker, R.G. & James, N.P. 1992. *Facies Models: response to sea level changes*. Canada, Geological Association of Canada, 407p.

Weijermars, R., Jackson, M.T. & Vendeville, B. 1993. Rheological and tectonic modeling of salt provinces. *Tectonophysics*, 217(1-2): 143-174.

Winter, W.R., Jahnert, R.J. & França, A.B. 2007. Bacia de Campos. *Boletim de Geociências da Petrobras,* 15(2): 511-529.

8 Impacto da Morfologia Rifte na Fase Sag Pré-sal – Bacia do Espírito Santo

A análise do impacto da morfologia herdada da fase rifte na sedimentação e tectônica sag pré-sal está apresentada na forma de um artigo científico, publicado na revista Journal of South American Earth Sciences, volume 98, em março de 2020. Os dados para a pesquisa foram provém da ANP (Agência Nacional do Petróleo, Gás Natural e Biocombustíveis), adquiridos pela UFRGS no Projeto Mucuri (Contrato UFRGS/Feeng/Shell).

8.1 Artigo 1 - Seismic tectono-stratigraphic analysis of the Aptian pre-salt marginal system of Espírito Santo Basin, Brazil

Francyne Bochi do Amarante[1,#], Juliano Kuchle[1], David Iacopini[2,3], Claiton Marlon dos Santos Scherer[1], Renata dos Santos Alvarenga[1], Patrycia Leipnitz Ene[1], André Basso Schilling[1]

[1] Instituto de Geociências, Universidade Federal do Rio Grande do Sul, 9500 Bento Gonçalves Avenue, Building 43137, Agronomia; 91501-970 Porto Alegre, RS, Brazil

[2] School of Geosciences, University of Aberdeen, United Kingdom

[3] Dipartimento di Scienze della Terra, dell'Ambiente e delle Risorse (DiSTAR) Università degli Studi di Napoli Federico II

[#] Corresponding author. Email: francyne.amarante@ufrgs.br

ABSTRACT

The Aptian sedimentary sequence of Mucuri Member, lower Mariricu Formation, constitutes the pre-salt of Espírito Santo Basin. Proximal successions are dominantly clastic consisting of fluvial and coastal sediments deposited within the margins of a wide lake, thus corresponding to the marginal deposits of lacustrine carbonate reservoirs located in distal portions of the basin. Economic interest for oil is centered on such distal reservoirs, thus proximal sections lack detailed studies. The Espírito Santo Basin is located near pre-salt official polygon, with oil exploration active for over six decades. The main objective of this study is the tectono-stratigraphic analysis of the clastic Mucuri Member. Leading methodology is a seismostratigraphic characterization based on 220 2D lines, 1 3D volume, 103 well log data and 1 cored well. Four seismostratigraphic units were identified, delimited by three conformable horizons. Unit-bounding reflectors coincide with gamma ray maxima or minima interpreted to reflect shale or anhydrites deposited in deep water environments, corresponding to lacustrine maximum flooding surfaces. The structural framework is characterized by minor faults in the north onto shallow basement platforms, and in the south by half-graben bounded by normal faults developed during the rift phase. The Mucuri Member records an enlargement in depositional area from its base to top unit witnessing an overall lacustrine base level rise during depositon. The geometry of depositional area was initially influenced by the paleorelief of the preceding rift basins. The seismic units record a decrease in thickness as remnant topography was gradually filled and the upper units – MUC3 and MUC4 – extended beyond the rift boundaries, covering a larger area. The Early Cretaceous Mucuri Member composes the first post-

rift sequence of Espírito Santo Basin marked by the cessation of fault activity and the onset of thermal subsidence.
Keywords: Pre-salt; South Atlantic; SE Brazil; Sag basin; Seismostratigraphy.

1 – Introduction

Sag basins of the south-eastern Brazilian coast are widely known as world-class hydrocarbon reservoirs (Abelha and Petersohn, 2018). Along Brazilian and African margins such sag Aptian sequences of lacustrine clastic and carbonate deposits are named pre-salt, because they precede the extensive evaporitic packages deposited in confined marine basin context. Since the first discoveries of offshore pre-salt hydrocarbon reservoirs in the early 2000's, the rift and sag systems of Brazilian coast have become a target of several research projects. However, there is still a lack of detailed studies regarding the geodynamic evolution of the sag interval and the tectonic and stratigraphic relations with the underlying rift basin. Published works focus on the depositional, diagenetic and geochemical aspects of the distal pre-salt lacustrine carbonate reservoirs (e.g. Muniz and Bosence, 2015; Wright and Barnett, 2015; Herlinger *et al.*, 2017; Pietzsch *et al.*, 2018; Lima and De Ros, 2019) or in the geodynamic aspects related to regional tectonic regime that originated and deformed the Brazilian and correlated African basins (e.g. Karner and Gamboa, 2007; Davison, 2007; Strozyk *et al.*, 2017; Kukla *et al.*, 2018), with only a few studies that detail the stratigraphic filling and paleoenvironmental evolution of the sag interval (e.g. Ceraldi and Green, 2016; Saller *et al.*, 2016).

Main objective of this study is to comprehend the tectono-stratigraphic evolution of the proximal sag basin or succession (Mucuri Member – Espirito Santo Basin) using seismostratigraphic analysis as a main tool. Specific objectives comprise: (i) to establish clear and precise criteria to differentiate the rift (Cricaré Formation) from the sag (Mucuri Member) sequences; (ii) recognition and delimitation of seismostratigraphic units within the sag succession; (iii) to determine of sedimentological and stratigraphic interpretation of the identified seismostratigraphic units from cored wells and gamma ray well log analysis (iv) to map the main sedimentation-controlling structures;

Espírito Santo Basin represents a key area to advance knowledge on the proximal Aptian sedimentary record. Oil exploration in the region is active since the 1950's and it has been highly stimulated during the last twenty years due to recent

discoveries (e.g. Milani *et al.*, 2000; Zalán, 2002). The basin is supported by large seismic reflection data coverage and it is located near the official pre-salt polygon defined by Brazil's National Oil, Natural Gas and Biofuels Agency (ANP).

2 – Geological context

The Espírito Santo Basin is located on the Brazilian central-eastern continental margin (Fig. 8.1A), constituting a part of the major rift basin system that originated from the break-up of Gondwana Supercontinent followed by the opening of the South Atlantic Ocean in the Late Jurassic/Early Cretaceous (Szatmari, 2000). The basin is delimited to the north by the Mucuri Basin and to the south by the Campos Basin by the Vitoria High (Vieira, 1994). The basin area is approximately 41,500 km² – considering the eastern border coincident with the continent-ocean boundary – from which 3,000 km² refer to the terrestrial portion (Fig. 8.1B).

Geodynamic model of South Atlantic is composed of four mega-sequences, which are recognized on both Brazilian and African margins (Cainelli and Mohriak, 1999; Beglinger *et al.*, 2012). During the pre-rift mega-sequence (Late Proterozoic – Jurassic), early subsidence and stretching originated sag basins that together formed a larger basin known as Afro-Brazilian Depression (Chang *et al.*, 1992). Syn-rift mega-sequence (Late Jurassic – Early Cretaceous) is characterized by increasing lithospheric stretching that led to large faults generation, which affected the continental crust and formed half-grabens. Rifting process caused a rotation of the rift blocks by an increase of lithospheric extension. The transitional (or sag) mega-sequence (Aptian – Early Albian) marks the cessation of rifting, crustal stretching and most basement-involved fault activity; erosion of rotated rift blocks originated a regional unconformity that reshaped the topographic level, named "pre-Alagoas unconformity" (Karner *et al.*, 2003). The post-rift (or drift) mega-sequence (Early Albian – Present) is characterized by oceanic accretion and continental drifting that led to the opening of the South Atlantic Ocean; increasing thermal subsidence is due to cooling and contraction of the lithosphere.

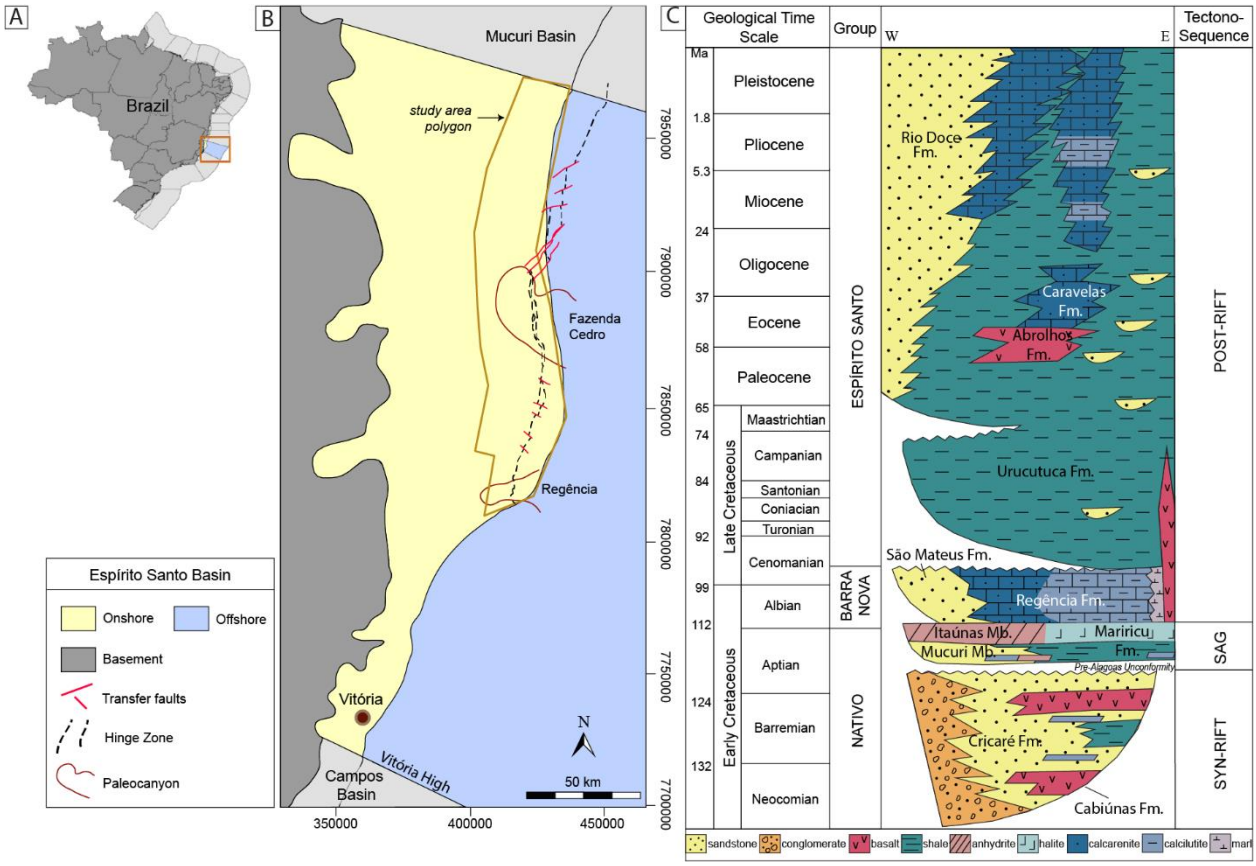

Figure 8.1. (A) Marginal basins of Brazilian east coast, Espírito Santo Basin evidenced by red box; (B) Coastal Espírito Santo Basin with the study polygon, paleocanyons and main structures: transfer faults and Hinge Zone – according to Vieira (1998); (C) Chronostratigraphic chart of Espírito Santo Basin (modified from Mohriak, 2003).

Espírito Santo Basin is composed of the three upper mega-sequences (Mohriak, 2003) (Fig. 8.1C): syn-rift (Valanginian – Early Aptian), transitional or sag (Aptian – Early Albian) and post rift or drift (Albian – Recent). The basement of the basin consists of metamorphosed igneous intrusions and sedimentary successions of the Brasiliano/Pan-African fold belds (Mohriak *et al.*, 2008). Sedimentation in the basin started with the Nativo Group, constituted by the Cricaré and Mariricu formations (Vieira *et al.*, 1994; Mohriak, 2003). The Cricaré Formation (Valanginian – Early Aptian) was deposited in a rift setting, and comprises alluvial and fluvial-lacustrine sediments intercalated with volcanic and volcanoclastic rocks of Cabiúnas Formation (Vieira, 1998; França *et al.*, 2007).

The end of deposition of the syn-rift mega-sequence along the Brazilian central-eastern continental margin basins was marked by the onset of a period of relative tectonic quiescence, registered in the proximal portions by subaerial exposure and erosion of rift shoulders (Dias, 1998). This resulted in the generation of a regional unconformity known as “Pre-Alagoas Unconformity” (Karner *et al.*, 2003) that preceded the deposition of the Mariricu Formation (Fig. 8.1C).

The Mariricu Formation (Aptian – Early Albian) is subdivided into two members, the Mucuri, target unit of this study, and the Itaúnas Member (Fig. 8.1C; Asmus *et al.*, 1971; Mohriak, 2003). The formation unconformably overlies either the basement or the Cricaré Formation. The geodynamic context of Mariricu Formation has been previously interpreted as a sag basin (Beglinger *et al.*, 2012), as it marks the cessation of most basement-involved fault activity and the beginning of thermal subsidence. At this time, sedimentation, initially conditioned by syn-rift inherited topography, transcends the limits of the pre-existing half-grabens, under a period of relative tectonic quiescence with more significant faulting occurring only locally (Dias, 2004). In previous studies, the mega-sequence composed of the Mariricu Formation has been interpreted as transitional because the formation accumulated in an environmental setting between continental rifting and the development of a marine passive margin (Vieira *et al.*, 1994; Cainelli and Mohriak, 1999). The upper contact of Mariricu Formation is conformable with the Barra Nova Group and unconformable against the Urucutuca Formation in the vicinities of Upper Cretaceous paleocanyons (Mohriak, 2003).

The Mucuri Member is composed of arkosic to lithic sandstone and conglomerate, intercalated with shale, siltstone and evaporitic levels of anhydrite and halite mixed with shale laminae (Vieira *et al.*, 1994). Thickness reaches 2000 m towards the basin depocenter, however, it is highly variable due to the rift remnant topography (França *et al.*, 2007). The Itaúnas Member, the upper unit of Mariricu Formation (Fig. 8.1C), consists of thick evaporitic successions dominantly composed of halite and anhydrite, with minor mudstone, sandstone and limestone (Vieira, 1998). Thickness is highly variable, from 50 m on the continent to 2000 m offshore (França and Tschiedel, 2006; Karner and Gamboa, 2007). The deposition of the large evaporitic successions is interpreted as a result of marine-water influx by episodic transgressions across the volcanic system Walvis Ridge/Rio Grande Rise, a physiographic barrier located offshore Angola/South Brazil that isolated the basin from open ocean to the south (Szatmari, 2000).

The drift mega-sequence (Albian – Recent) reflects the onset of an oceanic crust spreading ridge between the South American and African tectonic plates, and the subsequent opening of the South Atlantic Ocean. In the Espírito Santo Basin, the sedimentation in drift context commenced with the Barra Nova Group (Albian) that includes shallow water platform limestones of the Regência Formation and sandstones

to conglomerates of the São Mateus Formation (Fig. 8.1C), recording a shallow marine environment with epicontinental characteristics (Mohriak, 2003; França *et al.*, 2007).

The continuous eastward tilting of the carbonate platform due to thermal subsidence and crustal flexure gradually increased the ramp gradient. This resulted in a major unconformity by the end of Albian, responsible for developing the Regência and Fazenda Cedro submarine canyons that are located onshore and extend to the shallow marine portion of the basin (Fig. 8.1B) (Lindseth and Beraldo, 1985; França *et al.*, 2007). With the onset of a transgressive event in Cenomanian to Early Eocene times, the restricted marine sequence drowned and was covered by the siliciclastic open marine sequence (Cainelli and Mohriak, 1999) of the Espírito Santo Group (Fig. 8.1C). A retrograding interval of the group is recorded in the Urucutuca Formation (Cenomanian – Recent), composed of turbidites concentrated in the Regência and Fazenda Cedro paleocanyons, and more pelitic clastic sediments to the west. During the Paleogene, the Espírito Santo Basin underwent a distinct tectonic phase that caused sea-level fall and deposition of prograding deltaic and platform limestones of Rio Doce and Caravelas formations (Eocene – Recent) (Mohriak, 2003; França *et al.*, 2007).

3 – Data and methodology

The database for this study includes 220 2D seismic lines, 1 3D seismic volume and 103 wells in the onshore Espírito Santo state eastern region, covering an area of approximately 2300 km² (Fig. 8.2). The seismic lines include seven different surveys acquired from the year of 1970 to 1992; final migrated data were loaded as available in the Brazilian National Agency of Petroleum, Natural Gas and Biofuels (ANP) platform, with no reprocessing. All lines are set in zero phase, in American polarity (SEG convention), with no time to depth conversion.

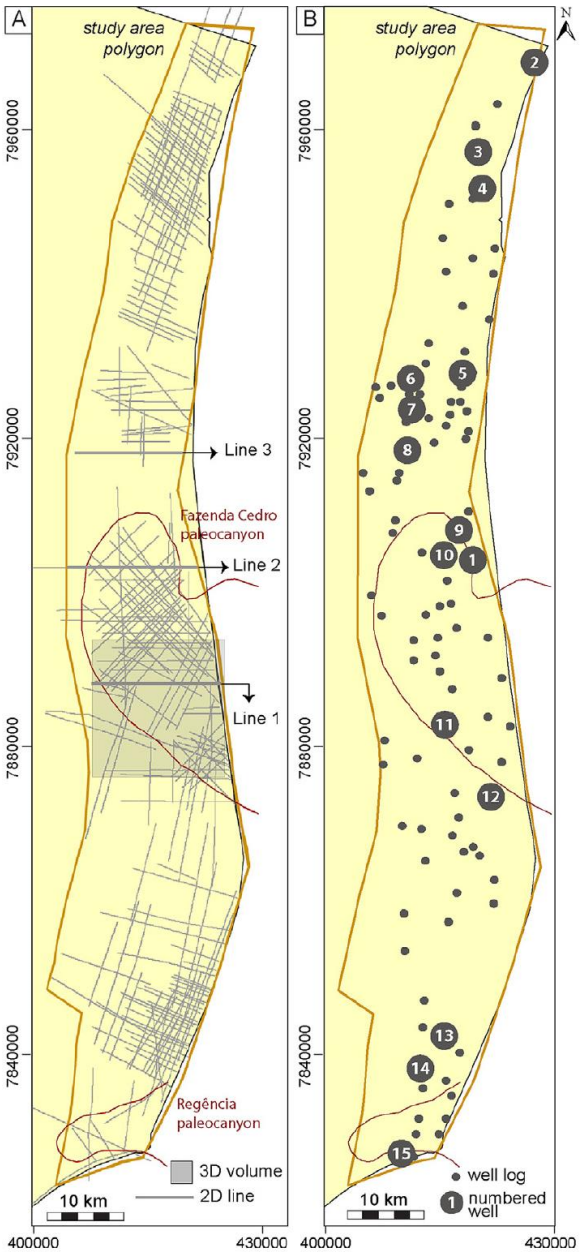

Figure 8.2. (A) Location of the used 2D seismic lines and 3D seismic volume; (B) Location of well-logs from the database. Nomenclature of named data (ex.: 'Line 1') is used throughout the article.

Lack of reliable checkshot data for the wells leads to an interpretative connection between well depth and seismic time. Wells were tied to seismic lines by two methods: (1) the peaks and troughs of the seismic wavelets of the relative acoustic impedance (RAI) attribute were correlated to the peaks and troughs of the sonic log curves (DT – delta time transit log). (2) In the absence of both sonic and density logs, Mucuri Member top and base surfaces of the well logs were visually connected to preliminary interpreted horizons in seismic lines. For this procedure, the base of evaporites was chosen as a main reference surface marking the first strongly continuous reflector with high amplitude (a result of elevated velocity-density contrast; Mitchum *et al.*, 1977), as evidenced by RAI and Root Mean Square (RMS) amplitude

seismic attributes. Hence, the base of salt is an easily recognizable and traceable surface. After setting well-to-seismic ties, systematic seismic mapping of the Mucuri Member was performed on all loaded lines.

Both literature reviews and well log analysis revealed uncertainties regarding the position of the lower contact of the Mucuri Member, especially when observed against the syn-rift Cricaré Formation. To solve the problem, we first identified rift basins by mapping major faults that delimit half-grabens using the cosine of phase seismic attribute. Then, we fine-tuned the positioning of the unconformity between both units (Pre-Alagoas Unconformity; Karner *et al.*, 2003) by applying a structurally-oriented filtering for noise suppression and then a frequency spectral decomposition attribute on a 3D seismic volume. We created an RGB blend volume by assigning the red, green and blue colors to three main frequencies of 10, 20 and 40 Hz (Fig. 8.3). The spectral decomposition was applied using the continuous-wavelet transform methodology of Chopra and Marfurt (2007).

We selected eight key seismic lines for seismostratigraphic interpretation to represent the main sedimentary features and depositional patterns within the study area. The interpretation followed the methodology developed by Vail *et al.* (1977) and Neal and Abreu (2009), starting with the interpretation of reflectors and their main terminations, which are onlap, downlap, toplap or erosional truncation.

The low-resolution of seismic lines and irregular spacing and coverage prevented a study-area wide mapping of seismic facies. However, the selected seismic lines allowed the identification of reflection pattern combinations from the association of reflection amplitude, continuity and frequency, with external geometry signature and spatial relations which permitted the interpretation of facies from the seismic record (Brown and Fisher, 1977).

Sets of reflector terminations along a horizon outline the bounding surfaces of stratigraphic units, which correspond to chronostratigraphically related strata (Brown and Fisher, 1977). Then, stacking of the units according to their relative age defines spatio-temporal charts for the purpose of interpreting the controls on the stratigraphic evolution of the basin.

The identified seismostratigraphic units were systematically mapped throughout the study area, enabling the generation of isochron and isopach maps for each interval in two-way travel time (TWT) milliseconds (ms). These maps document relative thickness variations.

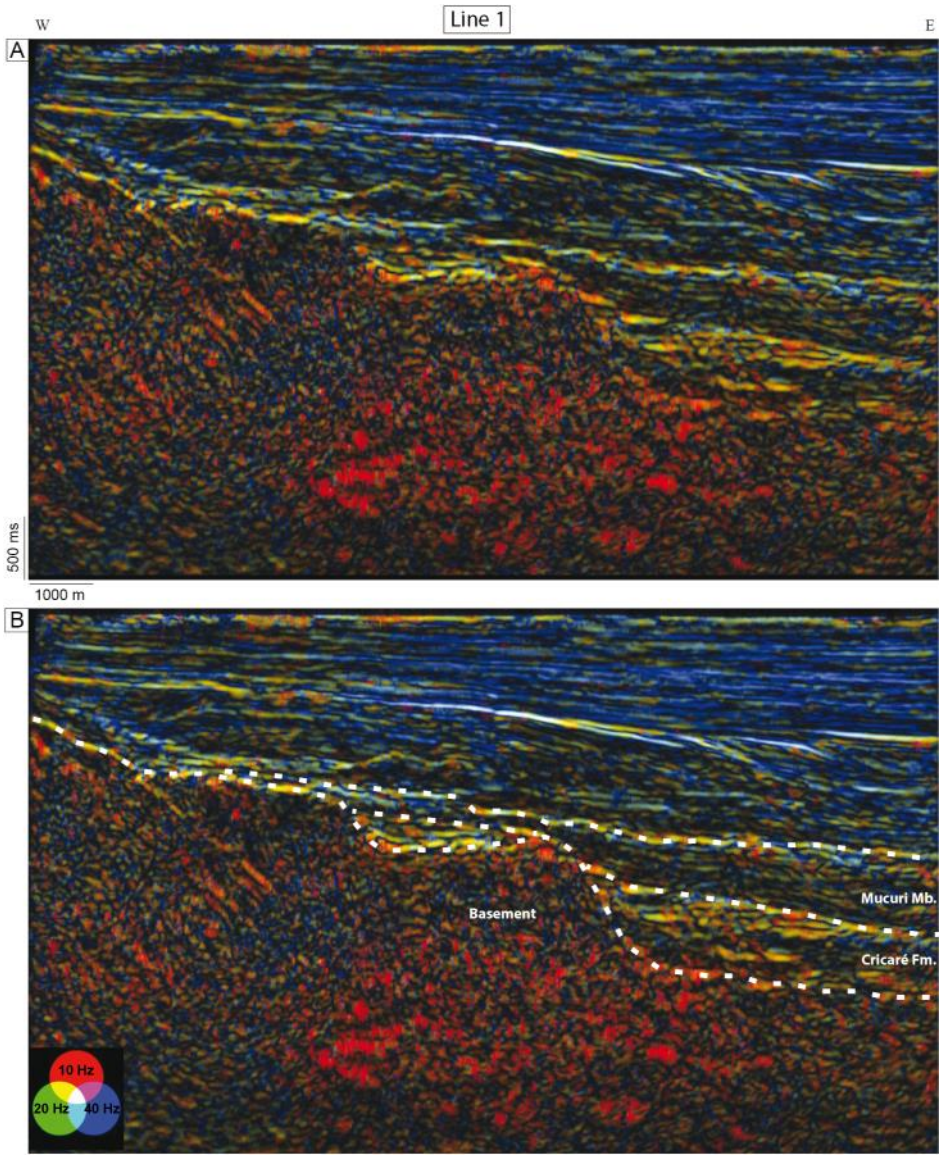

Figure 8.3. Line 1 with frequency spectral decomposition attribute, obtained and represented through a volume color blend for different frequencies (red: 10 Hz; green: 20 Hz; blue: 40 Hz). (A) Not interpreted; (B) Interpreted line, with depositional limits individualizing the basement, Cricaré Formation and Mucuri Member highlighted in white dotted line.

To designate a stratigraphic meaning for the identified units, gamma ray curves of well logs (positioned within 1000 m of proximity to a seismic line) were plotted on each seismic line. Description and interpretation of one cored well (well 6 – Fig. 8.2) were also performed to support an interpretation for the identified seismic units. The cored well detailing totalized 154 m of vertical section in a 1:50 scale. Lithofacies were classified according to grain-size and structures (*sensu* Miall, 1977) and grouped in facies associations. After defining a connection between the well and seismic data, a correlation section of the well logs was constructed.

Structural interpretation of the seismic dataset started with the identification of half-grabens. Subsequent mapping targeted the most relevant structures by observing abrupt terminations across the main horizons – the top and the base of Mucuri

Member. The delineation on 2D lines was guided by cosine of phase seismic attribute and by constantly crosschecking the interpretation on 3D maps.

4 – Results

4.1. Systematic seismic mapping of Mucuri Member

Mucuri Member is observed either overlying the syn-rift sedimentary-volcanic sequence of Cricaré Formation in rift troughs or the basement. Positioning the unconformity that delimits the rift-sag boundary is complex, because the unconformity presents neither pronounced angular contacts nor numerous reflection terminations. The usage of a frequency spectral decomposition attribute helped us to elucidate the Mucuri Member – Cricaré Formation contact and enhanced the top of the basement (Fig. 8.3).

The RGB color blend of the frequency spectral decomposition attribute is shown in Figure 8.3. Red, green and blue were assigned to different frequencies (10, 20 and 40 Hz) – the white color represents reflections where all frequencies contribute equally. Frequency decrease with depth is not constant, but there are intervals of frequency patterns separated by marked levels. Each level corresponds to a boundary between distinct geological units. Results regarding the interval of interest are: (1) the basement is dominated by red color, pointing to lower frequencies (10 Hz); (2) the Cricaré Formation has frequency variation dominantly from 10 to 20 Hz, predominating greenish to reddish colors; (3) the Mucuri Member attests a frequency increase from 20 to 40 Hz, characterized by blueish to greenish colors.

The Mucuri Member underlies the evaporitic sequence of Itaúnas Member (Fig. 8.1C) in most mapped seismic lines. Exceptions occur in the vicinity of Fazenda Cedro and Regência paleocanyons, where erosive truncation reflection terminations define the upper contact with the Urucutuca Formation; also, in the southern region between the paleocanyons, the Mucuri Member directly underlies either Regência or São Mateus formations. Main upper and lower boundary relations and the general geometry of the Mucuri Member cross-cut by the Fazenda Cedro paleocanyon are displayed in Figure 8.4.

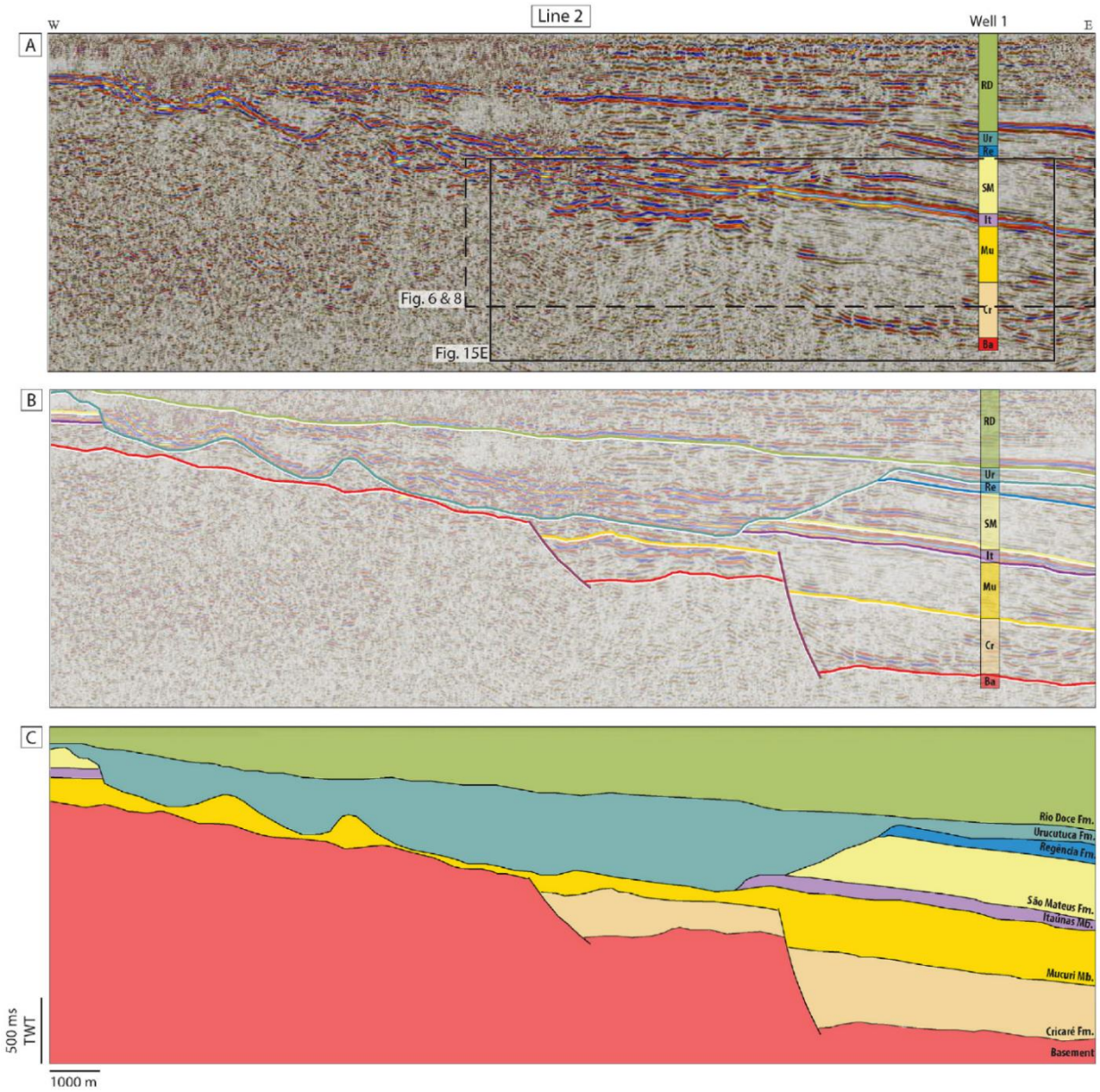

Figure 8.4. (A) Non-interpreted seismic line 2 with lithology column of well 1; (B) Interpreted horizons delimiting stratigraphic units in seismic line 2; (C) Interpreted stratigraphic units.

Systematic mapping of Mucuri Member in 220 2D seismic lines resulted in two time-structural maps of basal and top surfaces (Fig. 8.5 A, B), and one isopach map (Fig. 8.5C). The Mucuri Member base varies between 450 and 2800 ms (TWT), and the top between 350 and 2300 ms (TWT). Both stratigraphic surfaces dip to the east, the top showing a gradual increase in depth from west to east (Fig. 8.5B), differing from the base, which shows an abrupt eastward deepening around longitude 410000 and 418000 m E (Fig. 8.5A). Isopach map presents a relative TWT thickness of 20 and 500 ms, locally reaching 650 ms, showing localized erosion within Fazenda Cedro and Regência paleocanyons where the Mucuri Member may be absent due erosion. The isochron map shows a general thickening to the east, and the Mucuri Member is thinner in the north than in the central and southern parts of the study area.

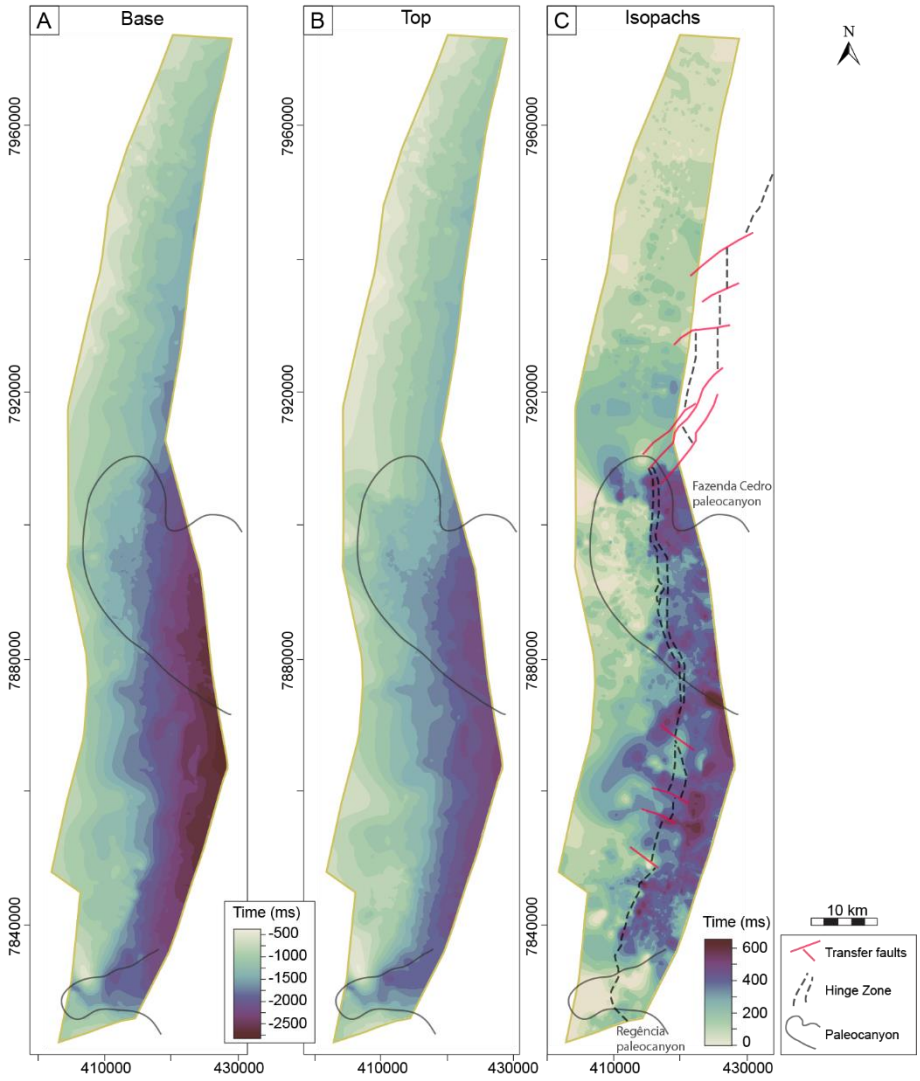

Figure 8.5. Surface map of Mucuri Member: (A) base and (B) top horizons; (C) Isopach map of the Mucuri Member.

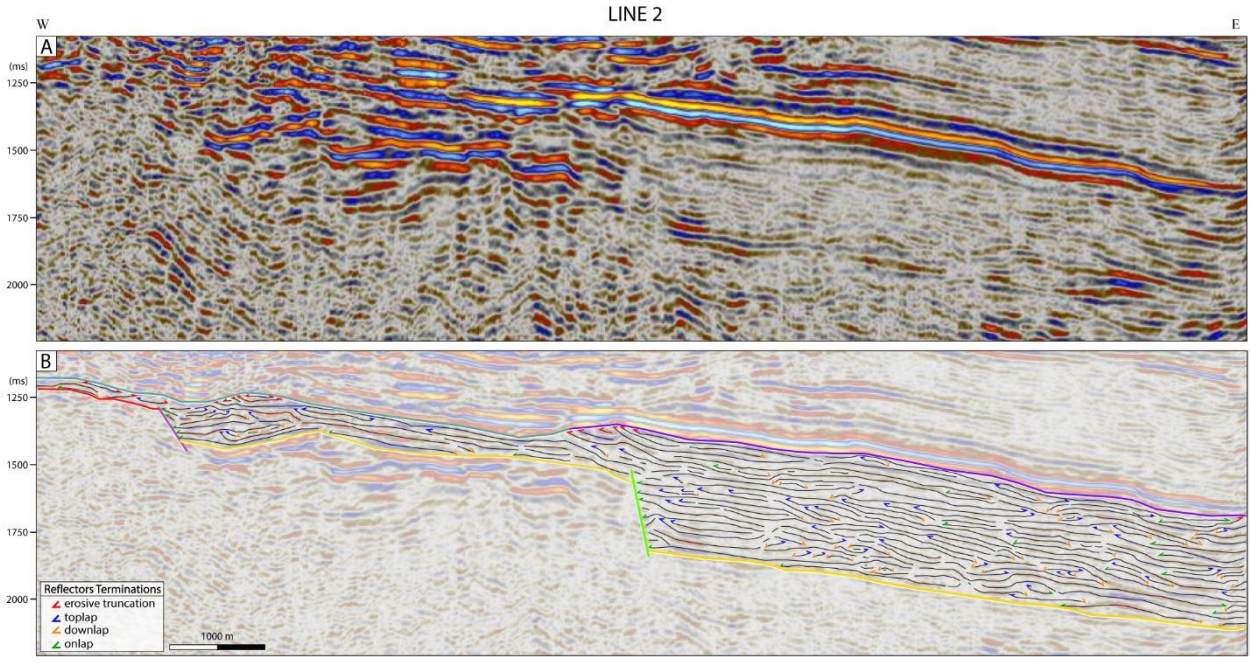

Figure 8.6. (A) Non-interpreted seismic line 2; (B) Reflection interpretation of line 2, with the top and base horizons and main faults.

4.2. Reflection interpretation

The reflectors within Mucuri Member show low to medium amplitudes, with continuous and discontinuous, parallel to wavy and discontinuous mounded configurations (Fig. 8.6). The internal geometry is composed of non-sequential termination patterns, evidencing a complex seismic facies arrangement.

The external geometry of reflector terminations outlines an overall onlap pattern to the west against either the basement or the volcano-sedimentary succession of the Cricaré Formation. There are no major erosive truncations in the Mucuri Member, indicating lack of regional unconformities on a reflection seismic scale.

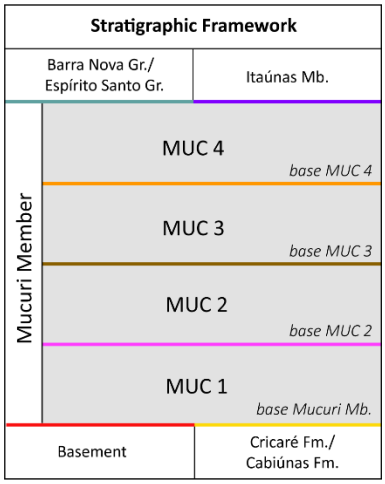

Figure 8.7. Stratigraphic framework of the Mucuri Member, with the identified seismostratigraphic units and the main horizons colored according to its designated colors.

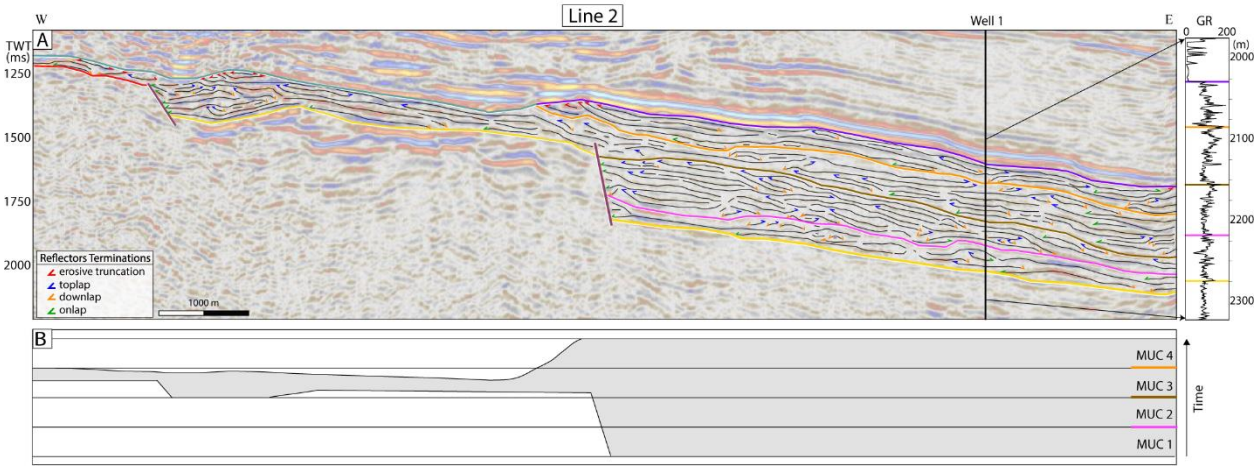

Figure 8.8. (A) Seismostratigraphic interpretation of line 2, with reflections interpretations, identified unit-bounding reflectors (colored according to Figure 8.7), location of well-log 1 and gamma ray curve; (B) Spatio-temporal chart of the seismic units according to their relative temporal position.

4.3. Seismostratigraphic units

The interpretation of reflectors and terminations along the selected seismic lines resulted in the establishment of three bounding reflection surfaces delimiting four seismostratigraphic units, defining the internal stratigraphic framework of the Mucuri Member (Fig. 8.7).

Seismostratigraphic units are named MUC1 to MUC4 from the base upwards, and are delimited at their bases by concordant reflectors and reflector terminations in onlap and downlap (Figs. 8.8, 8.9). The top of each unit is characterized by terminations in toplap or concordant reflectors (Figs. 8.8, 8.9), indicating a lack of internal unconformities within the Mucuri Member, also shown by the spatio-temporal chart (Fig. 8.8B). Besides the major erosive structures related to paleocanyons affecting MUC3 and MUC4 (Fig. 8.8), discrete erosive truncations occur only at the top of MUC4 unit in restricted zones, interpreted as deformed and scarred zones possibly reflecting evaporites halokinetic movement (Figs. 8.8, 8.9).

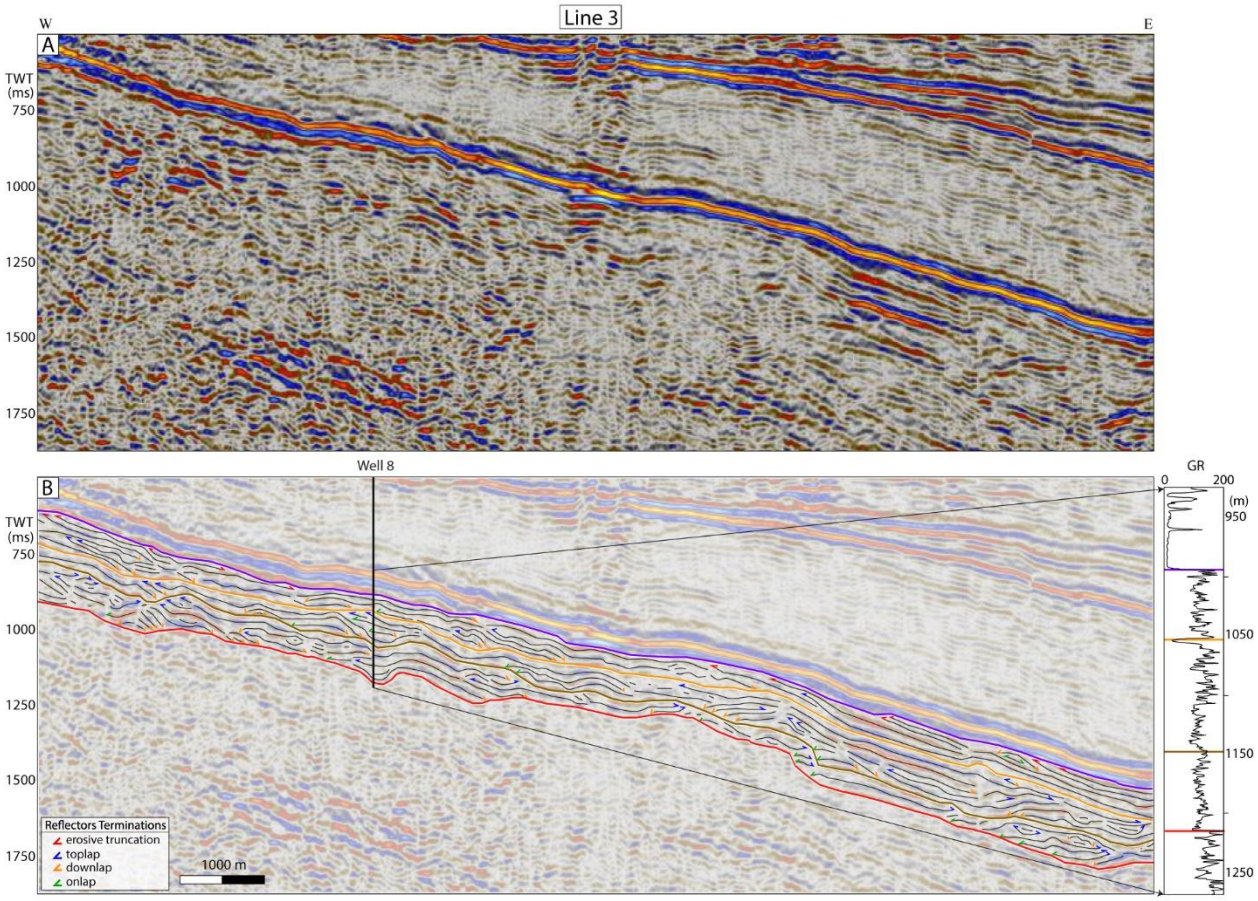

Figure 8.9. (A) Non-interpreted seismic line 3; (B) Seismostratigraphic interpretation of line 3, with reflections interpretations, identified units-bounding reflectors (colored according to Figure 8.7), position of well-log 2 and gamma ray curve.

The unit-bounding reflectors were mapped following their seismic characteristics at a more detailed scale. MUC1 deposited on 173 km² restricted to the

central-eastern portion (Fig. 8.10A); MUC2 extends to the north and to the south over 918 km² (Fig. 8.10B); MUC3 expands mainly to west and north over 1545 km² (Fig. 8.10C); MUC4 covers 2143 km² (Fig. 8.10D), almost the entire studied region. The Regência paleocanyon completely eroded the top units MUC4 and MUC3 for over 45 km², while Fazenda Cedro paleocanyon completely eroded MUC4 and partially removed MUC3 over 20 km² (Fig. 8.10). The basal surfaces of the units dip towards the east, coinciding with the general trend of the surfaces that delimit the Mucuri Member.

The isopach maps for each seismostratigraphic unit were generated by subtracting their top and base (Fig. 8.10). Unit's isopachs range as follows: MUC1 varies from 10 and 170 ms (TWT); MUC2 presents general values between 10 and 200 ms (TWT), reaching 270 ms in isolated portions; MUC3 varies between 10 and 200 ms (TWT), locally reaching 350 ms; MUC4 ranges between 10 and 250 ms (TWT), up to 370 ms in isolated regions. There is a general thickening to the south in the three upper units, but each unit has isolated locations of higher thickness values.

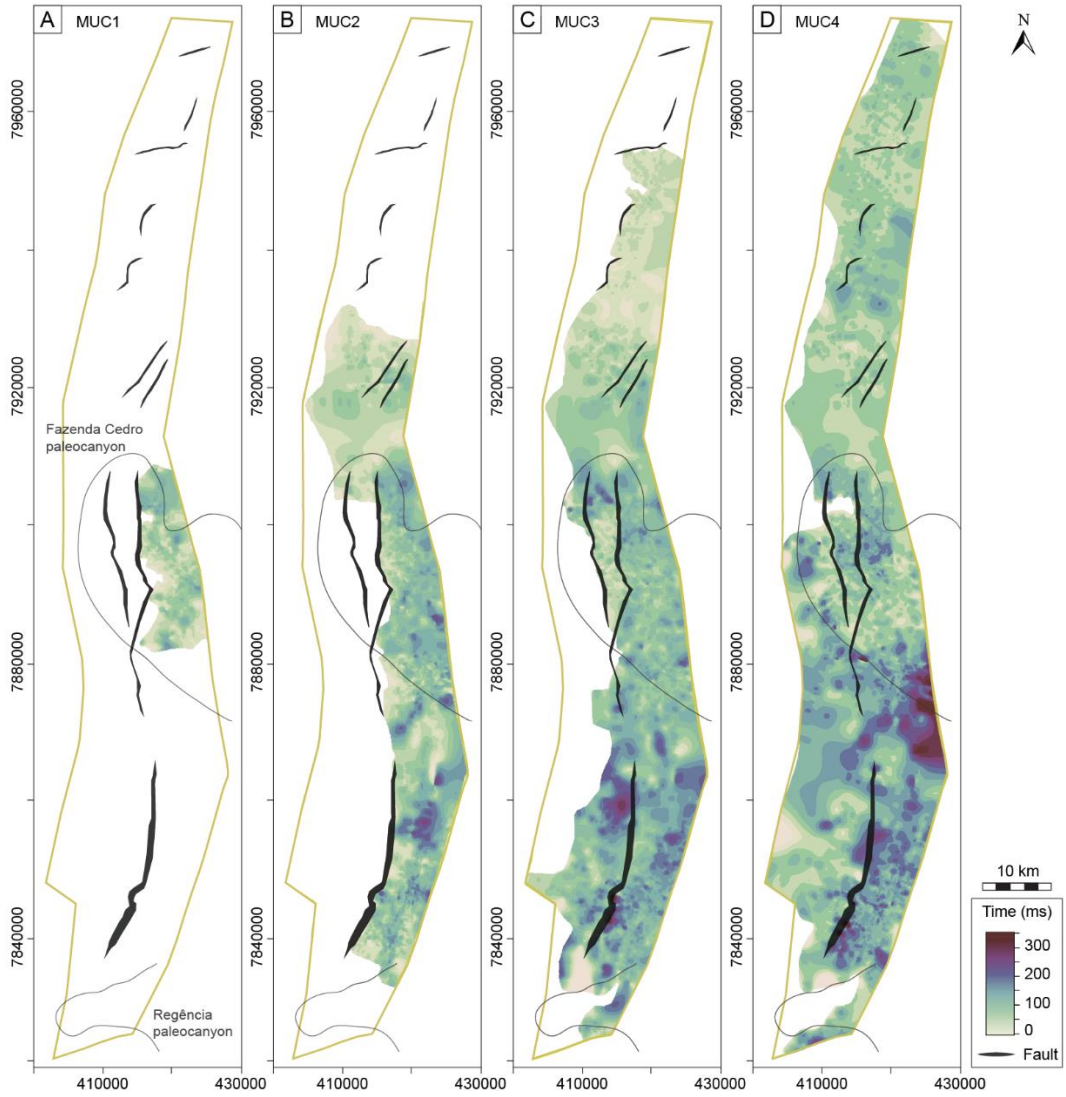

Figure 8.10. Isopach maps showing the relative TWT thickness variations of units: (A) MUC1; (B) MUC2; (C) MUC3; (D) MUC4; mapped faults segments in Mucuri Member in black.

4.4. Depositional systems inferred by lithofacies and seismic facies

The detailed sedimentological description of well 6 (Fig. 8.11) resulted in the individualization of seventeen lithofacies. Dominant grain size is fine- to coarse- sand, which composes ten sandstone lithofacies. Subordinately there are conglomerates, mudstones and anhydrites. The anhydrites occur as nodules displacing and replacing mud or fine sand layers post-deposition. Photos of the described well core are found in Supplementary Material.

The lithofacies were grouped into five facies associations according to the classification proposed by Althaus *et al.* (2019): (1) poorly-confined fluvial channel, (2) upper shoreface, (3) lower shoreface, (4) offshore and (5) hyperpycnal. The description, interpretation, component lithofacies and representative vertical log for each facies association are displayed in Table 8.1.

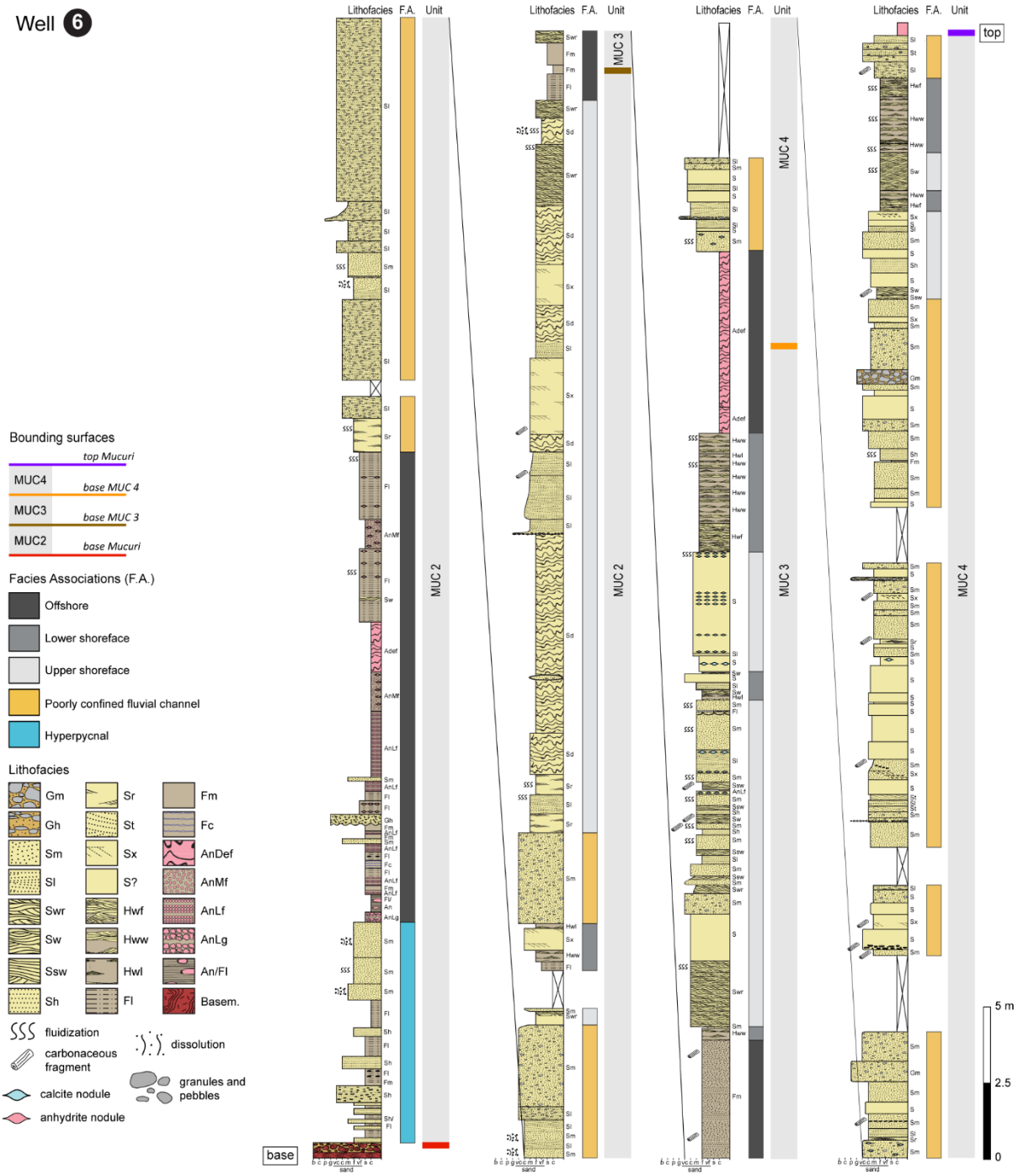

Figure 8.11. Cored-well (well 6) sedimentological and statigraphic interpretation.

Table 8.1. Facies associations and their lithofacies, description, interpretation and representative vertical log. Lithofacies codes are explained in the last line.

Facies association	Lithofacies	Description	Interpretation	Vertical Log
POORLY CONFINED FLUVIAL CHANNEL	Gm, Sr, Sl, Sm, St, Sx, Sh, Fm.	Successions of fining-upward cycles from 60 cm to 2.8 m thick, composing packages of up to 9.3 m. The base of each cycle consists Gm or coarse to very coarse-grained Sm or Sl. Overlying these strata there are medium- to coarse-grained, poorly to moderately-sorted Sm, Sl, St or Sx.. The cycles end with fine- to very fine-grained Sh or Sr, and rarely with Fm. Presence of carbonaceous fragments and mudclasts.	Shallow and poorly confined fluvial channels with highly-fluctuating discharges during sheetflood events.	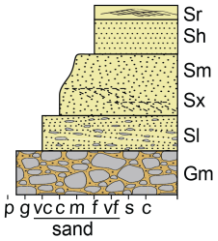
UPPER SHOREFACE	Swr, Ssw, Sw, Sd, Sx, Sl, Sr, Sh, An(Lf), Fl.	Fine- to very coarse-grained, well- to poorly-sorted mainly Sr, Sw and Swr. Less commonly, there are Ssw, Sl or Sx; presence of soft deformation structures (Sd) and carbonaceous fragments. Rarely there are Fl, AnLf and Sh.	Upper shoreface; oscillatory reworking of sandstones delivered by deltaic systems.	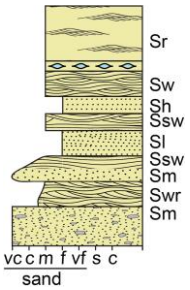
LOWER SHOREFACE	Sw, Sl, Sx, Hw(l,w,f).	Alternation between fine- to medium-grained well-sorted sandstones and very-fine grained sandstones to siltstones in heterolithic bedding with wave ripple cross lamination (Hw, linsen to flaser). Presence of medium- to very coarse-grained Sw, Sl or Sx.	Shoreface - shelf transition environment, below fair weather base level (lower shoreface).	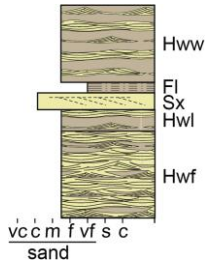
OFFSHORE	Gh, Sm, An(def, Lc, Lf, M), Fl, Fc, Fm.	Fl, Fc, Fm rich in organic matter; Nodules of anhydrite displacing laminations (An - def, Lc, Lf, M). Isolated intraformational Gh and medium- to coarse-grained Sm.	Offshore; eodiagenetic precipitation of anhydrites.	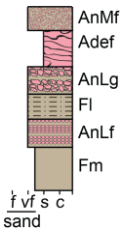
HYPER-PYCNAL	Sh, Sm, Fl, Fm.	Fining-upward cycles of fine- to very coarse-grained Sh and Sm in the base and Fl and Fm in the top.	Hyperpycnal flows deposited below storm waves base level.	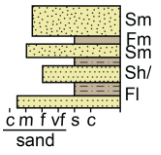
Lithofacies Codes	Conglomerates: massive (**Gm**); horizontally laminated (**Gh**). Sandstones:massive (**Sm**); low-angle cross-stratified (**Sl**); trough cross-bedded (**St**); indistinctly cross-bedded (**Sx**); horizontally laminated (**Sh**), current ripple cross-laminated (**Sr**); wave ripple cross-laminated (**Sw**) or combined-flow ripple cross-laminated (**Swr**); swaley cross-stratified (**Ssw**); soft deformated (**Sd**). Fines: massive (**Fm**); laminated (**Fl**); corrugated (**Fc**). Anhydrites: deformated (**Andef**); laminated (fine, **AnLf**; coarse, **AnLc**), massive (**AnM**). Heterolithic bedding: wave ripple-laminated (**Hw** + **l** linsen, **w** wavy, **f** flaser).			

Key seismic lines allowed the identification of three seismic facies with distinct external configurations and internal characteristics, which are found repeatedly in the

mapped area. Figure 8.12 presents the description of the three seismic facies, together with their respective interpretation and representative images, with and without application of an auxiliary seismic attribute used to enhance the internal facies structure (cosine of the phase in the first and third seismic facies to emphasize reflector discontinuities; RMS amplitude in the second, to enhance evaporite-related lithofacies). Seismic facies characterization and interpretation were based on seismic parameters – amplitude, frequency, continuity, geometry and internal patterns of reflectors, following Mitchum *et al.* (1977).

4.5. Wells correlation

The strike-oriented well-log correlation section (Fig. 8.13) is based on both lithological and gamma ray data, using the top of Mucuri Member as leveling-horizon. Differentiating the Mucuri Member from the Cricaré Formation was possible only by using the gamma ray curves, giving the similarities in sediment composition and facies succession of both units. The Cricaré Formation is characterized by high frequency and low amplitude variations, while the Mucuri Member is composed of low frequency and high amplitude gamma ray curves (Fig. 8.13, wells 9 to 14).

The reflectors that bound the seismostratigraphic units coincide with peaks of high value of gamma ray on wireline logs (Figs. 8.8A and 8.9B). High values of gamma ray are mostly associated to more expressive deposition of fine-grained sediments. In the Mucuri Member fine-grained sediments are deposited within offshore lacustrine context, characterized by mudstones and anhydrites facies successions (Fig. 8.11; Althaus *et al.*, 2019). Offshore anhydrites display anomalously low gamma ray values (Fig. 8.14). Deposition of the offshore facies association is a response to transgressive events, corresponding to maximum flooding surfaces (sensu Catuneau, 2011). Hence, the Mucuri Member is composed of four genetic stratigraphic sequences (sensu Galloway, 1989) bounded by lacustrine maximum flooding surfaces.

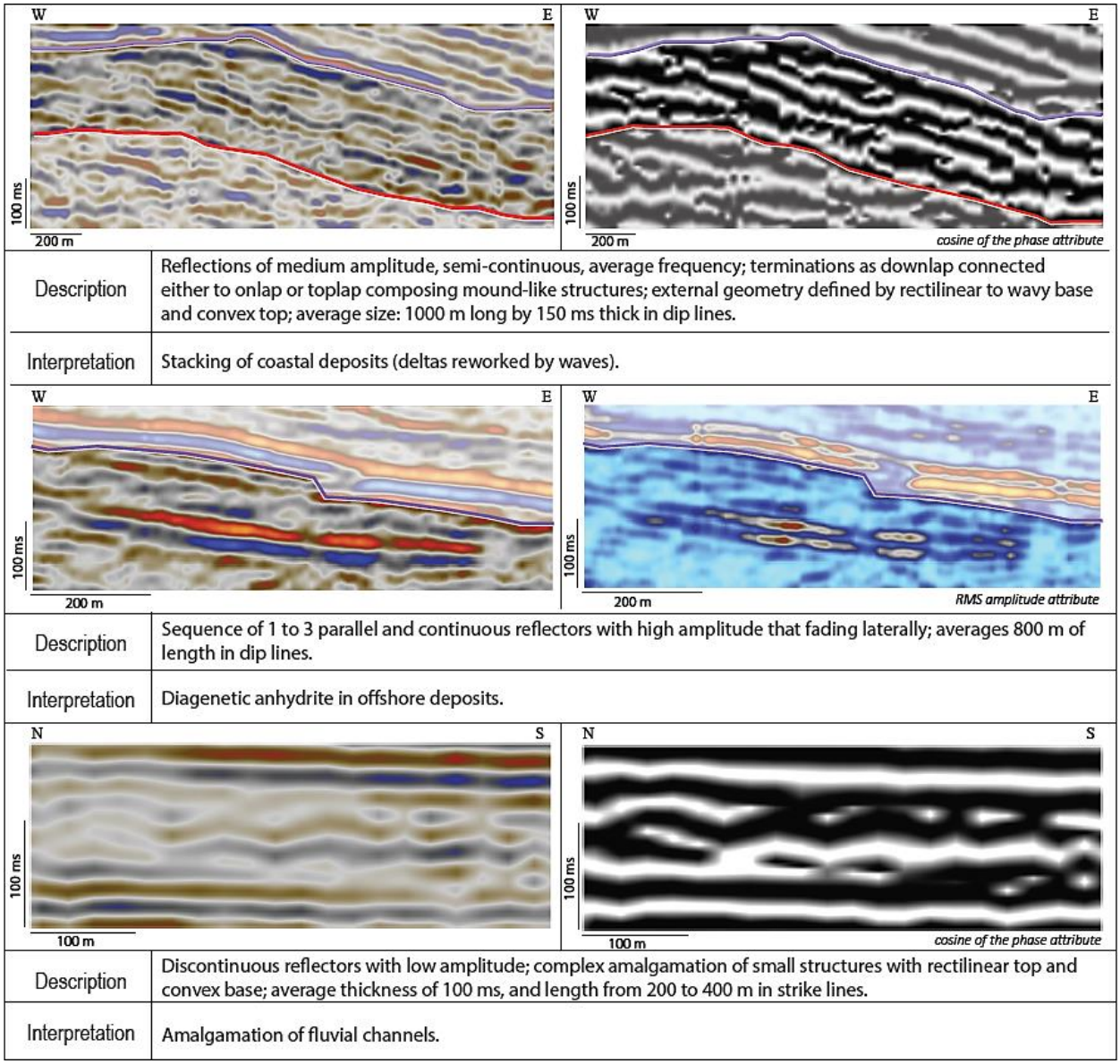

Figure 8.12. Description and interpretation of identified seismic facies, and their representative images, with and without application of the used auxiliary seismic attribute. The top of the Mucuri Member is in purple; the base, in red.

Based on these premises, an analysis of the stacking pattern of gamma ray values and stratigraphic units delimitation was performed (Fig. 8.14) and the surfaces that bound each unit were traced in the well-log correlation section (Fig. 8.13). Internal to each unit, there are other very high or very low peaks of gamma ray, suggesting a greater number of water-table rise events responding to higher frequency base-level variations, also attested by Althaus *et al.* (2019). The calculated average thickness for each unit from the well-correlation section (Fig. 8.13) shows a gradual decrease from the base upwards – MUC1, 96 m; MUC2, 74 m; MUC3, 60 m; MUC4, 53 m.

In the cored well three units were individualized from the vertical succession of the facies associations, bounded by maximum flooding surfaces within offshore deposits (Fig. 8.11). Lateral correlation (Fig. 8.13) shows that these units correspond

to MUC2, MUC3 and MUC4. Sedimentation within MUC2 commences with hyperpycnal flows associated with offshore deposits in deep water context; fluvial channel sediments cover these lacustrine associations and are superimposed by shallow water deposits, upper shoreface, that grade to offshore in continuous transgression. MUC3 records solely lacustrine facies successions: an alternation between upper and lower shoreface; to the top there is a transgression marked by the passage from upper shoreface to lower shoreface to offshore. Unit MUC4 is mostly composed of fluvial facies associations; in the top there are high frequency alternations with lower and upper shoreface deposits.

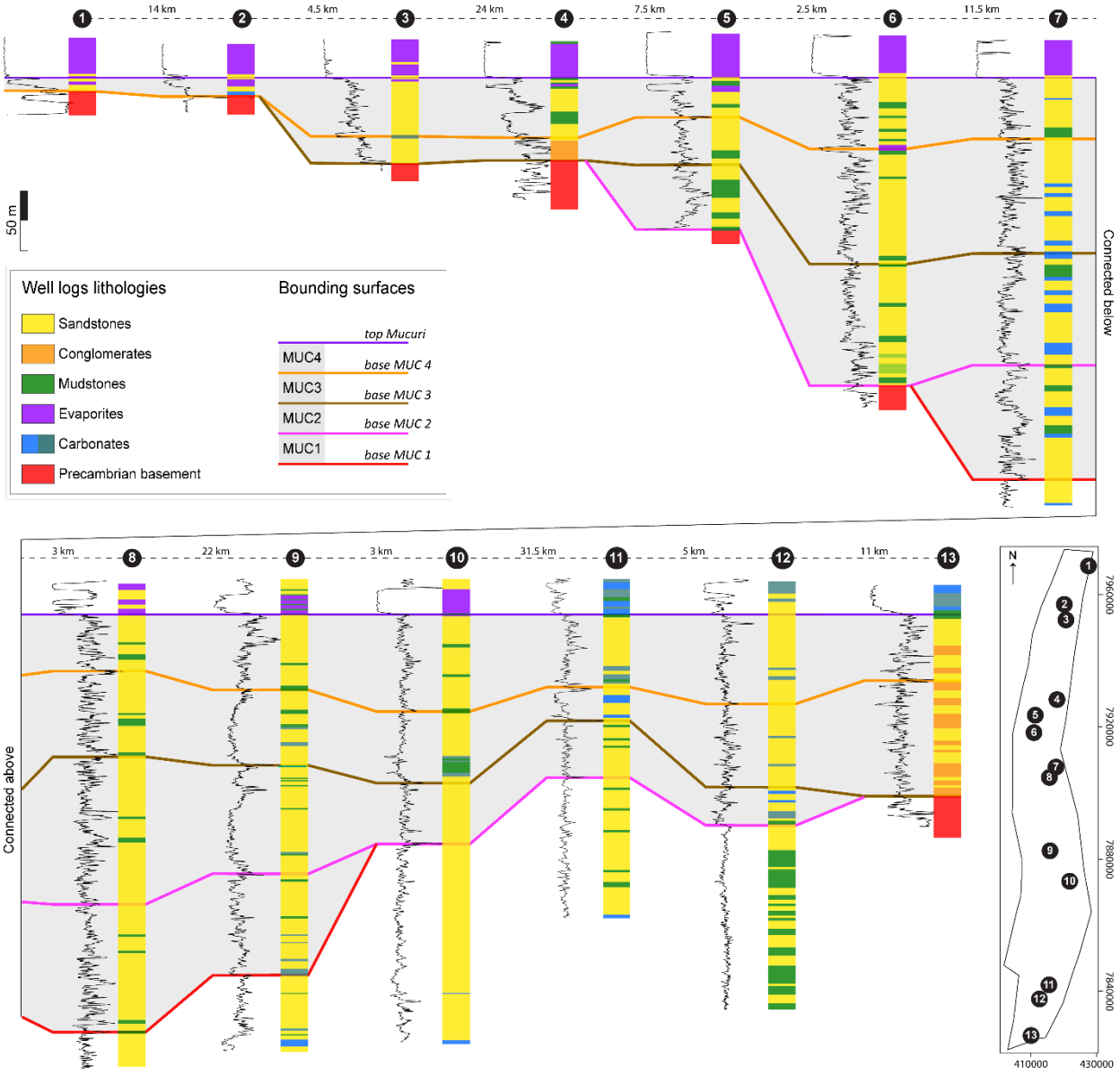

Figure 8.13. Well-log correlation section, with the gamma ray and/or lithology curves of each well.

4.6. Structural characterization

The structural framework of Mucuri Member is subdivided into two domains: north and south. The northern area is characterized by a series of short (3–8 km), NE-SW-oriented normal faults (Fig. 8.15A), with small displacement up to 50 ms (Fig. 8.15B-D). Occasionally the prominent reflectors of the evaporites that compose the Itaúnas Member are folded coupled to the basement, indicating there are structural events that postdated salt deposition (Fig. 8.15B). In this area, the basal surface of the member is irregular because it originated from the intense erosive processes that predated the deposition of Aptian sediments (Pre-Alagoas Unconformity – Karner *et al.*, 2003). Syn-rift deposits, if once present, were completely eroded and the Mucuri Member directly overlaps the basement, which is positioned relatively shallow, 400 to 1450 ms from west to east (Fig. 8.5). Such geomorphological framework was described as a prolongation of basement highs into the basin and named “shallow basement platforms” by Vieira (1998).

The southern portion is characterized by half-graben delimiting normal faults, inherited from the syn-rift stage of the basin. Three main fault segments were mapped (Fig. 8.15A faults 1-3) exclusively where they affect the interval of interest. Fault 1 (Fig. 8.15F) is 27 km long and it causes a maximum displacement of 550 ms; fault 2 (Fig. 8.15E) extends for 35 km, generating a maximum displacement of 300 ms; fault 3 (Fig. 8.15E) is 21 km long, and its displacement is the smallest, reaching 100 ms. The fault orientation varies from N-S to NE-SW with vergence to the east. The faults segments are related to the Espírito Santo Basin Hinge Zone (Fig. 8.1B; Vieira, 1998), a group of normal faults with important displacements and wide lateral distribution, which abruptly mark the thickening of the sedimentary package of the Mucuri Member. Such thickness increase east from the Hinge Zone is shown in Figure 8.5C. The Hinge Zone delimits the “shallow basement platforms” to the east. North from Fazenda Cedro Paleocanyon, such zone is deflected towards the east by a zone of transfer faults, NE-SW oriented (Fig. 8.1B; Fig. 8.15A - faults 4?). Northwards from that region, the Hinge Zone is located offshore, outside of the study area (Vieira, 1998).

The internal reflection patterns of the Mucuri Member close to the faults are parallel to wavy. These reflectors configurations indicate uniformity in depositional rates, attesting that faults movement during deposition was absent or minimal. Such interpretation is confirmed by the fact that divergent reflectors – the signature of lateral

variations in depositional rates caused by, among others, expressive fault activity – were not identified.

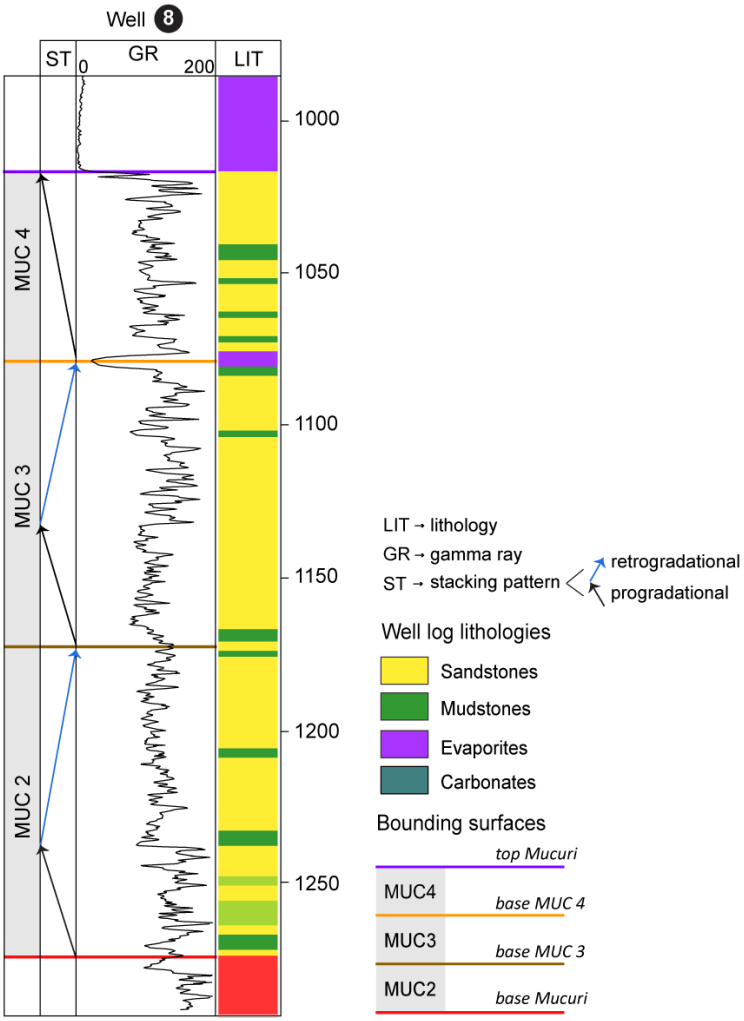

Figure 8.14. Gamma ray and lithology curves of well-log number 8, with the interpreted stacking patterns and identified units (named according to seismic units MUC2-MUC4).

5 – Tectono-stratigraphic evolution of Mucuri Member

We showed that the Mucuri Member is composed of four genetic stratigraphic sequences delimited by three lacustrine maximum flooding surfaces. The units' areal distribution did incrementally expand from the base upwards during each transgressive event. Seismic interpretation evidence that there was no prominent internal erosion within the interval sedimentation (Figs. 8.8 and 8.9), attesting the absence of seismic visible regional erosive episodes.

On a regional scale, in the southeastern Brazilian context, the Mucuri Member records the marginal deposits of a major lacustrine basin that hosts the pre-salt carbonate deposits of the substantial reservoirs of Santos, Campos and Espírito Santo basins. In the distal pre-salt carbonate successions of the Campos Basin, Dias (1998)

identified a cyclic repetition using a detailed well log analysis, and subdivided the sedimentary succession into four units, similar to what we describe and propose for the onshore Espírito Santo Basin in this work. In case the four units identified in Espírito Santo Basin (this work) and in Campos Basin (Dias, 1998) are synchronous and stratigraphically connected, successive increments in depositional area are expected on these reservoirs. The tectonic quiescence observed in Mucuri Member upper units is similar to what is observed in the distal carbonate deposits, discarding the existence of important syn-depositional fault movements.

From a structural point of view, sedimentation of the Mucuri Member units occurred onto two distinctive settings. A northern domain includes minor normal faults and basement irregularities; sediments of the Mucuri Member directly overlap the basement onto “shallow basement platforms”. In the area of interest as a trend the faults did not control the depositional boundaries mapped within this domain (Fig. 8.10). However, some of the faults traced did delimit the unit MUC3 to the west (Fig. 8.15B-C). This indicates that MUC3 was occasionally filling previous negative topography controlled by faulting.

A southern domain is composed of half-grabens delimited by normal faults inherited from the rift stage within the Hinge Zone (Figs. 8.1B, 8.15E,F), and the Mucuri Member is overlying mostly syn-rift sediments. Faults within this structural domain exert a clear control on the depositional limits of the Mucuri Member (Figs. 8.10, 8.15E,F). MUC 1 is completely delimited by fault 2; MUC 2 by faults 1 and 2, with minor areal increase to the north; MUC 3 limit is locally controlled by fault 3, with significant expansion to the north, south and west; MUC 4 limit is independent of structural relations. The fault segments were locally mapped up to the top of MUC4 unit (Fig. 8.15E). In both northern and southern structural domains faulting was probably inactive throughout the deposition Mucuri Member, indicating the identified faults segments were a backbone of the structural framework from the rift stage, yet providing a pre-existing topography later filled or draped by the Mucuri Member deposits.

Isopach maps show that the relative thicknesses of units MUC2 to MUC4 are thinner north of the Fazenda Cedro paleocanyon (Fig. 8.10) due to the relatively shallow position of the basement. Local variations were caused by basement irregularities likely originated by exposure and erosion (Pre-Alagoas Unconformity). In the southern structural domain, the upper units that deposited across rift-inherited normal faults (MUC3 and MUC4) indicate that there was no direct connection between thickness and fault location (Figs. 8.10, 8.15). Calculated average thickness for each

unit from the well-correlation section (Fig. 8.13) shows a gradual decrease from the base upwards, from 96 m in MUC1 to 53 m in MUC4. Thickness decreased with areal enlargement and the filling of the remnant topography likely under homogeneous subsidence.

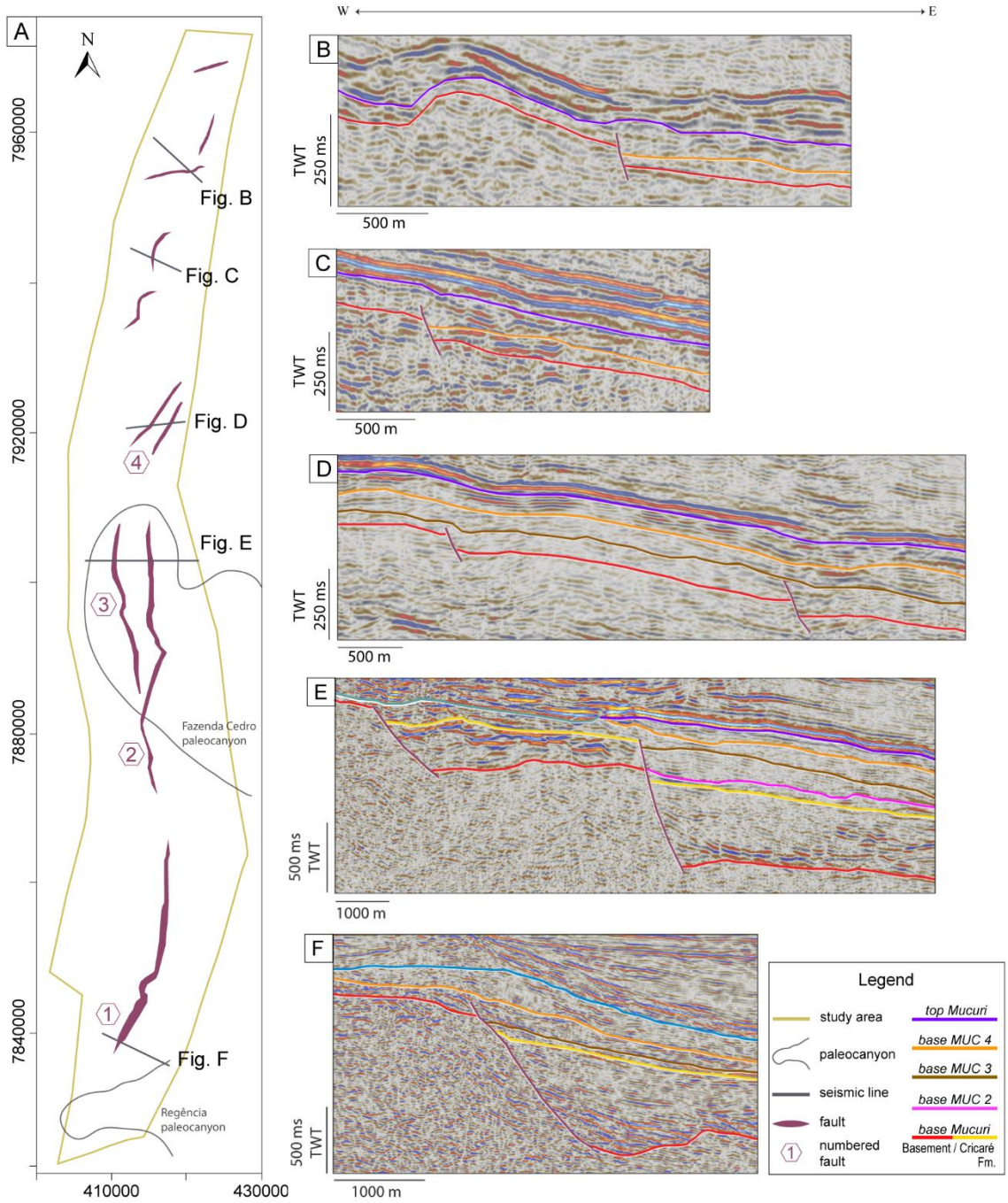

Figure 8.15. (A) Map of study area with the mapped fault segments, and location of the seismic lines presented; (B – F) Interpreted seismic lines, with faults and main horizons.

Therefore, the combined stratigraphic and structural analysis attests that the dominant controlling factor for the sedimentary distribution was base level rise. The depositional area was initially conditioned by the preexisting topography of the rift stage, as MUC1 and MUC2 are overall confined in paleo rift troughs; units MUC3 and

MUC4 were deposited onto a relatively smoother surface covering a broader area and evidence a peneplanation of the relief after the rift inherited topography was filled.

From a tectono-stratigraphic point of view we show that Mucuri Member in the onshore Espírito Santo Basin is defined by system tracts (*sensu* Prosser, 1993). The post-rift stage marks the end of active tectonism, implying a cessation of differential fault controlled subsidence and the onset of a more homogeneous subsidence caused by lithospheric thermal cooling. Such change in tectonic regime produces a tectonically-generated onlap surface. Succeeding reflectors of the immediate post-rift system tract have parallel internal patterns and terminate in onlap against hangingwall dip slope (Figs. 8.7, 8.15); as the rift-inherited depressions are filled the typical stacking pattern is aggradational. In the late post-rift system tract, the deposition transcends and drape the rift boundaries, indicating a peneplanation of the topography (Prosser, 1993); in this context, in the Mucuri Member, MUC1 and MUC2 can be interpreted as immediate post-rift sequences; MUC3 and MUC4 correspond to the late post-rift as they drape the rift basin and mark the gradual peneplanation of the topography.

Many studies document worldwide a similar tectono-sedimentary configuration in late-stage rift basins. These e.g. include: the Magnus Basin in the northern North Sea (Prosser, 1993), Cretaceous Taranaki-Aotea Basin in New Zealand (Strogen *et al.*, 2017) and North Falkland Basin (Lohr and Underhill, 2015). This study also documents clear examples of how inactive rift inherited space can be substantial in controlling the thickness of post-rift depositional units: in the Magnus Basin, for example, fault scarp relief 2 km of thickness existed at the end of rifting (Prosser, 1993).

6 – Conclusions

- The frequency spectral decomposition attribute allowed the identification of the Pre-Alagoas Unconformity within rift troughs, thus permitting to distinguish the Mucuri Member from the underlying Cricaré Formation.
- The Mucuri Member is composed of four genetic stratigraphic sequences (MUC1, MUC2, MUC3, MUC4), delimited by three lacustrine maximum flooding surfaces, identified and mapped both in seismic and well log data.
- The marginal system of Espírito Santo Basin is characterized by two structural domains. A northern one defined by minor faults and basement highs. A sourthern one defined by half-graben delimiting normal faults inherited from the

rift phase. In both domains faulting was inactive during the deposition of Mucuri Member.

- The Mucuri Member records an enlargement in the depositional area upwards triggered by transgressive events. MUC 1 and MUC2 architectures were significantly influenced and constrained by the rift inherited topography, with accumulation confined to rift troughs; the sediment distribution of MUC3 and MUC4 units transcended and draped rift basins limits. The upper unit MUC4 deposited on a smoothly dipping basal surface, indicating peneplanation of the area as the pre-existing syn-rift topography was filled.
- The basal units MUC1 and MUC2 can be interpreted as the expression of an immediate post-rift system tract (*sensu* Prosser, 1993); the upper units MUC3 and MUC4 form a late post-rift system tract.

Acknowledgments

F.B.D. Amarante thanks CNPq (National Council for Scientific and Technological Development of Brazil) for the doctorate scholarship. The authors gratefully acknowledge support from Shell Brasil Petroleo Ltda and the strategic importance of the support given by ANP (Brazil's National Oil, Natural Gas and Biofuels Agency) through the R&D levy regulation. Special thanks to Léo A. Hartmann for valuable suggestions and revision of the manuscript. The authors are very grateful to Gonzalo Zamora and the anonymous reviewer for their constructive comments.

Appendix A. Supplementary data

Supplementary data to this article can be found online at https://doi.org/10.1016/j.jsames.2019.102474.

References

Abelha, M., Petersohn, E., 2018. The State of Art of the Brazilian Pre-Salt Exploration. AAPG Search and Discovery Article #30586.

Althaus, C.E., Scherer, C.M.S., Kuchle, J., Reis, A.D.D., Ferronatto, J.P.F., De Ros, L.F., Bardola, T.P., 2019. Depositional model of alluvial to lacustrine sag margin, Aptian pre-salt Mucuri Member, Espírito Santo Basin. Manuscript in preparation.

Asmus, H.E., Gomes, J.B., Pereira, A.C.B., 1971. Integração Geológica regional da Bacia do Espírito Santo. São Paulo, XXV Congresso Brasileiro de Geologia 3, 215–226.

Beglinger, S.E., Doust, H, Cloetingh, S., 2012. Relating petroleum system and play development to basin evolution: West African South Atlantic basins. Marine and Petroleum Geology 3, 1-25.

Bosence, D.W.J., 1998. Stratigraphic and sedimentological models of rift basins. In: Purser, B. H.; Bosence, D.W.J. Sedimentation and Tectonics of Rift Basins: Red Sea, Gulf of Aden. London: Chapman e Hall, 9-25.

Brown, L.F., Fisher, W.L., 1977. Seismic-Stratigraphic Interpretation of Depositional Systems: Examples from Brazilian Rift and Pull-Apart Basins: Section 2. Application of Seismic Reflection Configuration to Stratigraphic Interpretation. AAPG Special Volumes 165, 213-248.

Cainelli, C., Mohriak, W.U., 1999. Some remarks on the evolution of sedimentary basins along the eastern Brazilian continental margin. Episodes, 206–216.

Catuneanu, O., 2011. Sequence stratigraphy: methodology and nomenclature. Newsletters on stratigraphy. E. Schweizerbart'sche Verlagsbuchhandlung. 44 (3), 190.

Catunenanu, O., Zechin, M., 2013. High-resolution sequence stratigraphy of clastic shelves II: Controls on sequence development. Marine and Petroleum Geology 39, 26-38.

Ceraldi, T. S., Green, D., 2016. Evolution of the South Atlantic lacustrine deposits in response to Early Cretaceous rifting, subsidence and lake hydrology. In: Ceraldi, T. S., Hodgkinson, R. A., Backe, G. (Eds.) Petroleum Geoscience of the West Africa Margin. Geological Society, London, Special Publications 438.

Chang, H.K., Kowsmann, R.O., Figueiredo, A.M.F., Bender, A., 1992. Tectonics and stratigraphy of the East Brazil rift system: an overview. Tectonophysics 213, 97-138.

Chopra, S., Marfurt, K.J., 2007. Seismic Attributes for prospect identification and reservoir characterization. SEG Geophysical Developments Series 11, 136-141.

Davison, I., 2007. Geology and tectonics of the South Atlantic Brazilian salt basins. Geological Society, London, Special Publications 272(1).

Dias, J.L., 1998. Análise sedimentológica e estratigráfica do Andar Aptiano em parte da Margem Leste do Brasil e no Platô das Malvinas: considerações sobre as primeiras incursões e ingressões marinhas do Oceano Atlântico Sul Meridional. Porto Alegre: Universidade Federal do Rio Grande do Sul. Thesis (Doctorate).

Dias, J.L., 2004. Tectônica, estratigrafia e sedimentação no Andar Aptiano da margem leste brasileira. Boletim de Geociências da Petrobras 13(1), 7–25.

França, R.L., Tschiedel, F.E., 2006. Os evaporitos das Bacias do Espírito Santo e Mucuri: sedimentação e tectônica Aracaju, Congresso Brasileiro De Geologia 43.

França, R.L., Del Rey, A.C., Tagliari, C.V., Brandão, J.R., Fontanelli, P.R., 2007. Bacia do Espírito Santo. Boletim de Geociências da Petrobras 15 (2), 501–509.

Galloway, W.E., 1989. Genetic stratigraphic sequences in basin analysis. I. Architecture and genesis of flooding-surface bounded depositional units. American Association of Petroleum Geologists Bulletin 73, 125–142.

Herlinger Jr.R., Zambonato, E.E., De Ros, L.F., 2017. Infulence of diagenesis on the quality of Lower Cretaceous pre-salt lacustrine reservoirs from northern Campos Basin, offshore Brazil. Journal of Sediment Research 87, 1285–1313.

Karner, G. D., Driscoll, N. W, Barker, D. H. N., 2003. Synrift subsidence across the West African continental margin: The role of lower plate ductile extension. In: Arthur, T. J., Macgregor, D. S., Cameron, N. R. (eds) Petroleum Geology of Africa: New Themes and Developing Technologies. Geological Society, London, Special Publications 207, 105-125.

Karner, G.D., Gamboa, L.A.P., 2007. Timing and origin of the South Atlantic pre-salt sag basins and their capping evaporates. In: Schreiber, B.C., Lugli, S., Bac¸bel, M. (eds) Evaporites Through Space and Time. Geological Society, London, Special Publications 285, 15–35.

Kukla, P. A., Strozyk, F., Mohriak, W. U., 2018. South Atlantic salt basins– witnesses of complex passive margin evolution. Gondwana Research 53, 41–57.

Lima, B.E.M., De Ros, L.F., 2019. Deposition, diagenetic and hydrotermal processes in the Aptian Pre-Salt lacustrine carbonate reservoirs of the northern Campos Basin, offshore Brazil. Sedimentary Geology 383, 55–81.

Lindseth, R.O., Beraldo, V.L., 1985. A Late Cretaceous Submarine Canyon in Brazil. In: Berg, O.R., Woolverton, D.G. (Eds.), Seismic Stratigraphy II: An Integrated Approach to Hydrocarbon Exploration. AAPG Memoir, 39p.

Lohr, T., Underhill, J.R., 2015. Role of rift transection and punctuated subsidence in the development of the North Falkland Basin. Petroleum Geosciences 21, 85–110.

Miall, A.D. 1977. Lithofacies types and vertical profile models in braided rivers deposits: a summary, in: Miall, A.D. (Ed.), Fluvial Sedimentology. Canadian Society of Petrology and Geology Memoir 5, 597–604.

Milani, E.J., Brandão, J.A.S.L., Zalán, P.V., Gamboa, L.A.P., 2000. Petróleo na margem continental brasileira: Geologia, exploração, resultados e Perspectivas. Revista Brasileira de Geofísica 18(3).

Mitchum Jr., R.M., Vail, P.R., Sangree J.B., 1977. Seismic stratigraphy and global changes of sea level, part 6: stratigraphic interpretation of seismic reflection patterns in depositional sequences, in: Payton, C. E. (Eds.), Seismic Stratigraphy – applications to hydrocarbon exploration. Tulsa, AAPG Memoir 26, 117–133.

Mohriak, W.U., 2003. Bacias Sedimentares Da Margem Continental Brasileira. In: Bizzi, L. A., Schobbenhaus, C., Vidotti, R. M. & Gonc¸ Alves, J. H. (eds) Geologia, Tectônica e Recursos Minerais do Brasil. Companhia de Pesquisas de Recursos Minerais, Brasília, 87–165.

Mohriak, W., Nemcok, M., Enciso, G., 2008. South Atlantic divergent margin evolution: rift-border uplift and salt tectonics in the basins of SE Brazil. In: Pankhurst, R.J., Trouw, R.A.J., Brito Neves, B.B., De Wit, M.J. (Eds.), West Gondwana: Pre-Cenozoic Correlations Across the South Atlantic Region. Geol. Soc. Spec. Publ 294, 365–398.

Muniz, M.C., Bosence, D.W.J., 2015. Pre-salt microbialites from the Campos Basin (offshore Brazil): image log facies, facies model and cyclicity in lacustrine carbonates. In: Bosence, D.W.J., Gibbons, K.A., Le Heron, D.P., Morgan, W.A., Pritchard, T., Vining, B.A. (Eds.), Microbial Carbonates in Space and Time: Implications for Global Exploration and Production. Geological Society, London, Special Publications 418, 221–242.

Neal, J., Abreu, V., 2009. Sequence stratigraphy hierarchy and the accommodation succession method. Geology 37, 779–782.

Pietzsch, R., Oliveira, D.M., Tedeschi, L.R., Queiroz Neto, J.V., Souza, R.S., 2018. Palaeohydrology of the Lower Cretaceous pre-salt lacustrine system, from rift to post-rift phase, Santos Basin, Brazil. Palaeogeography, Palaeoclimatology, Palaeoecology 507, 60–80.

Prosser, S., 1993. Rift-related linked depositional systems and their seismic expression. In: Williams, G. D.; Dobb, A. (Ed.) Tectonics and Seismic Sequence Stratigraphy. Geological Society, London, Special Publications 71, 35–66.

Saller, A., Rushton, S., Buambua, L., Inman, K., McNeil, R., Dickson, J.A.D., 2016. Presalt stratigraphy and depositional systems in the Kwanza Basin, offshore Angola. AAPG Bulletin 100(7), 1135–1164.

Sobreira, J.F.F., Szatmari, P., 2000. New Ar–Ar ages for the Abrolhos volcanic rocks, East Brazilian margin. Rio de Janeiro, 31st International Geological Congress.

Strogen, D.P., Seebeck, H., Nicol, A., King, P.R., 2017. Two-phase Cretaceous-Paleocene rifting in the Taranaki Basin region, New Zealand; implications for Gondwana break-up. Journal of the Geological Society 174(5), 929–946.

Strozyk F., Back, S., Kukla, P. A., 2017. Comparison of the rift and post-rift architecture of conjugated salt and salt-free basins offshore Brazil and Angola/Namibia, South Atlantic. Tectonophysics 716, 204–224.

Szatmari, P., 2000. Habitat of petroleum along the South Atlantic margins. In: Mello, M.R., Katz, B.J. (Eds.), Petroleum Systems of South Atlantic Margins. Tulsa, AAPG Memoir 73, 69–75.

Vail, P.R., Mitchum Jr., R.M., Todd, R.G., Widmier, J.M., Thompson, S., III, Sangree, J.B., Bubb, J.N., Hatlelid, W.G., 1977. Seismic stratigraphy and global changes of sea level, in: Payton, C. E. (Eds.), Seismic Stratigraphy – applications to hydrocarbon exploration. Tulsa, AAPG Memoir 26, 49–212.

Vieira, R.A.B., 1998. Análise Estratigráfica e Evolução Paleogeográfica da Seção Neoaptiana na Porção Sul da Plataforma de São Mateus, Bacia do Espírito Santo, Brasil. Porto Alegre: Universidade Federal do Rio Grande do Sul. Dissertation (Master's).

Vieira, R.A.B., Mendes, M.P., Vieira, P.E., Costa, L.A.R., Tagliari, C.V., Barcelar, L.A.P., Feijó, F.J., 1994. Bacia do Espírito Santo e Mucuri. Boletim de Geociências da Petrobras, 8(1), 191–202.

Wright, V.P., Barnett, A.J., 2015. An abiotic model for the development of textures in some South Atlantic Early Cretaceous lacustrine carbonates. In: Grotzinger, J.P., James, N. (Eds.), Microbial Carbonates in Space and Time: Implications for Global Exploration and Production. Geological Society, London, Special Publications 418, 209–219.

Zalán, P.V., 2002. O potencial petrolífero brasileiro além do pré-sal. Artigo Opinião. Portal Geofísica Brasil.

9 Impacto da Morfologia Rifte na Tectônica do Sal – Bacia de Campos

Os resultados da análise do impacto da morfologia rifte na tectônica do sal (e, consequentemente na sedimentação e tectônica posterior – fase drifte) estão apresentados na forma de um artigo científico, publicado em julho de 2021 na revista Basin Research. Os dados da pesquisa foram providos pela ANP (Agência Nacional do Petróleo, Gás Natural e Biocombustíveis), conforme o regramento próprio da agência para concessão de dados para estudos científicos acadêmicos das Universidades.

9.1 Artigo 2 - Pre-salt rift morphology controls salt tectonics in the Campos Basin, offshore SE Brazil

Francyne Bochi do Amarante[1,2,#], Christopher Aiden-Lee Jackson[2], Leonardo Muniz Pichel[3], Claiton Marlon dos Santos Scherer[1], Juliano Kuchle[1]

[1] Instituto de Geociências, Universidade Federal do Rio Grande do Sul, Porto Alegre, 90650 001, Brazil

[2] Basins Research Group (BRG), Department of Earth Science and Engineering, Imperial College London, London, SW7 2BP, United Kingdom

[3] Department of Earth Science, University of Bergen, Allegaten 41, 5007, Bergen, Norway

[#] Corresponding author. Email: francyne.amarante@ufrgs.br

ABSTRACT

Classic models of gravity-driven salt tectonics commonly depict kinematically-linked zones of overburden deformation, characterised by updip extension and downdip contraction, separated by a weakly deformed zone associated with downdip translation above a relatively smooth base-salt surface. We use 2D and 3D seismic reflection and borehole data from the south-central Campos Basin to show that these models fail to adequately capture the complex range of structural styles forming during salt-detached gravity-driven deformation above a rugose base-salt surface. In the Campos Basin the base-salt is defined by broadly NE-trending, margin-parallel, generally seaward-dipping ramps that have up to 2 km of structural relief. We define three domains of overburden deformation: an updip extensional domain, an intermediate multiphase domain, and a downdip contractional domain. The multiphase domain is defined by large, partly fault-bounded, ramp-syncline basins, the stratigraphic record of which suggest c. 28 km of seaward gravity-driven translation of salt and its overburden since the end of the Albian. We also identify three main types of salt structures in the multiphase domain: (i) contractional anticlines that were subjected to later extension and normal faulting; (ii) passive-to-active diapirs that were later extended and widened, and which are bound on their landward margins by landward-dipping, salt-detached normal faults; and (iii) reactive (extensional) diapirs that were subsequently squeezed. We argue that this multiphase deformation occurs because of basinward translation of salt and its overburden over complex base-salt relief, consistent with the predictions of physical models and several other seismic reflection data-based studies. Critically, these complex local strains overprint margin-scale patterns of deformation.

Keywords: base-salt relief, rift basin, passive margin, South Atlantic basins, ramp syncline basins, gravity-driven deformation, salt translation.

1 – Introduction

Salt-bearing passive margins typically deform in response to gravity gliding and gravity spreading (Peel, 2014). Such margins can be divided into kinematically linked domains of deformation, each associated with a distinct suite of salt and overburden structures (e.g. Rowan *et al.*, 2004; Brun and Fort, 2011; Peel, 2014). The upslope domain is characterised by thin-skinned (i.e. salt-detached) extension, which is associated with the formation of listric normal faults, rafts, and salt rollers (e.g. Lundin, 1992; Brun and Mauduit, 2009; Jackson and Hudec, 2017). Updip extension is accommodated by and kinematically linked to downdip contraction and the formation of salt-cored anticlines and salt-detached thrusts (e.g. Demercian *et al.*, 1993; Brun and Fort, 2004; Fort *et al.*, 2004). Domains of extension and contraction are separated by a domain of translation, in which deformation is typically described as being relatively mild (Brun and Fort, 2004; Davison *et al.*, 2012).

Recent studies on South Atlantic salt basins have demonstrated that this structural zonation is an oversimplification. More specifically, these studies show that various extensional and contractional structures, in addition to ramp-syncline basins (RSBs), can form in the translational domain due to the flow of salt and overburden across base-salt relief associated with prior rifting (Brun and Fort 2004, 2011; Dooley *et al.*, 2017; Hudec *et al.*, 2013; Pichel *et al.*, 2018, 2019a; Evans and Jackson, 2020; Erdi and Jackson, 2021). Local deformation can overprint regional patterns of deformation, resulting in multiphase structures with a complex kinematic history (Dooley *et al.*, 2017; Pichel *et al.*, 2019b; Erdi and Jackson, 2021).

The Aptian salt basin offshore southeastern Brazil contains substantial volumes of hydrocarbons and, because of this, has been intensively studied by the energy industry since the 1970's (e.g. Guardado *et al.*, 1989; Mohriak *et al.*, 1990; Bruhn *et al.*, 2003). There are presently 62 producing hydrocarbon fields in the Campos Basin (ANP, 2020). These fields relate to at least four petroleum systems, with reservoirs in pre- and intra-salt (i.e., pre-Aptian and Aptian) clastics and carbonates, post-salt (Albian-Cenomanian) marine carbonates, and most importantly, Upper Cretaceous to Miocene clastic turbidites (Guardado *et al.*, 1989; Bruhn *et al.*, 2003). The deposition and deformation of salt have strongly controlled the development of petroleum systems

in the Campos Basin (Guardado *et al.*, 1989; Mohriak *et al.*, 2012). For example, salt can be the seal rock, mainly to rift and Aptian pre-salt accumulations, and salt structures (more specifically thin-skinned faulting above salt anticlines and rollers) can form traps to post-salt sediments. The absence of salt, for example along welds, can define pathways for hydrocarbon migration, and salt-related faults can act as both migration pathways or traps, depending on their location and stratigraphic level. Despite its importance, there are surprisingly few international publications on the salt tectonics of the Campos Basin (Cobbold and Szatmari, 1991; Demercian *et al.*, 1993; Rouby *et al.*, 1993; Mohriak *et al.*, 2008 Davison *et al.*, 2012; Quirk *et al.*, 2012), and only a few present a detailed, regional-scale analysis of the geometry and kinematics of the salt and overburden structures (Demercian *et al.*, 1993; Rouby *et al.*, 1993). An improved knowledge of salt tectonics is required to understand the timing and style of salt-related deformation and deposition, and to extend hydrocarbon exploration further basinward into deeper waters.

In this study we use 2D and 3D seismic reflection and borehole data to characterise the salt-tectonic structural styles and related evolution of salt and overburden structures in the south-central Campos Basin, SE Brazil. We first describe the extensional and contractional domains, before focusing on the boundary between the two, which we herein name the multiphase domain. We then investigate the evolution of extensional and contractional deformation through time and space. We conclude by discussing the effects of base-salt relief on the distribution, origin and evolution of salt and overburden structures, and the implications of our work for post-salt hydrocarbon exploration in the deep-water Campos Basin.

2 – Geological context

The Campos Basin (c. 100,000 km²) is located on the southeastern Brazilian margin, offshore the states of Rio de Janeiro and Espírito Santo (Figure 9.1a) (Guardado *et al.*, 1989; Winter *et al.*, 2007). The basin originated during rifting of the Gondwana Supercontinent that culminated in the opening of the South Atlantic Ocean in the Late Jurassic-to-Early Cretaceous (Figure 9.1b) (Szatmari, 2000). The basin is limited to the north by the Vitória High, to the south by the Cabo Frio High (Figure 9.2a), to the east by oceanic crust, and to the west by exposures of crystalline basement rocks of the Ribeira Belt (Mohriak *et al.*, 1989; Heilbron *et al.*, 2000).

The syn-rift stage of the Campos Basin (Valanginian – Early Aptian) (Figure 9.1b) initiated at ~135 Ma with intense volcanic activity, coeval with the Serra Geral volcanism documented in the Paraná Basin (Baksi, 2018). Rifting was associated with the formation of NE-SW-striking normal faults that bound structural highs (horsts) and structural lows (grabens), including the External High and the External Low (Figure 9.2a) (Chang *et al.*, 1992; Guardado *et al.*, 2000). The inner (i.e. marginal) hinge line of the rift system is delineated by the Campos Fault (Figure 9.2a), a large structure that separates the shallow, western part, where Tertiary deposits rest directly on basement, from the deeper, eastern portion, where relatively thick accumulations of Barremian to Aptian sediment fill rift-related depocentres (Figure 9.2c) (Guardado *et al.*, 1989).

The early post-rift (i.e. sag) stage commenced in the Aptian (Figure 9.1b), marking the transition from basement-involved faulting and relatively rapid subsidence, to a period defined by very little faulting and long-wavelength, relatively slow subsidence driven by post-rift cooling of the lithosphere. Because of this change in subsidence pattern and rate, the depositional area enlarged and sedimentation progressively draped and essentially 'healed' rift-related relief (Quirk *et al.*, 2013; Kukla *et al.*, 2018; Amarante *et al.*, 2020). During the late Aptian, a thick salt layer was deposited in response to episodic marine-water influx through the Walvis Ridge volcanic high to the south (Davison *et al.*, 2012). Even though salt deposition occurred late in the sag phase, relief inherited from the rift phase still locally influenced salt distribution (Davison *et al.*, 2012; Dooley *et al.*, 2017).

The end of evaporite deposition is marked by a rapid marine transgression linked to the initiation of the drift (i.e. late post-rift) stage (Albian – Present) (Figure 9.1b) (Chang *et al.*, 1992). Focusing of thermally induced subsidence near the location of continental breakup caused the basin to tilt southeastward, inducing gravity gliding of Aptian salt and its overburden (Quirk *et al.*, 2012). Major progradation of basin-margin clastic wedges, linked to continental uplift and erosion, commenced in the Eocene and continues to the present day (Contreras *et al.*, 2010).

Salt-related deformation in the central South Atlantic region began in the Aptian (i.e. *during* salt deposition; Figure 9.1b) (Cobbold and Szatmari, 1991; Fiduk and Rowan, 2012; Davison *et al.*, 2012), with the major seaward flow of salt and its overburden continuing until the Maastrichtian (Figure 9.1b) (Quirk *et al.*, 2012). Based on salt (and overburden) structural style, the Campos Basin is divided into a proximal extensional domain (70 - 200 km wide) and a distal contractional domain (70 - 300 km wide), the latter terminating seaward in a broad (up to 37 km wide) allochthonous salt

sheet emplaced on the outer basement high (Figures 9.2b and 9.2c) (Davison, 2007; Davison *et al.*, 2012). Previous works identify rafts, salt rollers, extensional anticlines, triangular-shaped (reactive) salt walls, and collapsed diapirs in the extensional domain, with all of these structures related, in some way, to landward- and seaward-dipping, salt-detached normal faults (Demercian *et al.*, 1993; Mohriak *et al.*, 2008; Quirk *et al.*, 2012). Further seaward in the translation domain, Dooley *et al.* (2017) describe a large RSB. The contractional domain is characterized by elongate salt walls (Demercian *et al.*, 1993) and polyharmonic, salt-detached (buckle) fold belts (Cobbold and Szatmari, 1991; Dooley *et al.*, 2017).

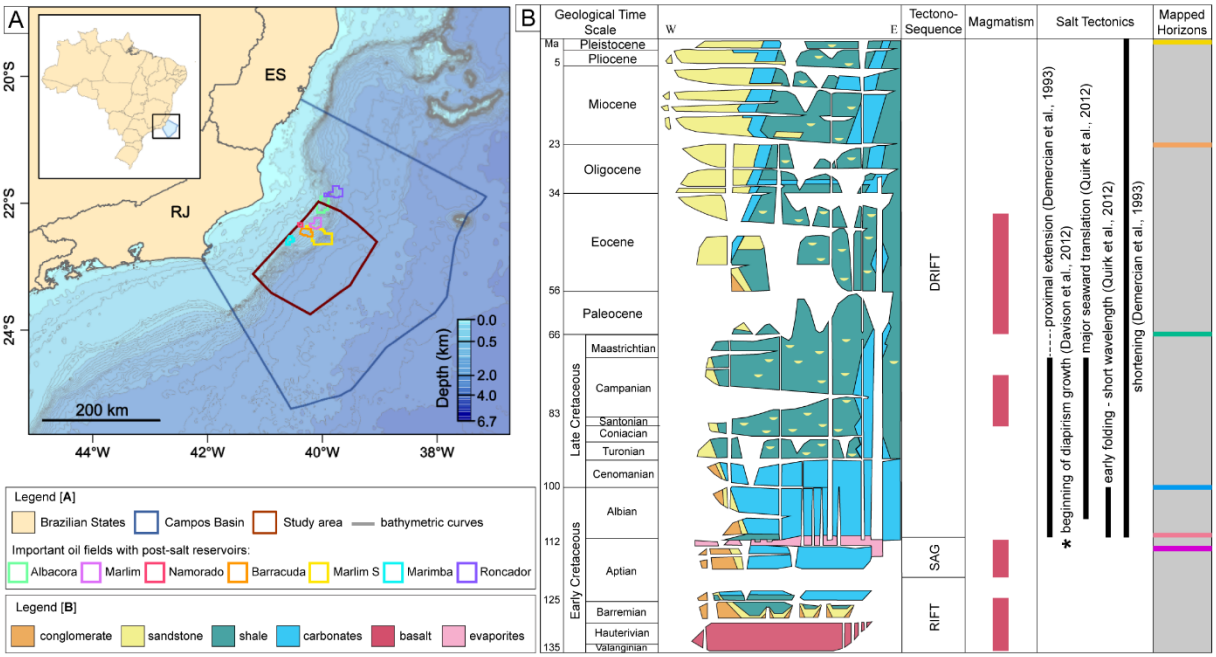

Figure 9.1. (A) Regional map showing the location of Campos Basin, the study area polygon and the main oil fields with post-salt reservoirs. (B) Simplified stratigraphic chart of Campos Basin (redrawn from Winter *et al.*, 2007), with the main magmatic events and timing of the salt tectonics from previous publications; the last column shows the mapped horizons of this study with their designed colours.

3 – Data base and methodology

Our seismic reflection database comprises 146 2D lines and one 3D volume from the ANP (Brazil's National Oil, Natural Gas and Biofuels Agency) data library, covering an area of c. 23,500 km² of the central-southern platform of Campos Basin (Figures 9.1a and 9.3). Spacing between the 2D seismic lines ranges from around 1 – 30 km. The 3D volume covers c. 2,900 km², with inlines (east-west) and crosslines (north-south) spaced 12.5 m (Figure 9.3). The seismic surveys are time-migrated (PTSM Kirchoff), zero-phase processed, with a display following SEG "normal" polarity; i.e. a downward increase in acoustic impedance is represented by a positive reflection event (i.e. white on displayed seismic profiles). All seismic lines and mapped horizons

(see below) are presented in two-way travel time (TWT) milliseconds (ms) and have not been depth-converted, meaning we describe relative rather than absolute changes in, for example, thicknesses between and within stratigraphic units, and changes in dip along seismically defined surfaces.

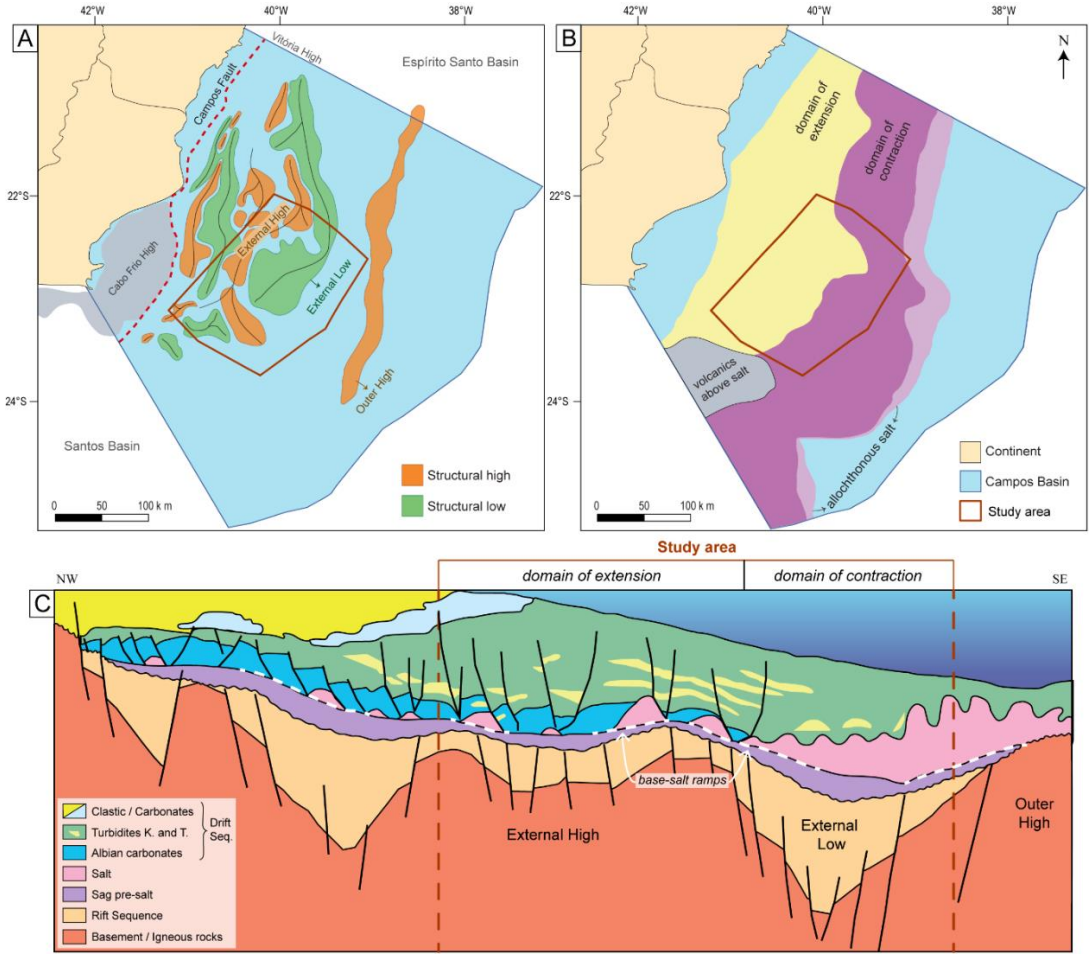

Figure 9.2. (A) Pre-salt structural framework of Campos Basin, redrawn from Guardado *et al.* (2000); Outer High and Cabo Frio High locations from Fetter (2009). (B) Salt-related structural provinces, modified from Davison *et al.* (2012); volcanics above salt location from Meisling *et al.* (2001). (C) Schematic cross section of Campos Basin, modified from Rangel *et al.*, 1994.

Within the study area there are 30 boreholes that contain well-logs (e.g. sonic travel time, bulk density, and gamma ray), and stratigraphic (i.e. age) and lithology data that help us constrain the age of the mapped horizons and the composition of the seismic-stratigraphic units they bound. These wells were tied to the seismic data through checkshot surveys. The interval velocity of the Aptian evaporites obtained from the well-logs ranges from 4000 – 7000 m/s depending on the proportion of halite, anhydrite, and potash salts. Overburden strata are defined by interval velocities ranging from 1800 – 6000 m/s due to the highly varying densities of different lithologies (e.g. mudstone, sandstones, conglomerates, carbonates) with varying porosities. We estimate that the vertical seismic vertical resolution in the interval of interest is 10 – 50 m; more specifically, 30 – 50 m within the salt layer (using a dominant frequency of 35

Hz), and 10 – 30 m within the overburden strata (considering a dominant frequency of 50 Hz). This is sufficient to map the kilometer-scale salt-related structures that form the focus of this study.

In addition to the seabed, we mapped four key horizons across the dataset: base of salt, top of salt, top Cretaceous, and top Paleogene. Where possible, we mapped the top Albian (Figure 9.1b). We mapped the top Cretaceous and top Paleogene horizons because they represent regional seismic-stratigraphic unconformities that are easily identifiable throughout the Campos Basin and which record major periods of salt-related deformation. The mapped surfaces display the present basin geometry, whereas isochron (i.e. thickness) maps derived from these surfaces show the distribution and evolution of salt-related sedimentary depocentres, allowing us to infer salt kinematics and dynamics.

Evaporites are generally defined by significantly higher seismic velocities than encasing sedimentary rocks. In time-migrated seismic sections, thick salt structures may be underlain by velocity pull-ups in the base-salt surface and underlying, sub-salt reflections. Velocity pull-ups mimic the geometry of the overlying salt structures and may erroneously be interpreted as sub-salt structural highs (Marfurt and Alves, 2015). Such seismic artifacts occur in the SE portion of the study area where high-relief salt structures are present (Figure 9.4a); we therefore manually corrected our interpretation of the base-salt horizon to compensate for these pull-ups (Figure 9.4b). We then mapped the base-salt ramps and calculated the dip-angle of these ramps in varying locations (Figure 9.4c), converting time (TWT, ms) to depth using a velocity of 4600 m/s (i.e. the average interval velocity of the underlying rocks calculated from the well logs). Local base-salt dip angles were also calculated using the same methodology (Figure 9.4d).

We chose the most representative, dip-oriented seismic profile to perform a structural restoration and develop a balanced kinematic model for the salt tectonics in the study-area. We combine decompaction and unfolding by simple vertical shear, and move-on-fault algorithms, following established restoration workflows for salt-related deformation (see Rowan and Ratliff 2012, Pichel and Jackson, 2020). The profile is restored to a gently dipping (~1°), clinoform-like seabed, characteristic of the prograding margin of the Campos Basin (cf. Figures 9.2c and 9.8). We reconstruct the approximate palaeo-seabed through time using the present seabed as a template, and local erosional unconformities and toplaps as additional constraints (cf., Pichel and Jackson, 2020). Decompaction is performed using the Sclater and Christie (1980)

function, assuming a clastic-dominated (i.e. post-Albian) overburden; this assumption is supported by lithological data provided by the available boreholes, and by previous studies (Winter *et al.*, 2007; Contreras *et al.*, 2010). Note that we did not depth-convert the time-migrated seismic profile and that the restored sections are shown with 2-3 times vertical exaggeration. Nonetheless, the restored profile balances, helping us quantify and illustrate the magnitude of gravity-driven salt-related deformation and overburden translation through time.

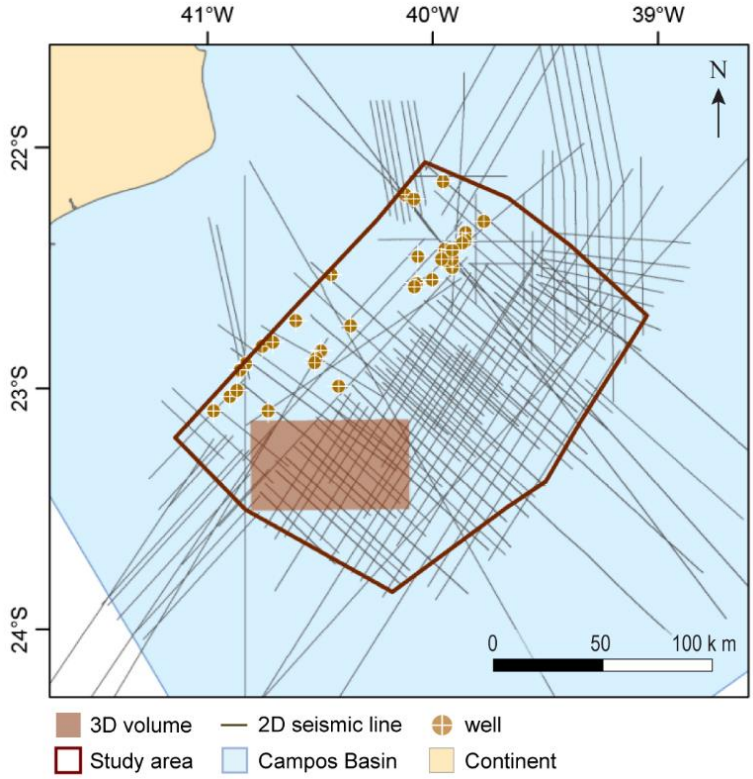

Figure 9.3. Dataset used in this study: 146 2D lines (or lines segments), one 3D volume and 30 boreholes.

4 – Base-salt structures

The base-salt surface dips regionally to the SE, with a mean dip of 2º (Figure 9.4a,b). Local changes in dip angle and direction define base-salt ramps (Figure 9.4c). In plan-view, these ramps trend NE, broadly subparallel to the margin, are locally concave- or convex-seaward, and are c. 20 – 180 km long and c. 3 – 20 km wide. The main belt of base-salt ramps define the boundary between the External High and the External Low (Figures 9.2 and 9.4b,c). These ramps have a maximum structural relief of c. 900 ms TWT (c. 2 km) and they dip seaward c. 3º – 9º (Figure 9.4c). The heights of the ramps are thus consistent we those previously reported from the Campos Basin (1.4 – 1.6 km - figure 24 in Dooley *et al.*, 2017; figure 6 in Davison *et al.*, 2012).

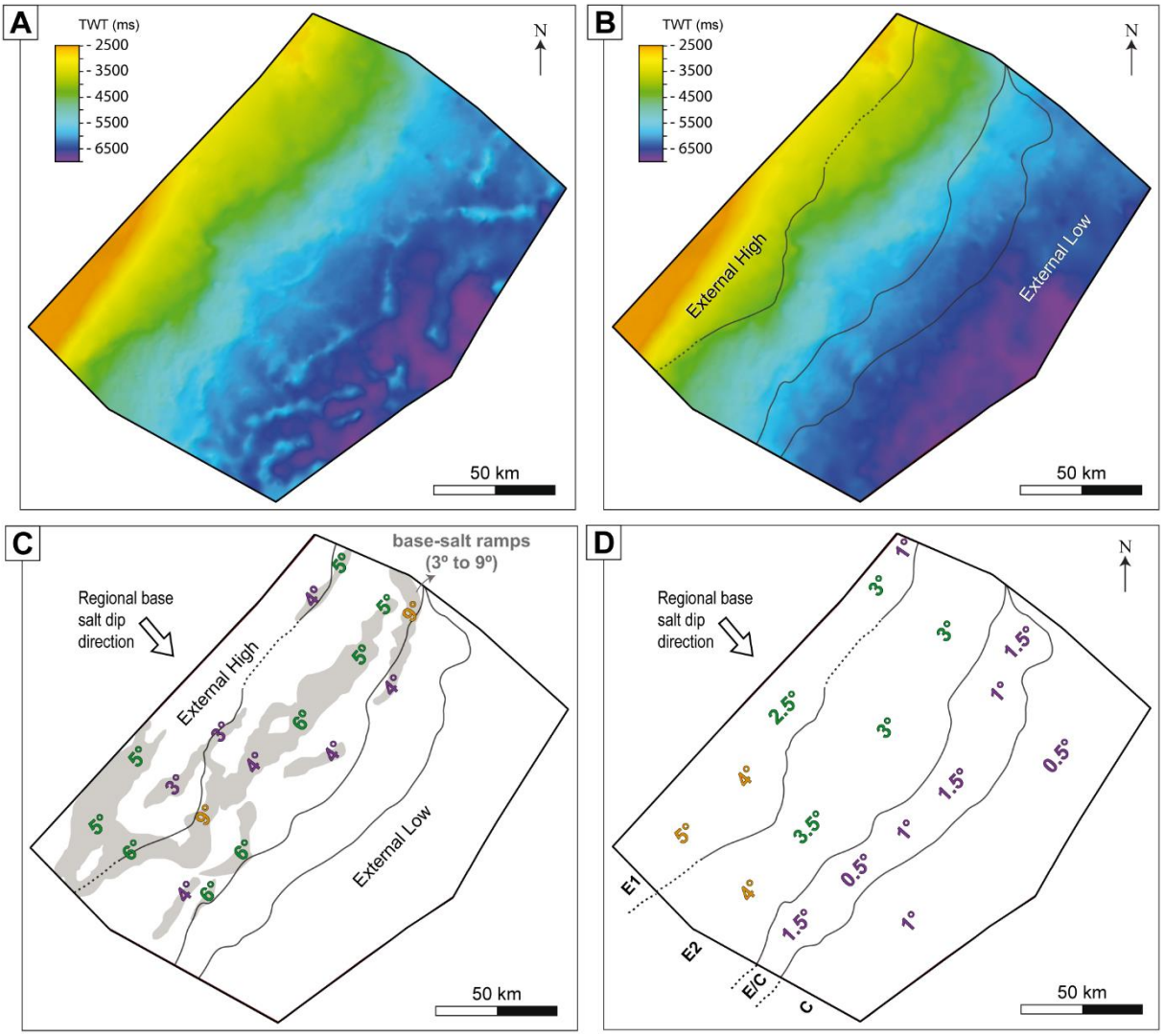

Figure 9.4. Time maps of the base-salt surface before (A) and after (B) the pull-up correction, showing doming dip to SE. (C) Mapped base-salt ramps shown in grey and their dip angles; the ramps are broadly subparallel to the margin, but with variable geometry along strike. The dip angles are plotted where they were calculated; they vary from 3º to 9º. (D) Average base-salt dip angles in different regions of each domain of deformation (shown in Figure 9.5).

5 – Structural style of the salt and its overburden

The salt structures interpreted from the salt isochron map (Figure 9.5) present varying geometries and structural styles. Most structures trend broadly NE, sub-parallel to the underlying pre-salt, rift-related ramps (Figure 9.5c). Exceptions to this occur in the SW of the study area, where salt-rollers trend N, and in the northeast, where a single E-trending salt wall is found. Salt structures are flanked by apparent primary welds or areas of relatively thin, depleted salt; in these regions, sub-salt and supra-salt strata appear to be in direct contact (white areas in Figure 9.5a).

Key overburden structures are displayed on the Top Salt to Top Cretaceous isochron map (Figure 9.6). These structures have broadly the same orientation as underlying salt structures (see detailed descriptions below), and where the underlying

salt has pierced the entire Cretaceous succession the latter is absent (white areas in Figure 9.6a,b). The types, dimensions, and interpreted origins of the salt and overburden structures are summarized in Tables 9.1 and 9.2, respectively. We now present the distribution of these structures, which define the three main domains of thin-skinned, salt-detached deformation: extensional, contractional, and multiphase.

5.1. Extensional domain (E)

5.1.1. Description

The extensional domain trends NW and corresponds to nearly half of the study area, with a minimum average width of c. 77 km (Figure 9.5). All the major base-salt ramps described above occur within this domain, which results in relatively high average values of base-salt dip (c. 2.5°-4.5°) that increase south-westwards (Figure 9.4d). The base-salt dips increase south-westwards because, even though they maintain the same average dip, they become wider and/or more numerous (Figure 9.4c). Seaward (i.e. south-eastwards) changes in salt and overburden structures within the extensional domain define two subdomains: E1 (proximal) and E2 (distal).

Subdomain E1 defines the proximal, upslope portion of the extensional domain. In E1 the salt is relatively thin (0-300 ms, with an average of 80 ms), with limited top-salt relief and thickness variations (Figures 9.5, 9.6 and 9.7). To the southwest, we observe small (200 to 300 ms high) salt rollers bounded by seaward-dipping, salt-detached normal faults (Table 9.1, Figure 9.7d,e,f), and tilted raft-like blocks of Albian strata (Table 9.2). Where salt rollers are absent, for example along-strike to the northeast, salt is largely depleted (<50 ms) to (apparently) welded, or it forms small pillows (Figure 9.7a,b). The mean base-salt dip is 3º seaward, locally reaching 6º on well-defined, NE-trending ramps (Figures 9.4c,d and 9.8).

Subdomain E2 occurs immediately downdip of E1. Salt thickness varies from 0-1450 ms, and numerous elongate, NE-to-N-trending structures are visible on the salt thickness map (Figure 9.5). The average base-salt dip is 3º, with NE-trending base-salt ramps dipping up to 9º, defining linear to locally concave- or convex-seaward geometries (Figures 9.4c,d and 9.8). The key salt and overburden structures in E2 are: (a) salt rollers and their associated salt-detached growth faults/rollover systems, which can laterally pass into RSBs or extensional turtle structures; and (b) collapsed diapirs overlain by grabens and half-grabens (Tables 9.1 and 9.2; Figure 9.7).

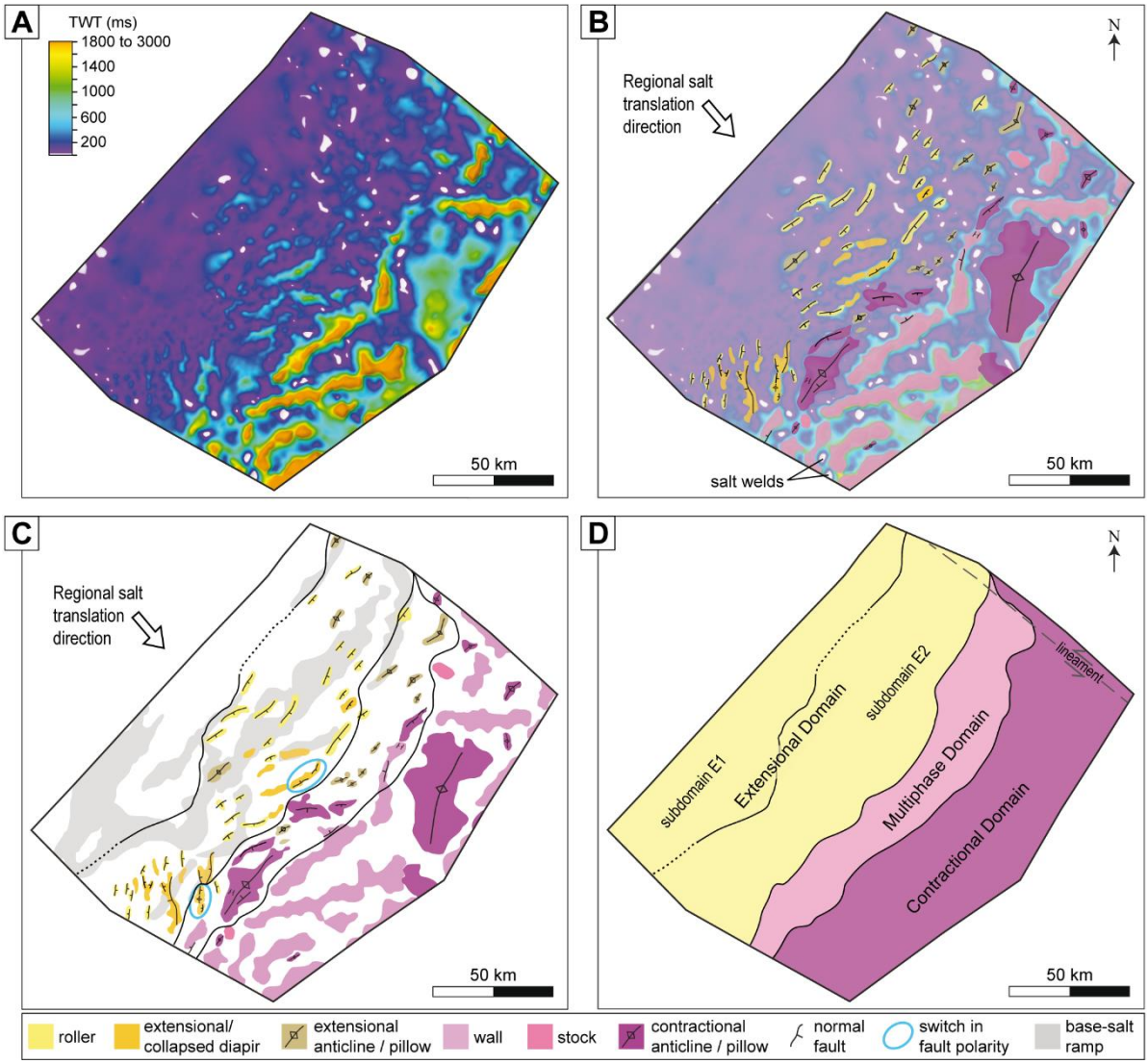

Figure 9.5. Salt isochron thickness map (A) with the interpreted salt structures in (B); areas of minimal thickness shown in white represent regions where salt is completely to incompletely welded. (C) Distribution of the salt structures across the study area, with the location of base-salt ramps in grey – colours of the structures within the multiphase domain follow their primary deformation. (D) Location of the domains of thin-skinned deformation; the boundary between E1 and E2 is partially dotted due to the scarcity of seismic lines in this region.

Table 9.1. Salt structures, their description, dimensions and genetic interpretation.

Structure	Example	Description (e.g. geometry, distribution, and overburden seismic-stratigraphy)	Dimension	Genetic Interpretation
Extensional salt rollers	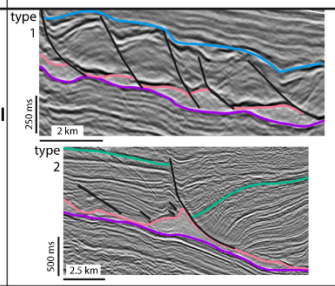	Relatively narrow, low-relief salt diapirs, bound on at least one side by a salt-detached normal fault (see Table 2). Strata in the footwall of this fault are up-turned and concordant with top salt; in the hanging wall, strata are in faulted contact with the salt. In upslope positions (Type 1 rollers; see column to right) they are relatively small, typically underlying and separating rafts (Table 2), and may be separated by primary welds; in downslope positions (Type 2 rollers; see column to right) they occur next to landward- or seaward-dipping salt-detached normal faults and associated extensional turtle structures (Table 2) or rollover systems. In toe-of-slope positions, salt rollers can also occur on top of salt anticlines.	(1) 1–2 km wide; up to 200 ms TWT high. (2) 4.7–20 km long; 1.5–5.5 km wide; up to 600 ms TWT high.	In upslope positions the seaward flow of salt drives overburden extension, which is accommodated by normal faulting. Differential loading of salt drives reactive diapirism and the formation of salt rollers that rise into the immediate hangingwall of salt-detached faults. In toe-of-slope positions, in the multiphase domain, later extension and faulting of salt contractional anticlines locally drove reactive rise and the formation of salt rollers. *Source*: Fort et al. (2004); Brun and Mauduit (2009); Jackson and Hudec (2017).
Extensional/ collapsed diapiric salt walls	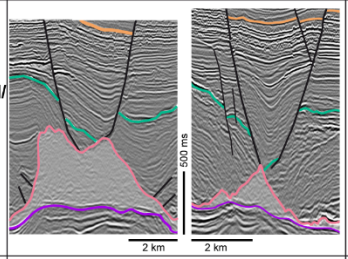	Triangular-shaped diapirs defined by wide bases and narrow crests. They are located in downslope positins, adjacent to Type 2 rollers. Diapirs are flanked and overlain by small, inward-dipping, salt-detached normal faults (Table 2). Flanking strata onlap or downlap onto, and often upturned against, top salt. Diapir crests are either rounded or U-/V-shaped; in the latter case, the shape arises due to the presence of horn-link cusps located in the hangingwall of overlying crestal faults (cf. salt rollers). The size and orientations of the faults vary, but they typically define crestal grabens filled with growth strata.	5.3–12.3 km long; 1.4–5 km wide; up to 1300 ms TWT high.	Thin-skinned extension of the overburden causes normal faulting and the formation of grabens and half-grabens. Differential loading of underling salt drives reactive diapirism and salt wall formation. Continuing extension may cause diapirs to widen until the salt source layer becomes depleted and/or strongly restricted; diapir crests then begin to sag, driving normal faulting of and graben formation in overburden rocks. *Source*: Vendeville and Jackson (1992a,b).
Salt anticlines and pillows	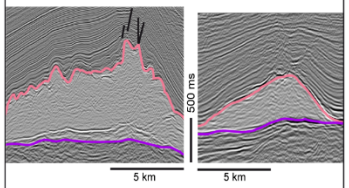	Convex-up bodies of salt that have a concordant (i.e. non-diapiric) contacts with overburden strata. These structures occur across the entire study area; their dimensions increase towards the the downdip end. In downslope positions these structures are the core of extensional turtle structures (Table 2). Overburden commonly faulted (salt-detached normal faults - Table 2) and folded (extensional anticlines and contractional folds - Table 2).	*extensional*: up to 15.8 km long up to 3.5 km wide up to 450 ms TWT high *contractional* 5.5–50.8 km long; 2.7–27 km wide; up to 1800 TWT ms high; λ = 10–25 km	Depending on their plan-view length-to-width ratio, these salt bodies are called pillows (ratio <2) or anticlines (ratio >2). In downslope they are associated to extensional turtle structures (Table 2), originated by thin-skinned extension (extensional salt anticlines and pillows). At the toe of slope and towards the downdip end of the study area, the structure form due to overburden shortening and salt inflation immediately seaward of base-salt ramps due to a salt flux imbalance associated with thickness variations of the salt layer (contractional salt anticlines and pillows). *Source*: Dooley et al. (2017) and (2018); Jackson and Hudec (2017).
Diapiric salt walls and stocks	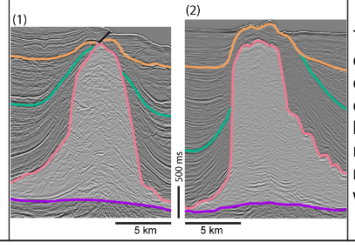	Triangular to columnar salt structures in cross-section, characterised by discordant (i.e. diapiric) contacts with their overburden. In map-view these bodies are either sub-circular or elongated, located downdip the toe of slope. Often capped by an arched and faulted roof. High-relief structures underlie relief at the present seafloor. Commonly flanked by upturned megaflaps (sensu Rowan et al., 2016) of overburden strata which can be partially eroded by exposure (see example 2).	*stocks*: up to 10 km long; up to 5.3 km wide; up to 1500 ms TWT high. *walls*: 14–72 km long; 2.2–14.4 km wide; up to 3000 ms TWT high.	Salt diapirs can grow via a range of mixed processes. Those in the contractional domain record mainly two mechanisms of diapiric rise: (a) passive diapirism, associated with syndepositional downbuilding of flanking diapirs); and (b) active diapirism, caused by regional thin-skinned compression, which also leads to overburden arching and faulting. Megaflaps may record a preceding stage of salt inflation and formation of a pillow or anticline, which was then broken through by a growing diapir. *Source*: Rowan et al. (2016); Jackson and Hudec (2017).

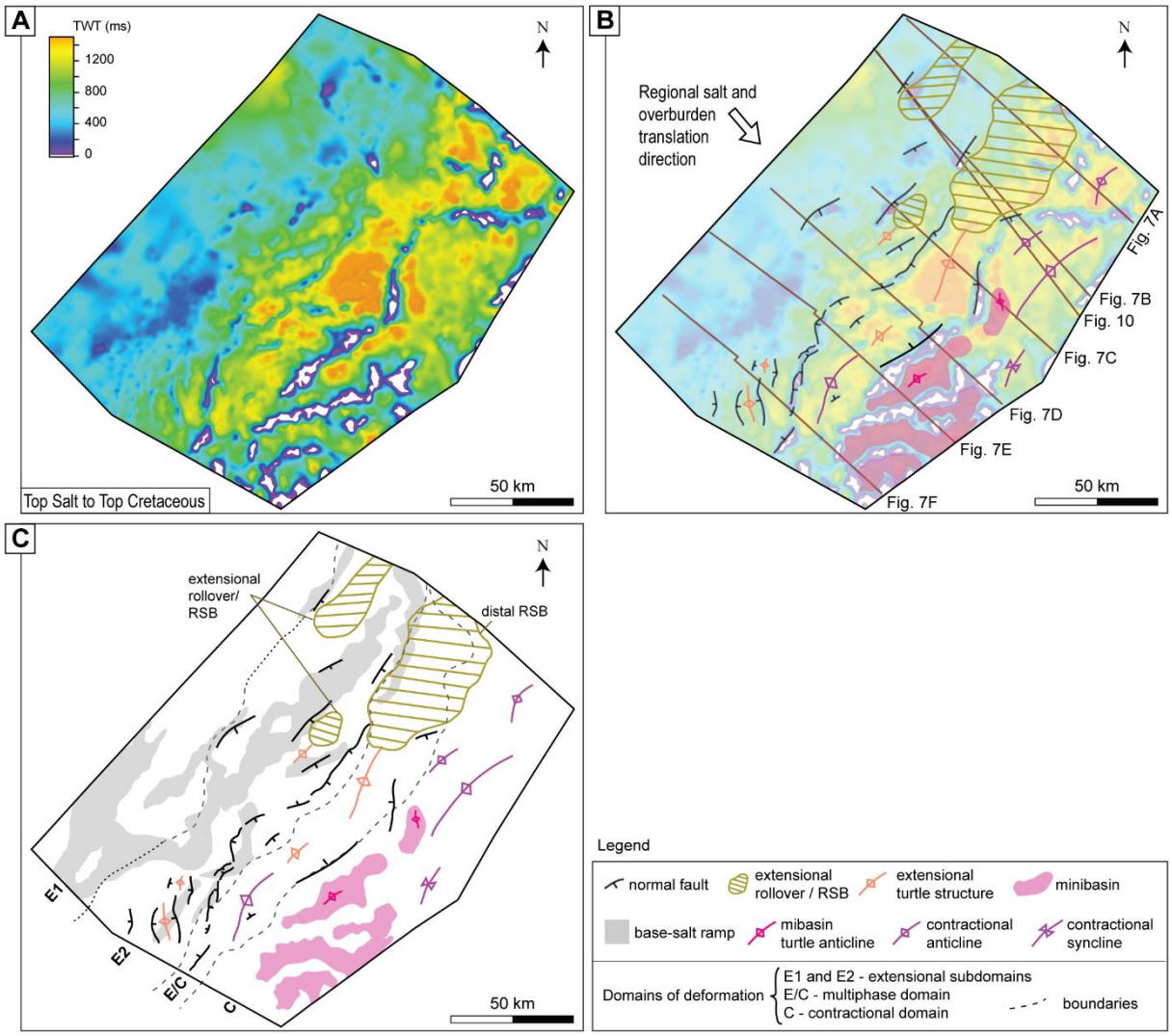

Figure 9.6. (A) Isochron thickness map from the Top Salt to the Top Cretaceous horizon. (B) Interpreted overburden structures related to salt tectonics onto the isochron thickness map of 6A; this map also shows the location of the seismic lines of figures 7 (and 8) and 10. (C) Distribution of the interpreted overburden structures in 6B, with base-salt ramps in gray and the domains of thin-skinned deformation.

Table 9.2. Salt-related overburden structures, their description, dimensions and genetic interpretation.

Structures	Example	Description	Dimension	Age of Growth Strata	Genetic Interpretation
Rafts	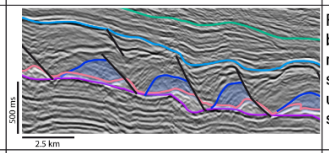	Rotated blocks (rafts) of overburden strata bound by salt-detached normal faults, separated by salt rollers and/or trough-like deposits of younger, synkinematic strata (see Table 1). Typically underlain by salt welds. Rafts occur updip in the study area.	2–3.2 km wide; 200–300 ms TWT high.	Early to mid-Albian.	Formed due to extensional dismemberment of overburden strata during gravity gliding. Synkinematic depocentres form between rafts. *Source*: Quirk et al. (2012); Jackson and Hudec (2017).
Salt-detached normal faults	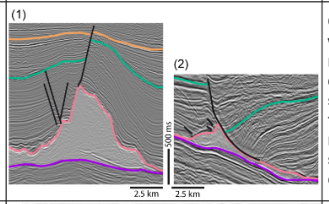	Overburden-restricted normal faults that detach within salt. Bound salt rollers and associated rollover systems (example 2) and rafts, and can displace overburden strata capping the crests of salt anticlines (example 1) and as well as various types of diapirs (Table 1). May offset strata filling ramp-syncline basins. The faults dip landward- or seaward-, and are either listric or planar in cross-section.	up to 37 km long; up to 750 ms TWT of vertical throw.	*subdomain E1*: Albian; *subdomain E2*: Albian–mid-Neogene; *E/C Domain*: Albian–mid-Neogene; *Cont. Domain*: Albian–Recent.	Salt-detached normal faults accommodate thin-skinned extension of overburden. They can form: (i) in the proximal domains (ie. E1 and 2) due to the seaward flow of salt and associated overburden stretching; (ii) in the distal domain (i.e. C domain) due to outer-arc bending-related stretching of overburden above salt pillows and anticlines; (iii) due to overburden stretching above extensionally collapsing diapirs. *Source*: Fort et al. (2004); Jackson and Hudec (2017).
Extensional turtle structures	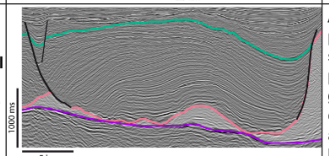	Anticlines bounded by oppositely and inward-dipping, salt-detached normal faults that also bound salt rollers and walls. Anticlines cored by salt pillows and anticlines (Table 1). Anticline-related growth strata are asymmetric, thickening towards one or both flanking faults. In map-view, the these anticlines are elongated and trend parallel to their bounding normal faults.	up to 32.1 km long; up to 30 km wide; up to 1500 ms TWT high.	Albian–Early Paleogene.	Salt-detached normal faults with opposite dips are generated by thin-skinned extension. Salt flow into fault footwalls causing local overburden collapse, and ultimately the formation of a salt-cored anticline called a 'turtle'. *Source*: Lundin (1992); Quirk et al. (2012).
Ramp syncline basins	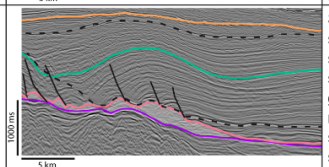	Synclinal basins located in the hanging-wall of salt-detached normal faults and associated rollover systems. Typically located above and slightly seaward of seaward-dipping base-salt ramps. RSB growth strata dip and thicken landward, defining a monoclinal geometry. Downdip, the detachment surface (lower black dotted line) is marked by strata onlap or apparent downlap.	16–63.7 km long; 10–35 km of translation.	Albian–mid-Paleogene.	RSBs that form in response to the downdip translation of salt and its overburden across major base-salt ramps. The lateral distance between the top of the ramp and the seaward--most onlap (or apparent downlap) termination defines the magnitude of translation. *Source*: Jackson and Hudec (2005); Jackson and Hudec (2017).
Minibasins	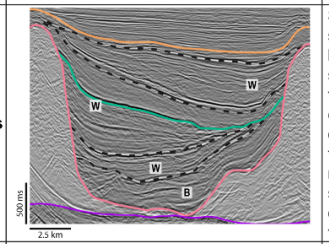	Synclinal depocentres bounded by thick, diapiric salt. Depocentre strata thin towards and onlap onto bounding diapirs. Basal depocentre strata are symmetric, defining "bowl-shaped" geometries (B); these can be overlain by more asymmetric wedges of strata (W) thicken towards onto of the bounding diapirs. Basal megaflaps are common. Depocentres are floored by salt or a primary weld. Locally, multi-wavelength folds are developed within basal strata. In map-view, these depocentres are elongated parallel to bounding salt walls. Depocentres can be isolated or partially connected.	amplitude: 35–110 ms TWT and up to 1500 ms TWT λ = 0.5–2.5 km and 10–25 km	Albian–Top Paleogene.	Minibasins formed by density-driven subsidence of overburden into underlying salt. Subsidence may occur during lateral shortening. Bowl-shaped stratal packages (B) record symmetrical subsidence, whereas wedge-shaped pacakges (W) record asymmetric subsidence and minibasin tilting. Abrupt shifts in wedge depocentre location may reflect syn-subsidence shortening, which causes one bounding diapir to inflate more rapidly than the other. *Source*: Jackson and Hudec (2017); Jackson et al. (2019).
Contractional folds	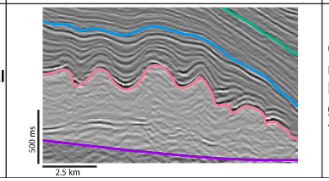	Convex-up bodies, typically polyharmonic, with multiwavelength growth composed by early high-frequency folds and a larger wavelength growth. There can be faults dissecting the crest of the antiforms.	25–52.3 km long; 4.3–17 km wide; up to 1500 ms TWT deep.	Early Albian–Early Neogene.	High frequency folds formed when the overburden was thin, due to shortening immediately seaward of base-salt ramps in response to a salt flux imbalance associated with thickness variations of the salt layer. Subsequent regional thin-skinned compression promoted fold growth in larger wavelength. *Source*: Cobbold and Szatmari, (1991); Fort et al. (2004)

In the NE portion of the study area, salt rollers and extensional rollovers dominate, and these can pass laterally into RSBs (Figure 9.6; Figure 9.7a,b) that are locally underlain by extensional anticlines or pillows (Figure 9.7a -structures 1; Figure 9.7b - structure 1). The central and south-western regions of the study area are characterized by salt rollers bounded by seaward- or landward-dipping growth faults and flanking rollover systems (Figure 9.7c to f); these structures occasionally define extensional turtle structures (Figure 9.7c - structure 2; Figure 9.7d - structure 2) or grabens above extensionally collapsed diapirs (Figure 9.7d - structure 3, Figure 9.7f - structures 1 and 2). There are also more complex extensional diapirs that may have grown from lower-relief rollers in response to periodic switches in the polarity of their bounding faults (see *flip-flop salt walls* of Quirk *et al.*, 2012; extensional diapir in Figure 9.9, inactive fault segment indicated by a white line near the diapir pedestal). Switches in fault polarity across extensional salt walls can be observed in the salt structure map (Figure 9.5c - blue ellipses). Salt rollers occur close to or above base-salt ramps (Figure 9.7d,e,f), whereas collapsed diapirs and grabens tend to overlie areas where the base-salt is flatter (Figure 9.7d,f). The extensional turtle structures are wider and longer in the central region in comparison to the north-eastern and south-western regions, where the growth faults are also longer (Figure 9.6b,c). The extensional turtle structures are associated with Cenomanian to Maastrichtian growth strata, and they are cored by salt anticlines or pillows (Figure 9.7d - structure 2; Figure 9.9), or folded Albian strata above welded salt (Figure 9.7c - structure 2). The salt-detached normal faults bounding salt rollers, or those flanking graben formed above collapsed diapirs, are associated with Albian to mid-Neogene growth strata (Table 9.2 and Figure 9.7).

5.1.2. Interpretation

The structures within the extensional domain vary along dip, defining the two previously described subdomains (E1 and E2), and along strike. According to Fort *et al.* (2004), the types of extensional structures formed during salt-detached gliding reflect variations in the strain rate within the ductile salt layer, with the strain rate being mainly controlled by the basal slope angle (i.e. the local dip of the base-salt surface). Relatively steep and gentle base-salt angles are associated with relatively high and low ductile strain rates, respectively. Fort *et al.* (2004) demonstrate that salt rollers form on steeper basal slopes, whereas diapirs dominate on gentler slopes. This general model appears to apply to the Campos Basin, with salt rollers overlying base-salt ramps in both subdomains (i.e. in E1 in the central and south-western parts of the study area, and in E2 along-strike of the entire studied part of the margin). The specific length

and steepness of the these ramps also appeared to control the specific type of overburden structure that formed, i.e., narrow and steep base-salt ramps in the north-eastern portion of the study area favoured the formation of extensional rollovers/RSBs (Figures 9.7 and 9.8 a,b,c), whereas wider ramps in the central and south-western parts of the study area favoured the formation of rollovers that pass laterally into extensional turtle structures (Figures 9.7 and 9.8 c-f).

In contrast, areas characterised by gentler base-salt angles are associated with extensional diapirs, that may ultimately widen and collapse with ongoing stretching (Fort *et al.*, 2004 - see their figure 7). Such structural styles are seen in the centre and SW of our study area, where collapsed diapirs tend to develop away from base-salt ramps, on shallower basal slope angles (Figure 9.7 and 9.8 d,e,f), and often in association with extensional turtle structures (Figures 9.7d - structure 2, Figure 9.9 - west end of the lines). In summary, we suggest that subdomain E1 corresponds to the *sealed tilted blocks* subdomain of Fort *et al.* (2004), and E2 is at the transition between the *growth fault and rollover systems* and *extensional diapirs* subdomains.

Finally, the formation of RSBs is conventionally defined as a product of translation of salt and its overburden across major base-salt ramps (Table 9.2) (e.g. Jackson and Hudec, 2005, 2017; Pichel *et al.*, 2018). The RSBs in the extensional domain here are slightly unusual in that they form along-strike of extensional rollovers (Figure 9.7a - structure 1, 9.7b - structure 1; Figure 9.10), which means that translation of salt and its overburden downdip is partially accommodated by the coeval formation of and slip on, salt-detached faults (Evans *et al.*, 2021).

5.2. Contractional domain (C)

5.2.1. Description

The contractional domain defines the downslope portion of the study area. This domain trends NE and has an average width of c. 39 km, being widest in the NE where it is up to 75 km wide, just to the north of a NW-trending, basement-involved lineament (Figure 9.5d). Base-salt is smoother in the contractional domain than in the extensional domain, with the mean seaward dip varying from 0.5º to 1º (Figure 9.4d). Salt is thickest in this domain (up to 3000 ms), being arranged into NE-to-E-trending broad salt anticlines underlying buckle folds, and salt walls and stocks (Table 9.1 and Figure 9.5) that are flanked by minibasins (Table 9.2 and Figure 9.6b,c).

One of the most prominent structures within the contractional domain is a large, salt-detached fold belt (51 km long and up to 27 km wide; Figure 9.5), comprising stacked, multiwavelength folds, i.e., relatively short-wavelength (0.5-2.5 km) and low-amplitude (35-110 ms) folds at top salt pass upwards into longer wavelength (10-25 km) and higher-amplitude (up to 650 ms) folds in the overburden (Figure 9.7b - structure 4; Figure 9.7c - structure 5). Similar structures are described by Davison *et al.* (1996), Demercian *et al.* (1993), Dooley *et al.* (2017) and Erdi and Jackson (2021).

Diapiric structures, commonly salt walls, predominate in the contractional domain (Figure 9.5c). These structures are up to 72 km long and 14 km wide, and are triangular to columnar shaped in cross-section (Table 9.1). The diapirs are often capped by an arched or uplifted roof (Figure 9.7a - structure 3, 9.7b - structure 5, 9.7d - structure 7, 9.7e - structure 5, 9.7f - structure 3). Upturned megaflaps (*sensu* Rowan *et al.*, 2016), frequently topped by erosional truncations flanking one side of the diapirs, are also common (Figure 9.7a - structure 3, 9.7e - structure 8, 9.7f - structures 3 to SE and 6), and they are sometimes ornamented by now-rotated and uplifted trains of the high-frequency buckle folds described above (Figure 9.7d - structure 7).

Post-salt Cretaceous overburden is thin to absent over salt walls in the contractional domain, but is very thick (up to 1800 ms) in the flanking minibasins (Figures 9.6 and 9.7d,e,f). Minibasins occur in the centre and SW portions of the study area (Figure 9.6c), where they are overall symmetric (Figure 9.7e - structures 6) or asymmetric (Figure 9.7d – structure 6) and are floored by salt (Figure 9.7f - structures 4) or primary welds (Figure 9.7f - structure 5). The minibasins can sometimes assume an antiformal, turtle-like shape (Figure 9.7c - structure 4).

5.2.2. Interpretation

We interpret that the high-frequency buckle folds formed by thin-skinned shortening when the overburden is thin (Cobbold and Szatmari, 1991; Fort *et al.*, 2004; Dooley *et al.*, 2017), meaning contraction started soon after salt deposition (i.e. during the earliest Albian; cf. Demercian *et al.*, 1993; Quirk *et al.*, 2012 - Figure 9.1c). Early, short-wavelength folds at the base of the polyharmonic folds form when the overburden is thin, either by local variations in salt flux across a seaward-dipping ramp (Dooley *et al.*, 2017), or by regional shortening (Fort *et al.*, 2004). After the formation of these early folds, the strength of the folded layer increases in response to synkinematic sedimentation, resulting in a progressive increase of fold wavelength (Cobbold and Szatmari, 1991; Fort *et al.*, 2004). Shortening then becomes concentrated within the growing anticlines, trapping and pinching salt within the anticlinal cores and leading to

the generation of contractional diapirs (see Figure 9.7d - structures 7 and 8) (Fort *et al.*, 2004; Rowan *et al.*, 2016 – see their figure 13). Shortening-driven active rise of these diapirs resulted in the uplift and outward-tilting of the flanking megaflaps and arching of their roofs (Table 9.2) (Jackson and Hudec, 2017) Diapirs formed in this way can subsequently rise passively if they reach the free surface (Jackson and Hudec, 2017).

Not all diapiric structures in the study area have geometric or seismic-stratigraphic features diagnostic of their formation due to thin-skinned shortening nor extension, suggesting they largely grew in response to passive diapirism (e.g. Figure 9.7d - structure 7). However, we interpret that these structures are kinematically part of the contractional domain given they are spatially associated with contractional structures and were thus likely triggered by (or are associated with) shortening.

Minibasins form primarily by due to subsidence of overburden into underlying salt. This subsidence is load-driven (i.e. overburden sinks and salt is expelled laterally), recorded by the deposition of bowl-shaped, symmetrical packages, or wedge-shaped, asymmetrical packages of sedimentary strata (Table 9.2). Abrupt shifts in the wedges depocentres locations (Figure 9.7e - structure 6a; 9.7f - structure 5; Table 9.2) may reflect coeval lateral shortening, which causes one bounding diapir to inflate more rapidly than the other (Jackson *et al.*, 2019). Turtle anticlines within minibasins (Figure 9.7c - structure 4) originate due to partial or full depocentre inversion caused by minibasin welding at the minibasin centres, and the onset of subsidence and salt expulsion at their flanks (Trusheim, 1960; Peel, 2014).

5.3. Multiphase domain (E/C)

5.3.1. Description

This domain is located between the extensional and contractional domains, presently located at the toe of the ramp between the External High and External Low. The domain has a mean width of 25 km (Figure 9.5) and base-salt has average seaward dip of 0.5º to 1.5º (Figure 9.4d). Salt thickness in the multiphase domain ranges from 0-2100 ms, commonly composing NE-trending, irregular to elongated structures, and more rarely, N- and E-trending structures (Figure 9.5).

In the NE, this domain is fundamentally translational (or transitional), characterized by a large ramp syncline basin (RSB) (Figure 9.6c) that is locally associated with salt rollers of subdomain E2 (Figure 9.7b - structure 2, 9.7c - structure

1; Figure 9.10). Along-strike to the southwest, the multiphase domain is characterized by three types of salt structures with a hybrid extensional-contractional evolution. The most common type consists of contractional anticlines, which were subjected to later extension and normal faulting (Figure 9.7d - structure 4) that locally drove reactive rise and formation of salt rollers (Figure 9.9 - structure 2) and overlying grabens (Figure 9.7b - structure 3). The second most frequent type of structure comprises diapirs with passive and active growth histories, and which are overlain and partly flanked by landward-dipping normal faults that displace the diapir roof (Figure 9.7c - structure 3; Figure 9.7d - structure 5) and that may bound extensional turtle structures (Figure 9.7c - structure 3). Lastly, we observe an extensional diapir that was subsequently squeezed, with the latter phase of active diapirism driving arching and normal faulting of the diapir roof (Figure 9.9b - structure 1) or folding and uplift of strata above the collapsed diapir graben (Figures 9.9c – structure 3, and 9.7f - structure 2, between the Top Cretaceous and Top Paleogene).

5.3.2. Interpretation

Like the smaller RSBs in the extensional domain, the large RSB in the multiphase domain records horizontal translation, which is partially accommodated by the formation of salt-detached faults (Figure 9.7b - structure 2, 9.7c - structure 1; Figure 9.10). The balanced kinematic model in Figure 10 shows the hybrid origin of these structures (see also section 6).

The contractional anticlines that were subjected to later extension and normal faulting of the multiphase domain have two alternative origins. The first is that salt and its overburden translated across two seaward-dipping, base-salt ramps, with an anticline initially forming across the contractional hinge of the first ramp, before this fold was subsequently extended above the extensional hinge of the second. Schematic illustrations in Figure 9.10f,g elucidate this mechanism. During the early Albian, salt flow across the updip base-salt ramp caused active salt upwelling across the contractional hinge at its base, folding the prekinematic strata (Figure 9.10g – structures 5 and 6). Further translation across the downdip ramp reactivated the antiform in response to extension, generating two normal faults and triggering reactive diapirism (Figure 9.10f – structure 5). This multiphase deformation mechanism may also be applied to smaller structures in this domain (Figures 9.5c, 9.7b - structure 3, 9.7d - structure 4), which record deformation ceasing by the end of the Cretaceous (Figure 9.10 – structure 5). Complex salt structure with a similar origin and evolution are documented in the Kwanza Basin, offshore Angola (Erdi and Jackson, 2021 – see

their figure 9b), in the Santos Basin, offshore Brazil (Pichel *et al.*, 2019a), and from numerical models (Pichel *et al.*, 2019b).

The second origin for the formation of contractional anticlines that were subjected to later extension is the seaward migration of extension through time, resulting in extensional inversion of previously contractional structures (Brun and Fort, 2011). Downdip migration of extension occurs after grounding of updip structures due to salt welding and/or margin progradation. This model may apply to the largest contractional structure to the SW (Figures 9.5c, 9.9 - structure 2). This structure initially grew into a multiwavelength salt anticline during the Albian and Late Cretaceous (see section 5.2.2), and later was extended, locally developing salt rollers as indicated by the presence of salt-detached normal faults associated with Paleogene growth strata (Figure 9.9 - structure 2). The salt was welded updip of the structure so that the system became pinned further updip whilst the downdip salt anticline was still able to translate and extend. The weld-driven migration of extension may also account for the evolution of diapirs that witnessed phases of active and passive growth, given these structures are associated with relatively young (late Cretaceous – Paleogene) salt-detached normal faults (Figure 9.7c - structure 3, 9.7d - structure 5) that likely formed after the adjacent primary welds.

Finally, in the SW of the multiphase domain there is one extensional diapir that underwent later contraction (Figure 9.9 - structure 1). Differential salt flow along base-salt steps may have caused the later contraction of the extensional diapir. The abundance of magmatic intrusions and intense faulting in the south-west part of the study area (Figures 9.7e,f, and 9.9) may also, in some way, have influenced the complex evolution history of this structure.

(next two pages)

Figure 9.7. nterpreted dip lines in the north (A), (B), centre (C), (D), and south (E), (F) of the study area, with the interpreted seismic horizons, salt and overburden structures, and domains of deformation; the map left from (C) shows the locations of the lines onto the interpreted salt structures. Salt and overburden structures are numbered to facilitate indications in the text. The dotted white line in (F) represents the shift from bowl-shaped (B) minibasin to wedge-shaped (W). Seismic data supplied by ANP.

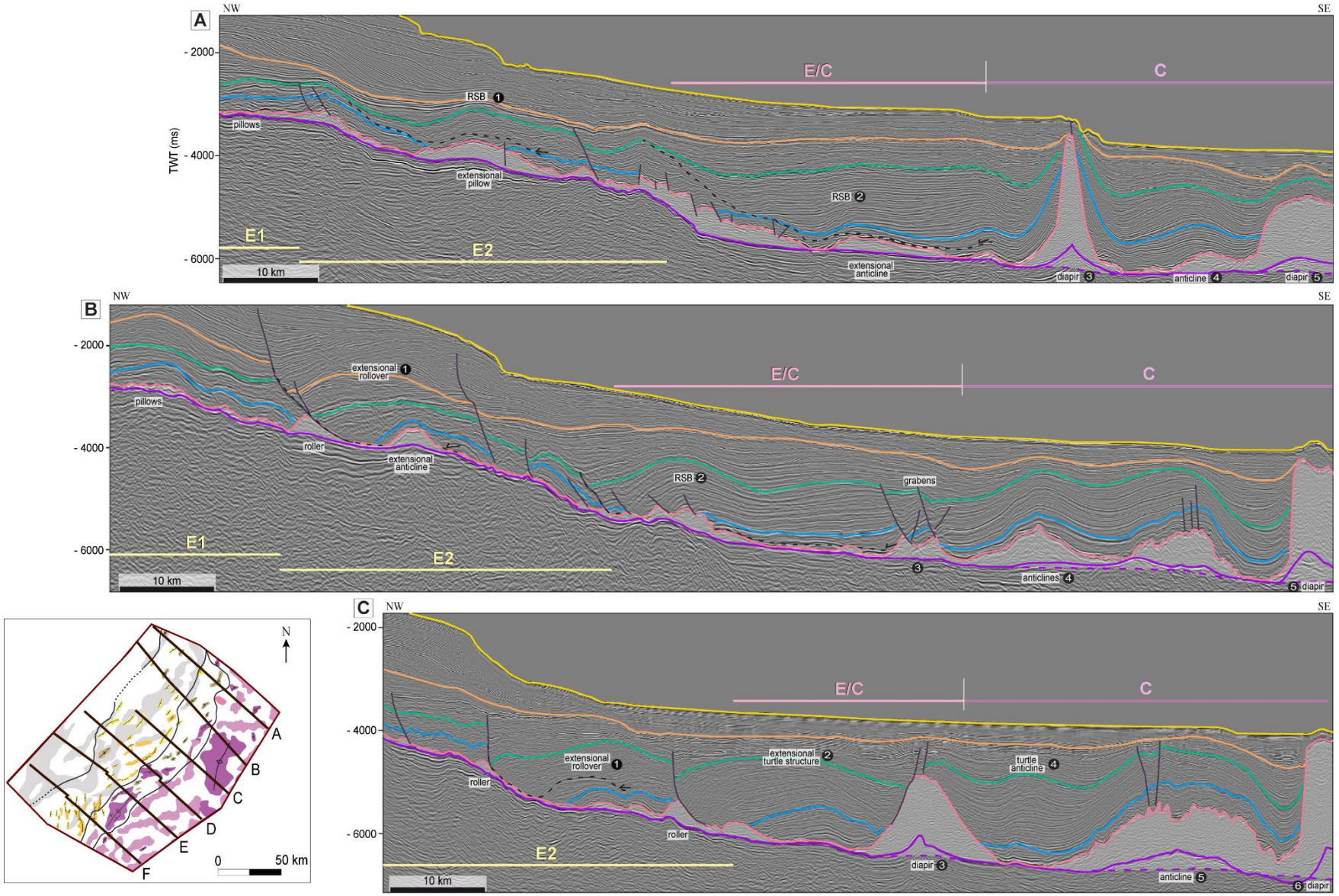
A
NW
SE
- 2000
- 4000
- 6000
TWT (ms)
E/C
C
RSB 1
pillows
extensional pillow
RSB 2
E1
E2
10 km
extensional anticline
diapir 3
anticline 4
diapir 5
B
NW
SE
- 2000
- 4000
- 6000
extensional rollover 1
pillows
roller
extensional anticline
E/C
C
RSB 2
grabens
E1
E2
10 km
3
anticlines 4
5 diapir
C
NW
SE
- 2000
- 4000
- 6000
E/C
C
extensional rollover 1
extensional turtle structure 2
turtle anticline 4
roller
roller
E2
10 km
diapir 3
anticline 5
6 diapir
N
A
B
C
D
E
F
0
50 km

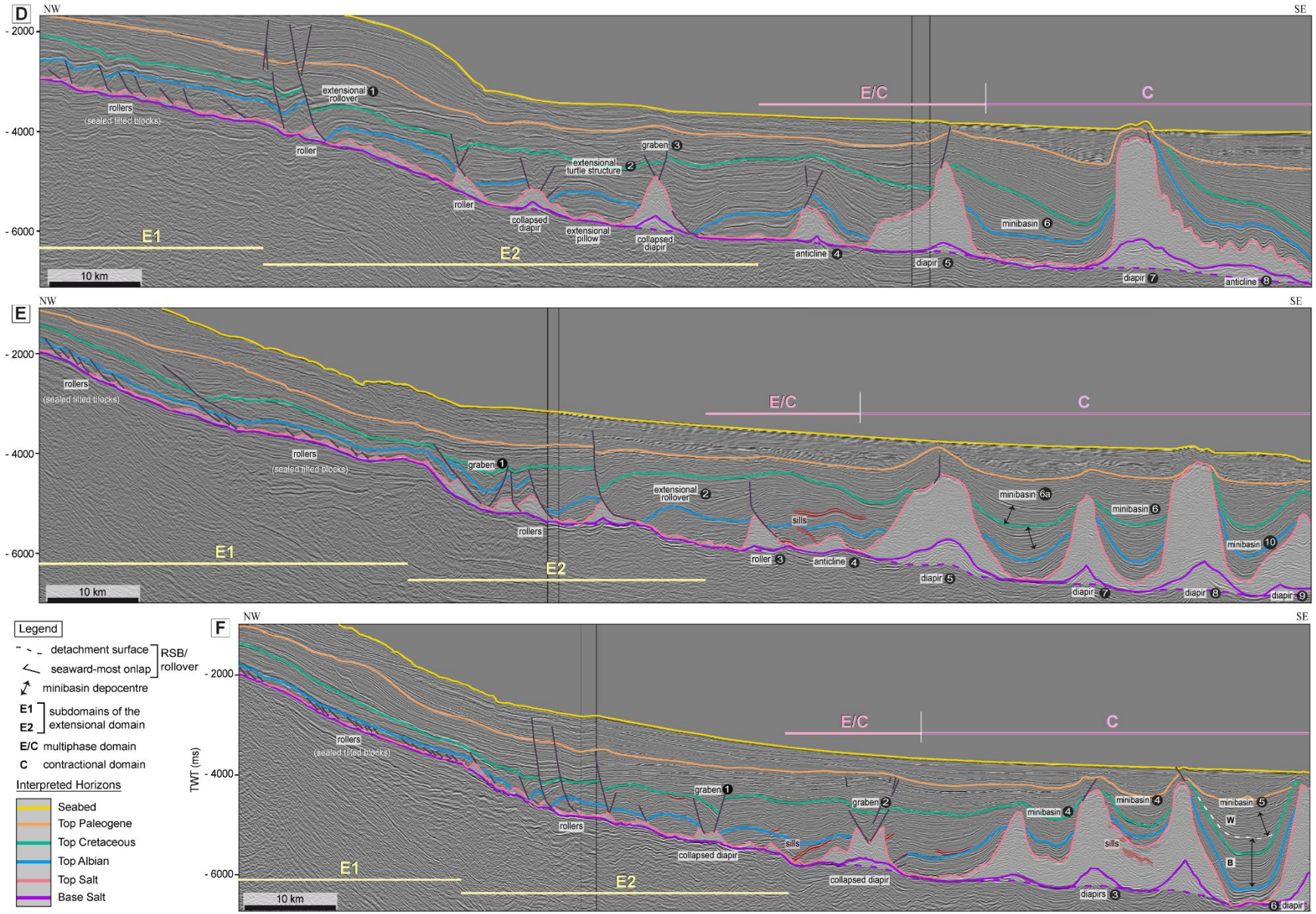
D
NW
SE
- 2000
- 4000
- 6000
rollers
(sealed tilted blocks)
extensional rollover 1
roller
graben 3
extensional turtle structure 2
roller
collapsed diapir
extensional pillow
collapsed diapir
E1
E2
E/C
C
anticline 4
minibasin 6
diapir 5
diapir 7
anticline 8
10 km
E
NW
SE
- 2000
- 4000
- 6000
rollers
(sealed tilted blocks)
rollers
(sealed tilted blocks)
graben 1
extensional rollover 2
rollers
sills
roller 3
anticline 4
minibasin 6a
minibasin 6
minibasin 10
diapir 5
diapir 7
diapir 8
diapir 9
E1
E2
E/C
C
10 km
Legend
detachment surface
seaward-most onlap
RSB/ rollover
minibasin depocentre
E1
E2
subdomains of the extensional domain
E/C multiphase domain
C contractional domain
Interpreted Horizons
Seabed
Top Paleogene
Top Cretaceous
Top Albian
Top Salt
Base Salt
F
NW
SE
TWT (ms)
- 2000
- 4000
- 6000
rollers
(sealed tilted blocks)
graben 1
graben 2
rollers
sills
collapsed diapir
sills
collapsed diapir
minibasin 4
minibasin 4
minibasin 5
W
B
diapirs 3
6 diapir
E1
E2
E/C
C
10 km

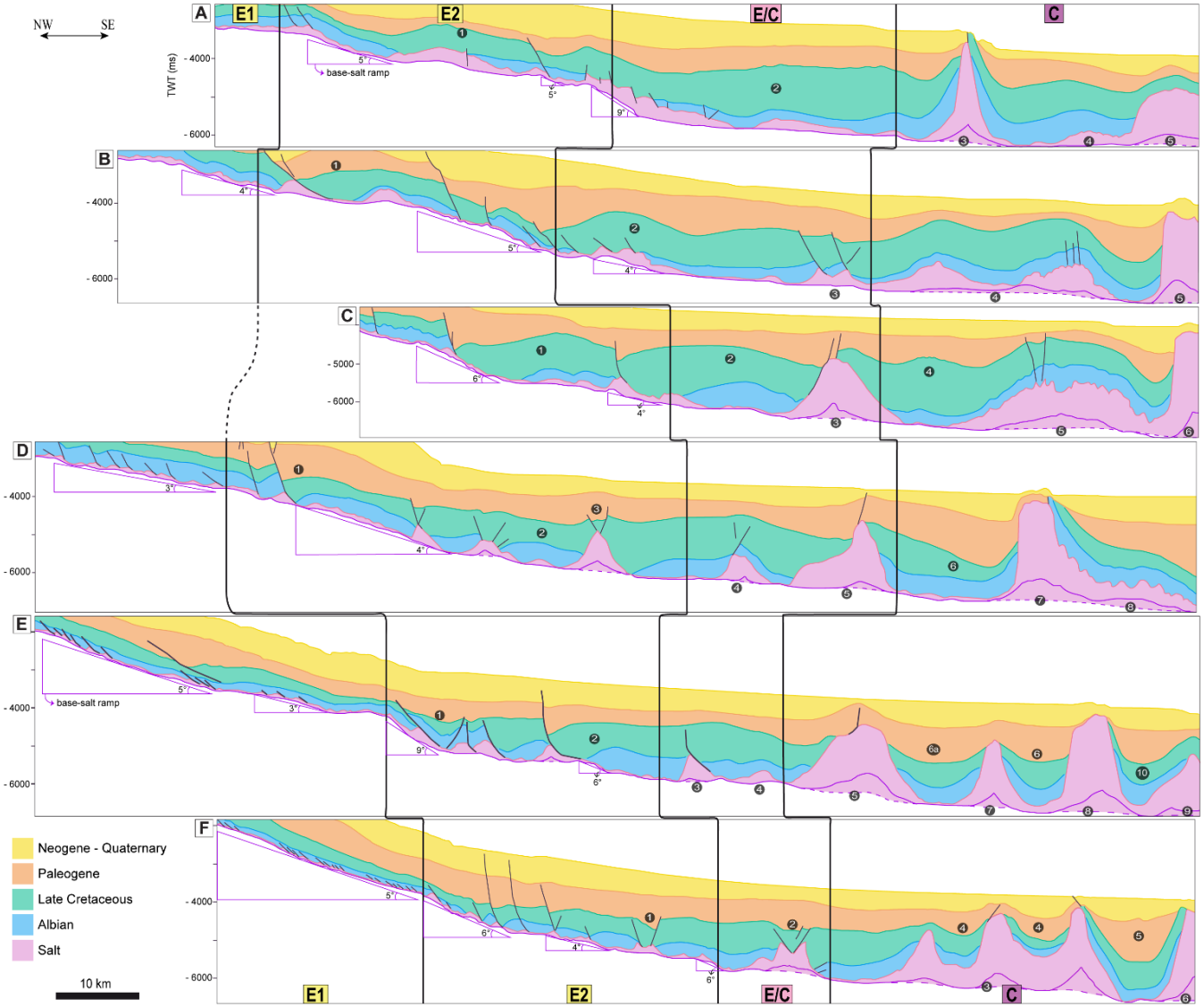

Figure 9.8. Stratigraphic intervals of the seismic geosections shown in Figure 7, with the spatial distribution of the deformation domains. The stratigraphic intervals have been coloured to highlight thickening and thinning relationships, indicating timing of the deformation. Base-salt ramps are indicated with triangles, together with their dip angles. Salt and overburden structures are numbered according to Figure 9.7.

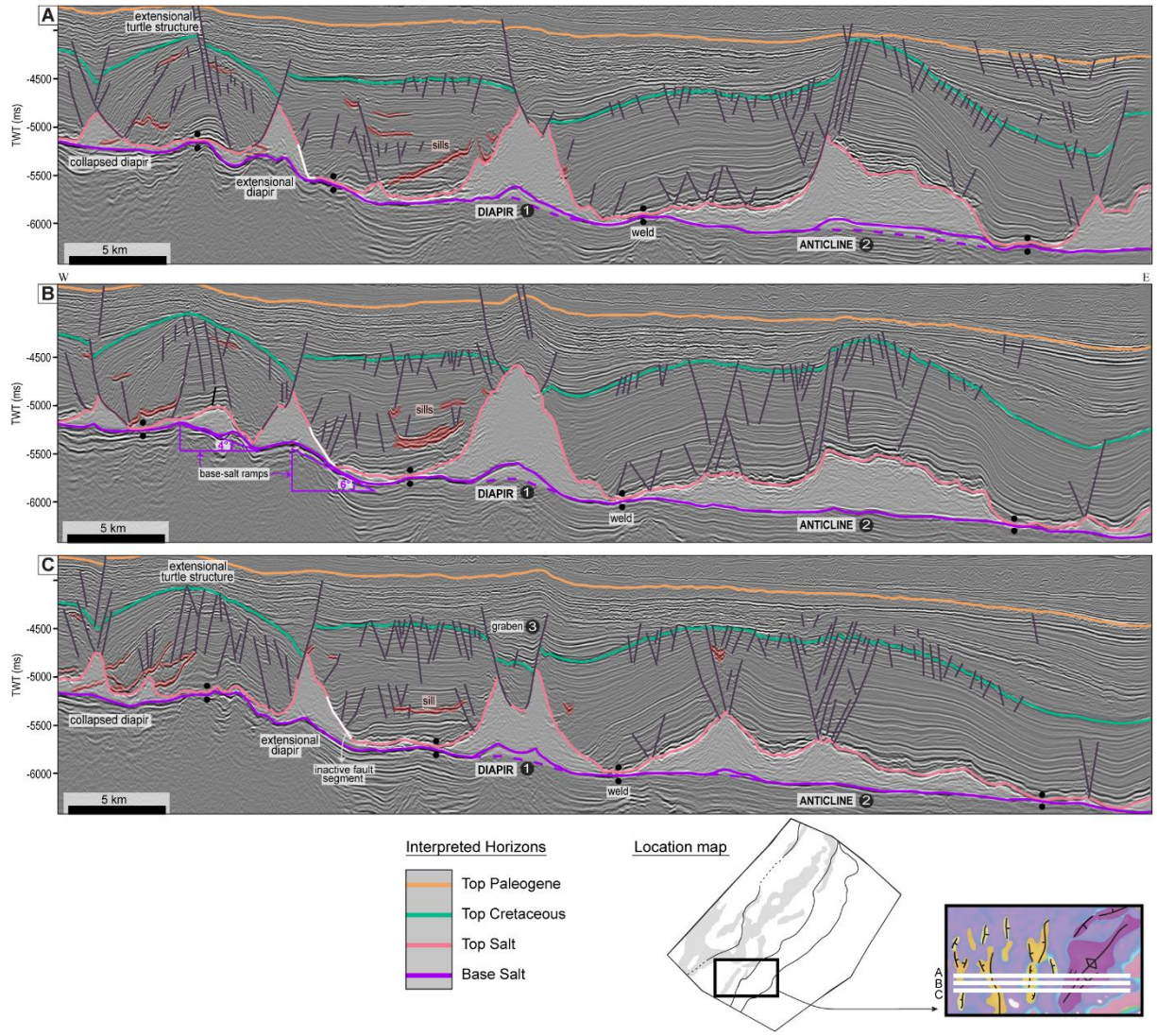

Figure 9.9. Interpreted seismic inlines of the 3D volume, with the interpreted seismic horizons, labelled salt and overburden structures, and base-salt ramps with their dip angles. (A) is north, (B) centre and (C) south – spacing between the lines is 1.6 km (see map in the bottom right for location). The sections show the boundary between the extensional domain (subdomain E2) and the multiphase domain. Salt and overburden structures are numbered to facilitate indications in the text. Note the abundance of sills and faults. Seismic data supplied by ANP.

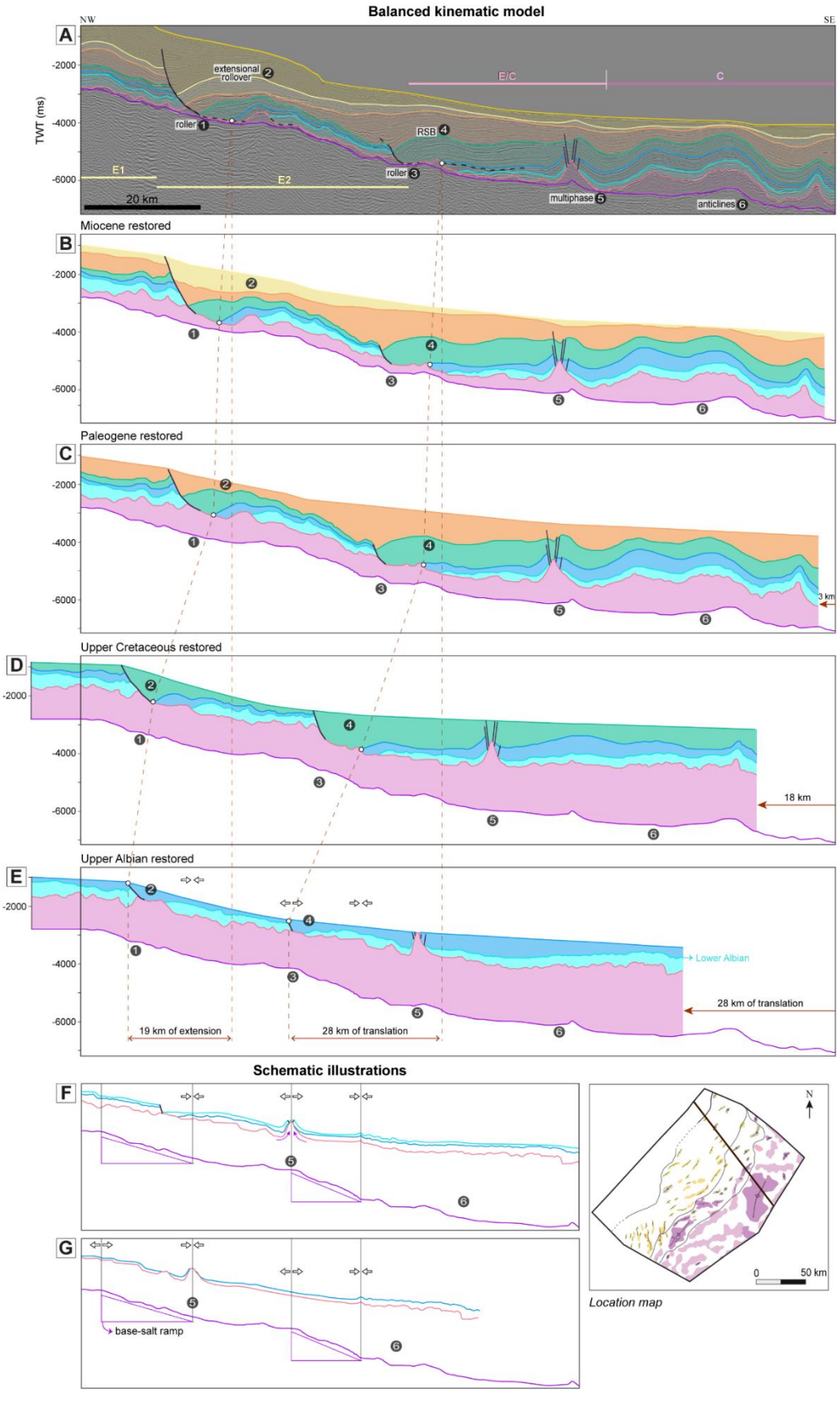
Balanced kinematic model
NW
SE
A
TWT (ms)
-2000
-4000
-6000
extensional rollover 2
E/C
C
roller 1
RSB 4
roller 3
E1
E2
20 km
multiphase 5
anticlines 6
Miocene restored
B
Paleogene restored
C
3 km
Upper Cretaceous restored
D
18 km
Upper Albian restored
E
Lower Albian
28 km of translation
19 km of extension
28 km of translation
Schematic illustrations
F
G
base-salt ramp
N
0
50 km
Location map

(previous page)

Figure 9.10. (A) Interpreted seismic line 0239-0362 (see the map in the bottom right for location) used in the balanced kinematic model, shown in (B) to (E) – (B) is the restoration of the Miocene; (C) Paleogene; (D) Upper Cretaceous and (E) Upper Albian. See the methodology item for development details. (F) and (G) are schematic illustrations of salt deformation across base-salt ramps during the Albian. Salt and overburden structures are numbered to facilitate indications in the text. The dotted lines indicate the seaward salt movement (translation/extension). The colours of the horizons are indicated in Figures 9.2 and 9.7.

6 – Evolution of extensional and contractional deformation through time

Using temporal changes in sediment thickness patterns, seismic-stratigraphic relationships (i.e. onlap, erosional truncation), and balanced structural restorations, we reconstruct the evolution of the study area during three key time intervals: Albian to End-Cretaceous, Paleogene, and Neogene to Recent.

6.1. Albian to Top Cretaceous

Thin-skinned extensional and contractional deformation had already begun during the Albian (and possibly as early as the Aptian; Cobbold and Szatmari, 1991; Fiduk and Rowan, 2012; Davison *et al.*, 2012) as salt began to flow downdip towards the basin. Regional thin-skinned extension of overburden in the proximal subdomain E1 commenced and ceased during the Albian as shown by the occurrence of fault-bound Albian growth strata, with the fault tips sealed by post-Albian strata (Figures 9.7 and 9.8d to f). By the late Albian, salt welds had formed, associated with grounding of Albian rafts and the cessation of faulting (Fort *et al.*, 2004). In subdomain E2, extension continued for longer, finishing near the end of the Cretaceous. Salt-detached normal faults and salt rollers formed in the central and southwestern parts of the study area, bounding extensional turtle structures (Figures 9.7c - structure 2, 9.8c and 9.9). Early reactive diapirs formed and subsequently collapsed, with most of this deformation ceasing by the end of the Cretaceous (Figures 9.7d-f and 9.8d-f). In the northeast of E2 and in the multiphase domain, extensional rollovers developed, as illustrated by the balanced kinematic model of line 0239-0362 in Figure 9.10a-e. The salt-detached normal faults bounding the salt rollers formed during the Albian (Figure 9.10e). As salt and its overburden flowed downdip, the salt-detached faults continued to slip and grow, continually creating accommodation as recorded by the deposition of packages of syn-kinematic strata that thicken towards the faults (Figure 9.10d).

Local contractional deformation induced by base-salt relief started in the early Albian, as recorded by the deposition of growth strata flanking high-frequency buckle folds in the contractional (Figures 9.7b - structure 4, 9.7c - structure 5, 9.7d - structures 7 and 8; Figure 9.10f,g) and multiphase domains (Figures 9.9 - structure 2, and 9.10f,g). With ongoing translation, early contractional structures that formed at the toe of seaward-dipping base-salt ramp were further shortened and evolved into larger-wavelength salt anticlines (Figure 9.7b - structure 4, 9.7c - structure 5, 9.7d - structure 8; Figure 9.9 - structure 2; Figure 9.10 – structure 6). Some of these early contractional structures were subsequently extended and faulted (Figure 9.7b - structure 3, 9.7d - structure 4, Figure 9.9 - structure 2; Figure 9.10c-f – structure 5), with deformation of these multiphase structures ceasing near the end of the Cretaceous.

Regional thin-skinned contraction also caused active diapirism near the end of the Cretaceous, as recorded by upturned megaflaps topped by erosional truncations (Figures 9.7a - structure 3, 9.7d - structure 7, 9.7f - structure 3; Figure 9.8a,d,f). Passive diapirism also occurred during much of this Period, as recorded by stratal thickening into flanking minibasins (e.g. Figure 9.7e - structure 6, 9.7f - structure 4). Near the end of the Cretaceous, downdip migration of regional extension led to the development of landward-dipping normal faults against two salt walls, bounding extensional turtle structures (Figures 9.5c, 9.7c - structure 2, and 9.8c).

6.2. Paleogene

Regional thin-skinned extension continued through the Paleogene, with faults related to extensional turtle structure formation continuing to slip in subdomain 2 (Figures 9.7c - structure 2, 9.8c and 9.9). Further downdip, in the multiphase domain, an RSB developed in response to further seaward translation of salt and its overburden (Jackson and Hudec, 2005; Pichel *et al.*, 2018) (Figure 9.10c,b – structure 4). The multiwavelength anticline was extended and faulted because of welding further updip; this extension locally caused the reactive rise of salt and the formation of a roller (Figure 9.9 - structure 2). Faulted salt walls bounding extensional turtle structures within the multiphase domain accumulated significant throw, becoming inactive by the mid-Paleogene (Figures 9.7c - structure 2 and 9.8c).

Regional thin-skinned contraction also occurred throughout the Paleogene. The extensional diapir in the multiphase domain was squeezed at this time, resulting in active rise and folding of its roof (Figure 9.9 - structure 1). Salt-detached anticlines in the contractional domain were amplified due to ongoing shortening and syn-kinematic sedimentation (Figures 9.7b – structure 4, 9.7c- structure 5, 9.8b,c and 9.10b,c – structure 6). Diapirs in the contractional domain continued to grow actively and passively, with deepening of flanking minibasins until salt welding (Figures 9.7d -structure 6, 9.7f - structure 5 and 9.8d,f) and folding of their roofs occurred (Figure 9.7a - structure 5).

6.3. Neogene to Recent

The period between the Neogene to Recent records very little thin-skinned extension, with salt-detached normal faulting being largely inactive by this time (Figures 9.7 and 9.8). The seaward flow of salt and overburden continued until the middle Neogene, at least in the area were the hybrid extensional rollover-RSB formed (Figure 9.6c; Figure 9.10a,b – structure 4). Anticline growth in the contractional domain ceased in the Miocene (Figure 9.10a,b –structure 6). Using a line-length method applied to the updip and downdip limits of the folded strata in the regions labelled ‘E/C’ and ‘C’ in the restoration, Figure 9.10, we estimate the magnitude of shortening is 5–6 km – as a result of both (sub-vertical) bending and (sub-horizontal) buckling. The active rise of diapirs, presumably due to ongoing horizontal shortening, continued until recently and may still be ongoing (Figures 9.7a - structure 3, 9.7b - structure 5, 9.7c structure 6, 9.7d - structure 7 and Figure 9.8a-d).

7 – Discussion

7.1. Base-salt relief as a control on salt tectonics

Even though the evaporites in the salt basins offshore SE Brazil were deposited during a period of relative tectonic quiescence, and the base-salt surface is overall quite smooth, there are a few large-displacement faults that offset this surface to form base-salt ramps with up to c. 2 km of relief. The major base-salt ramps in the study area are within the extensional domain, delineating the boundary between the External High and the External Low (Figures 9.2 and 9.4). The ramps are overall linear, but may be locally

concave- or convex-seaward (Figure 9.4c), and are c. 20-180 km long, c. 3-20 km wide, have a maximum structural relief of c. 900 ms TWT (c. 2 km), and dip 3º to 9º. The more linear, elongate ramps trend NE, perpendicular to the regional salt translation direction. Most salt and overburden structures also trend NE, with exceptions to this observed to the southwest, downdip from the concave- or convex-seaward ramps, where extensional salt and overburden structures trend north (Figure 9.5c). This is likely related to: (a) local changes in base-salt structure further updip, outside of our dataset, which redirected the salt flow to be bi-directional or radial (Cobbold and Szatmari, 1991); and/or (b) the presence of numerous volcanic sills in this area (Figures 9.7e,f and 9.9), which caused local changes in overburden strength and thus deformation patterns (Magee *et al.*, 2021).

In addition to influencing the *orientation* of salt and overburden structures, the geometry and scale of base-salt relief also affects the *types* of structures that form. For example, the extensional domain generally coincides with the area where the major base-salt ramps occur, near the boundary between the External High and the External Low (Figure 9.4d). More specifically, along-strike and down-dip zoning of the structures within the extensional domain may reflect variations in the strain rate within the ductile salt layer, with locally steeper base-salt angles being associated with locally higher strain rates and the formation of salt rollers as opposed to extensional diapirs (Fort *et al.*, 2004).

The multiphase (E/C) structures occur at the toe of the slope, on a relatively flat part of the base-salt surface adjacent to the External Low. Seaward translation of salt and its overburden across base-salt ramps from the high block (External High) to this low block (External Low), and the associated salt flux and volume variations, resulted in local belts of increased deformation (see Dooley *et al.*, 2017). As the salt flows off a structural high onto a low, the salt flux decelerates as it encounters thick and slower-moving salt at the base of seaward-dipping ramps, ultimately generating local extensional hinges at the top of the ramps, and contractional hinges at the base (Dooley *et al.*, 2017; 2018; Pichel *et al.*, 2019a-b). This mechanism is responsible for triggering at least some of the contractional fold belts and anticlines in Campos Basin, and the subsequent extension of some of these structures. Dooley *et al.* (2017) interpreted a wide fold belt with polyharmonic folds in Campos Basin; these are is geometrically similar and, we infer,

have a similar origin to the large antiform we identify in Figures 9.7b,c and 9.10 (see their figure 24 for comparison).

Through time, overburden structures on the high block of the External High become grounded due to salt welding, with extension migrating downdip, ultimately reaching the toe-of-slope. The migration of extension with time causes relatively late, relatively widespread (i.e. regional) extension of previously contractional structures and diapiric structures of the multiphase domain. This study shows that although classic models of gravity gliding and spreading on salt-influenced passive margins are broadly correct, they are rather oversimplified and fail to explain and adequately capture the diversity of salt and overburden structural styles interpreted in the Campos Basin and elsewhere (cf., Evans and Jackson, 2019; Pichel *et al.*, 2019a; Erdi and Jackson, 2021). It is important to stress that the multiphase evolution of the structures in the E/C domain are heterogeneous, and may go unnoticed in an isolated 2D analysis (e.g. Figure 9.9 - structure 1).

7.1.2. Estimating the magnitude and rate of salt-detached translation

Seaward gravity-driven translation of salt and its overburden in the Campos Basin started in the early Albian, lasting until at least the mid-Paleogene (Fig. 10). The distribution and evolution of key salt and overburden structures, and their relationship to base-salt relief, can constrain the magnitude of this translation.

RSBs have been used to determine the magnitude of salt-detached tectonic transport in passive margin basins, by measuring the distance between the top of the causal base-salt ramp and the (landward-directed) onlap point of the oldest intra-RSB strata (Jackson and Hudec, 2005; Pichel *et al.*, 2018; Oppo *et al.*, 2021). The RSBs in the Campos Basin are hybrid structures, evolving (in time) from and/or passing laterally (in space) into extensional rollovers due to ramp geometry, and temporal and spatial changes in salt thickness (see 5.1.2; Figure 9.10a-e). The hybrid extensional rollover-RSB in the NE (Figure 9.6c) started to form early in the Albian and was active until the mid-Neogene, recording post-Albian overburden extension of c. 19 km (Figure 9.10 – structure 2). The large, seaward RSB located further to the SW (Figure 9.6c) was active for a shorter period, containing Albian to mid-Paleogene growth strata, and recorded greater post-Albian translation (c. 28 km). Thus, the maximum seaward translation of the

overburden recorded by the RSBs since the end of the Albian is c. 28 km, comparable to that calculated by Dooley *et al.* (2017) elsewhere in the Campos Basin (see their figure 24).

An alternative way to estimate the magnitude of horizontal translation in salt basins is by measuring the distance between the most seaward end of a train of high-frequency buckle folds and the base of a seaward-dipping, base-salt ramp inferred to have generated them (Dooley *et al.*, 2017). Applying this methodology to our dataset, where such buckle folds may plausibly have developed during the Albian (i.e., the major seaward-dipping base-salt ramp in the NW of the study area; see Figure 9.7b-d), we calculate translation magnitudes of c. 40 km (Figure 9.7b), c. 50 km (Figure 9.7c), and c. 60 km (Figure 9.7d) in the NE, centre, and SW of the study area, respectively. The horizontal translation magnitudes estimated from the stratigraphic analysis of the RSBs (c. 28 km) thus differs significantly to those based on the present position of overburden buckle folds with respect to their inferred causal ramps (c. 40-60 km). We argue that RSBs provide a more certain record of the magnitude of horizontal translation in salt basins for the following reasons: (i) the translation magnitude calculated from RSB analysis is more consistent with the magnitude of salt-detached extension measured in the updip domain (Figs. 8 and 10); (ii) the salt nappe emplaced on oceanic crust at the seaward end of the Campos Basin, and which is at least partly the expression of the amount of horizontal translation updip (see Jackson *et al.* 2015), is < 40 km wide (Figure 9.2b) (Davison *et al.* 2012), a value consistent with the magnitude of translation calculated from the RSBs; (iii) translation magnitudes calculated by RSB analysis in conjugate (i.e., Angolan; 13-23 km; Evans and Jackson, 2020; Erdi and Jackson, 2021) and neighbouring basins (i.e., Santos Basin; 28-32 km; Pichel *et al.*, 2018) are more consistent with those defined here from comparable RSB analysis (c. 28 km); (iv) it is uncertain which ramp was responsible for the formation of the high-frequency buckle folds, i.e., was it the present toe-of-slope base-salt ramp or a more subtle ramp located further downdip?; (v) folding can occur due to regional overburden shortening and may not be diagnostic of translation. Based on this discussion, we infer that the Albian high-frequency folds in the multiphase domain (Figure 9.9 - structure 2) did not form at the same base of the base-salt ramp associated with the

formation of the RSBs, but may have instead formed at one or more subtle ramps located further downdip (Figures 9.4c and 9.5).

Having argued that the *magnitude* of salt-detached translation in the Campos Basin is more likely c. 28 km than c. 40-60 km, we can now calculate the *duration* and *rate* of translation. Growth strata within the RSBs indicate translation started lasted until the middle Paleogene, defining post-Albian duration of c. 55 Ma and a translation rate of c. 0.5 mm/year. Recent studies of RSBs in the conjugate Kwanza Basin, offshore Angola by Evans and Jackson (2019) and Erdi and Jackson (2021) demonstrate along-strike variability in both the magnitude and rate of Cenomanian-to-Recent salt-detached translation, i.e., from as little as 13 km at a rate of 0.13 mm/year in the NW of the study area, to 23.2 km at a rate of 0.23 mm/year in the SE. In the Santos Basin, offshore Brazil, Pichel *et al.* (2018) estimate a horizontal translation magnitude of 28-32 km lasting for c. 50 Myr (i.e., from the end-Albian until the middle Paleocene), thus defining a slightly faster translation rate than seen elsewhere (c. 0.7-0.8 mm/year). As argued by Pichel *et al.* (2018), Evans and Jackson (2019), and Erdi and Jackson (2021), this variability in the duration and rate of translation likely reflects changes in primary salt thickness and composition, the scale and distribution of base-salt relief, and local basement-involved tectonic processes driving salt-detached deformation (i.e., margin uplift) (see also Dooley *et al.*, 2017). Some combination of these controls may explain along-strike variation in RSB development and evolution in the Campos Basin. For example, the base-salt surface is overall steeper in the SW compared to the NE (Figure 9.4d), and it is defined by wider and more numerous base-salt ramps (Figure 9.4c). Davison *et al.* (2012) also suggest the primary salt thickness increased south-westwards from c. 1.2 km to 2 km (see their figure 7), which is consistent with our observations that the magnitude of translation was greatest in the SW.

7.2. Hydrocarbon exploration potential of Campos Basin

The Campos Basin is the second most prolific hydrocarbon basin in Brazil, being responsible for c. 33% of the hydrocarbon production in Brazil (ANP real-time panel, accessed in May, 2021). The first oil discovery in the basin dates from 1970’s, with the reservoir being Albian carbonates (Mohriak *et al.*, 1990). Further exploration through the

following decades led to the discovery of a further 41 oil and gas fields located 50-140 km off the Brazilian coast, in water depths of 80-2400 m. The fields are associated with a range of plays and have reservoirs in a variety of stratigraphic units (Bruhn *et al.*, 2003).

Known petroleum systems of the Campos Basin are composed of Barremian/Aptian (i.e. sub- to intrasalt) source rocks. Hydrocarbon migration from pre-rift source rocks to suprasalt reservoirs occurs through normal faults, or across areas of thin or welded salt (Guardado *et al.*, 1989). The most important fields include reservoirs in post-salt turbidites located in various stratigraphic levels, for example the Albacora (Miocene), Marlim (Oligocene to Miocene), Barracuda (Oligocene to Eocene), and Roncador (Maastrichian) fields (Figure 9.1a for field locations) (Bruhn *et al.*, 2003; ANP report, 2015). Salt-related faults form traps, controlling most of the oil and gas accumulations in these turbidite reservoirs (Bruhn *et al.*, 2003; Mohriak *et al.*, 2012). Subsalt reservoirs comprise rift (Barremian) and Aptian pre-salt carbonates (“coquinas”) and clastics, and fractured syn-rift volcanics (Hauterivian) (Goldberg *et al.*, 2017). The salt layer has a critical role for these deeper reservoirs, acting as an efficient seal rock.

The known post-salt reservoirs of the Campos Basin are mainly located within the thin-skinned extensional domain, which currently lies within relatively shallow water-depths (Figure 9.1a). This means significant unexplored areas may lie seaward of this location, in substantially deeper water. This study details the position and timing of salt-related deformation, key information required to push exploration further basinward into the multiphase and contractional domains. For example, we document multiwavelength salt anticlines in the multiphase domain (Albian – Top Cretaceous); these could represent structural traps, with later (end of the Cretaceous – Paleogene) extensional normal faults defining reservoir compartments (Figure 9.9 - structure 2). Hydrocarbon may have migrated from the pre-rift source rocks through welds adjacent to the large salt structures; given we infer these welds formed sometime during the end of the Cretaceous to the Paleogene, post-Paleogene migration is required to charge suprasalt traps, although the precise timing will vary based on the age of individual welds. High-frequency Albian buckle folds are common in the contractional domain (e.g. Figure 9.7b - structure 4, 9.7c - structure 5) and can also create structural traps (Jackson and Hudec, 2017) for hydrocarbons sourced from suprasalt source rocks, if they are mature. Megaflaps flanking

diapirs in the contractional domain (e.g. Figure 9.7a - structure 3, 9.7e - structure 8, 9.7f - structures 3 to SE), which began forming to the end of the Cretaceous, can compose three-way truncation traps against salt; megaflaps can also act as a lateral seal for stratigraphic traps and have implications for fluid pressures in minibasins (Rowan *et al.*, 2016). Diapirs could also be flanked by Cretaceous to Paleogene deep-water clastic reservoirs in pinch-out traps at the margins of minibasins (e.g. Figure 9.7d - minibasin 6 and adjacent diapirs 5 and 7, 9.7e – minibasins 6 and flanking diapirs 5, 7 and 8), similar to discoveries in the Gulf of Mexico (Booth *et al.*, 2003). Finally, turtle anticlines within salt-withdrawal basins (Cretaceous) (e.g. Figure 9.7c - structure 4) can cause structural inversion of stratigraphic units and can create stratigraphic/structural traps, similar to those documented in east Texas, US (Wescott and Hood, 1994).

8 – Conclusions

We use 2D and 3D seismic reflection and borehole data from the south-central Campos Basin to characterise salt-tectonic structural styles and related evolution of salt and overburden structures. The key conclusions of our study are:

- Variations in dip angle and direction in the base-salt surface define base-salt ramps, which define the boundary between the External High and the External Low, basement structures originated by rift tectonics. The dip angle of the base-salt ramps vary from 3° to 9°, and the dip direction trend broadly to NE, in overall linear geometries and locally concave-convex. The maximum structural relief of the ramps is c. 900 ms TWT (or c. 2 km).
- The distribution of the interpreted salt and overburden structures define three domains of thin-skinned, salt-detached deformation: extensional – subdivided into subdomains E1 and E2 –, contractional, and multiphase.
- We interpreted three multiphase structures: (i) contractional anticlines that were subjected to later extension and normal faulting; (ii) diapirs with passive and active growth later subjected to regional extension, developing landward-dipping normal faults on the landward flank; and, lastly, (iii) an extensional diapir that was subsequently squeezed. The structures in the

multiphase domain formed in response to multiple, kinematically-variable (extensional and contractional) phases of deformation over time and space.

- Base-salt relief caused local variations in salt flux, affecting the regional domains of deformation, controlling or influencing the types of generated salt and overburden structures, and their evolution through time and space.
- Ramp syncline basins provide a record of c. 28 km horizontal translation of salt and its overburden in a rate of c. 0.5 mm/year from the end of the Albian to the middle Paleogene.

Acknowledgments

F.B.d. Amarante thanks CNPq (National Council for Scientific and Technological Development of Brazil) for the Sandwich Doctorate Abroad Scholarship (SWE). We thank journal reviewers Mar Moragas and Ian Davison for their constructive insights, and the associate editor Craig Magee for his editorial handling. The authors gratefully acknowledge ANP (Brazil's National Oil, Natural Gas and Biofuels Agency) for providing the data and for the license to publish this article.

References

Amarante, F.B.d., Kuchle, J., Iacopini, D., Scherer, C.M.d.S., Alvarenga, R. dos S., Ene, P.L., Schilling, A.B., 2020. Seismic tectono-stratigraphic analysis of the Aptian pre-salt marginal system of Espírito Santo Basin, Brazil. Journal of South American Earth Sciences 98, 102474. https://doi.org/10.1016/j.jsames.2019.102474

ANP (Brazilian Agency for Petroleum, Natural Gas and Biofuels). 2015. Geological Summary and Sectors on Offer. Retrieved from http://rodadas.anp.gov.br/arquivos/Round_13/areas_oferecidas_r13/Sumarios_Geologicos/Sumario_Geologico_Bacia_Campos_R13.pdf

ANP Real-time Panel. 2021. Real-time web panel for production of oil and gas in Brazil. Retrieved from http://www.anp.gov.br/exploracao-e-producao-de-oleo-e-gas/paineis-dinamicos-de-producao-de-petroleo-e-gas-natural

ANP (Brazilian Agency for Petroleum, Natural Gas and Biofuels), Exploration and Production Database Web Maps – BDEP (Banco de Dados de Exploração e Produção). 2020. http://www.anp.gov.br/exploracao-e-producao-de-oleo-e-gas/dados-tecnicos

Baksi, A.K., 2018. Paraná flood basalt volcanism primarily limited to ~ 1 Myr beginning at 135 Ma: New 40 Ar/ 39 Ar ages for rocks from Rio Grande do Sul, and critical evaluation of published radiometric data. Journal of Volcanology and Geothermal Research 355, 66–77. https://doi.org/10.1016/j.jvolgeores.2017.02.016

Booth, J.R., Dean, M.C., DuVernay, A.E., III, Styzen, M.J., 2003. Paleo-bathymetric controls on the stratigraphic architecture and reservoir development of confined fans in the Auger Basin: central Gulf of Mexico slope. Marine and Petroleum Geology 20, 563–586. https://doi.org/10.1016/j.marpetgeo.2003.03.008

Bruhn, C.H.L., Gomes, J.A.T., Del Lucchese, C., Jr., Johann, P.R.S., 2003. Campos Basin: Reservoir Characterization and Management - Historical Overview and Future Challenges, in: Offshore Technology Conference. Presented at the Offshore Technology Conference, Offshore Technology Conference. https://doi.org/10.4043/15220-ms

Brun, J.-P., Fort, X., 2004. Compressional salt tectonics (Angolan margin). Tectonophysics 382, 129–150. https://doi.org/10.1016/j.tecto.2003.11.014

Brun, J.-P., Fort, X., 2011. Salt tectonics at passive margins: Geology versus models. Marine and Petroleum Geology 28, 1123–1145. https://doi.org/10.1016/j.marpetgeo.2011.03.004

Brun, J.-P., Mauduit, T.P.-O., 2009. Salt rollers: Structure and kinematics from analogue modelling. Marine and Petroleum Geology 26, 249–258. https://doi.org/10.1016/j.marpetgeo.2008.02.002

Chang, H.K., Kowsmann, R.O., Figueiredo, A.M.F., Bender, A., 1992. Tectonics and stratigraphy of the East Brazil rift system: an overview. Tectonophysics 213, 97–138.

Cobbold, P.R., Szatmari, P., 1991. Radial gravitational gliding on passive margins. Tectonophysics 188, 249–289. https://doi.org/10.1016/0040-1951(91)90459-6

Contreras, J., Zühlke, R., Bowman, S., Bechstädt, T., 2010. Seismic stratigraphy and subsidence analysis of the southern Brazilian margin (Campos, Santos and Pelotas basins). Mar. Petrol. Geol. 27 (9), 1952–1980.

Davison, I., 2007. Geology and tectonics of the South Atlantic Brazilian salt basins. Geological Society, London, Special Publications 272, 345–359. https://doi.org/10.1144/gsl.sp.2007.272.01.18

Davison, I., Alsop, I., Blundell, D., 1996. Salt tectonics: some aspects of deformation mechanics. Geological Society, London, Special Publications 100, 1–10. https://doi.org/10.1144/gsl.sp.1996.100.01.01

Davison, I., Anderson, L., Nuttall, P., 2012. Salt deposition, loading and gravity drainage in the Campos and Santos salt basins. Geological Society, London, Special Publications 363, 159–174. https://doi.org/10.1144/sp363.8

Demercian, S., Szatmari, P., Cobbold, P.R., 1993. Style and pattern of salt diapirs due to thin-skinned gravitational gliding, Campos and Santos basins, offshore Brazil. Tectonophysics 228 (3–4), 393–433.

Dooley, T.P., Hudec, M.R., Carruthers, D., Jackson, M.P.A., Luo, G., 2017. The effects of base-salt relief on salt flow and suprasalt deformation patterns — Part 1: Flow across simple steps in the base of salt. Interpretation 5, SD1–SD23. https://doi.org/10.1190/int-2016-0087.1

Erdi, A., Jackson, C.A.L., 2021. What Controls Contraction in the Translation Domain of the Outer Kwanza Basin, Offshore Angola? Basin Research. https://doi.org/10.1111/bre.12539

Evans, S.L., Jackson, C.A.L., 2019. Base-salt relief controls salt-related deformation in the Outer Kwanza Basin, offshore Angola. Basin Research 32, 668–687. https://doi.org/10.1111/bre.12390

Evans, S.L., Jackson, C.A.-L., 2021. Intra-salt structure and strain partitioning in layered evaporites: implications for drilling through Messinian salt in the eastern Mediterranean. Petroleum Geoscience. https://doi.org/10.1144/petgeo2020-072

Fetter, M., 2009. The role of basement tectonic reactivation on the structural evolution of Campos Basin, offshore Brazil: Evidence from 3D seismic analysis and section restoration. Marine and Petroleum Geology 26, 873–886. https://doi.org/10.1016/j.marpetgeo.2008.06.005

Fiduk, J.C., Rowan, M.G., 2012. Analysis of folding and deformation within layered evaporites in Blocks BM-S-8 & -9, Santos Basin, Brazil. Geological Society, London, Special Publications 363, 471–487. https://doi.org/10.1144/sp363.22

Fort, X., Brun, J.-P., Chauvel, F., 2004. Salt tectonics on the Angolan margin, synsedimentary deformation processes. Bulletin 88, 1523–1544. https://doi.org/10.1306/06010403012

Goldberg, K., Kuchle, J., Scherer, C.M.S., Alvarenga, R.S., Ene, P.L., Armelenti, G., De Ros, L.F., 2017. Re-Sedimented deposits in the rift section of the Campos Basin. Marine and Petroleum Geology 80, 412–431.

Guardado, L.R., Gamboa, L.A.P., Lucchesi, C.F., 1989. Petroleum geology of Campos Basin, Brazil: a model for producing Atlantic type basin. In: Edwards, J.D., Santagrossi, P.A. (Eds.), Divergent/Passive Margins Basins. AAPG Memoir 48, 3–36.

Guardado, L.R., Spadini, A.R., Brandão, J.S.L., Mello, M.R., 2000. Petroleum system of the Campos Basin, Brazil. In: Mello, M.R., Katz, B.J. (Eds.), Petroleum Systems of South Atlantic Margins. AAPG Memoir 73, 317–324.

Heilbron, M., Mohriak, W.U., Valeriano, C.M., Milani, E.J., Almeida, J., Tupinambá, M., 2000. From collision to extension: The roots of the southeastern continental margin of Brazil, in: Atlantic Rifts and Continental Margins. American Geophysical Union, 1–32. https://doi.org/10.1029/gm115p0001

Hudec, M.R., Jackson, M.P.A., Schultz-Ela, D.D., 2009. The paradox of minibasin subsidence into salt: Clues to the evolution of crustal basins. Geological Society of America Bulletin 121, 201–221. https://doi.org/10.1130/B26275.1

Hudec, M.R., Norton, I.O., Jackson, M.P.A., Peel, F.J., 2013. Jurassic evolution of the Gulf of Mexico salt basin. AAPG Bulletin 97, 1683–1710. https://doi.org/10.1306/04011312073

Jackson, C.A. -L., Duffy, O.B., Fernandez, N., Dooley, T.P., Hudec, M.R., Jackson, M.P.A., Burg, G., 2019. The stratigraphic record of minibasin subsidence, Precaspian Basin, Kazakhstan. Basin Research 32, 739–763. https://doi.org/10.1111/bre.12393

Jackson, C.A.-L., Jackson, M.P.A., Hudec, M.R., 2015. Understanding the kinematics of salt-bearing passive margins: A critical test of competing hypotheses for the origin of the Albian Gap, Santos Basin, offshore Brazil. Geological Society of America Bulletin 127, 1730–1751. https://doi.org/10.1130/b31290.1

Jackson, M.P.A., Hudec, M.R., 2005. Stratigraphic record of translation down ramps in a passive-margin salt detachment. Journal of Structural Geology 27, 889–911. https://doi.org/10.1016/j.jsg.2005.01.010

Jackson, M. P. A., Hudec, M. R., 2017. Salt Tectonics: Principles and Practice. Cambridge: Cambridge University Press. https://doi.org/10.1017/9781139003988

Kukla, P.A., Strozyk, F., Mohriak, W.U., 2018. South Atlantic salt basins – Witnesses of complex passive margin evolution. Gondwana Research 53, 41–57. https://doi.org/10.1016/j.gr.2017.03.012

Lundin, E.R., 1992. Thin-skinned extensional tectonics on a salt detachment, northern Kwanza Basin, Angola. Marine and Petroleum Geology 9, 405–411. https://doi.org/10.1016/0264-8172(92)90051-f

Magee, C., Pichel, L.M., Madden-Nadeau, A.L., Jackson, C.A. -L., Mohriak, W., 2021. Salt–magma interactions influence intrusion distribution and salt tectonics in the Santos Basin, offshore Brazil. Basin Research. https://doi.org/10.1111/bre.12537

Marfurt, K.J., Alves, T.M., 2015. Pitfalls and limitations in seismic attribute interpretation of tectonic features. Interpretation 3, SB5–SB15. https://doi.org/10.1190/int-2014-0122.1

Meisling, K.E., Cobbold, P.R., Mount, V.S., 2001. Segmentation of an obliquely rifted margin, Campos and Santos basins, southeastern Brazil. AAPG Bulletin 85 (11), 1903–1924.

Mohriak, W.U., Mello, M.R., Karner, G.D., Dewey, J.F., Maxwell, J.R., 1989. Structural and stratigraphic evolution of the Campos Basin, offshore Brazil. In: Tankard, A.J., Balkwill, H.R. (Eds.), Extensional Tectonics and Stratigraphy of the North Atlantic Margins. AAPG Memoir 46, 577–598.

Mohriak, W.U., Mello, M.R., Dewey, J.F., Maxwell, J.R., 1990. Petroleum geology of the Campos Basin, offshore Brazil. Geological Society, London, Special Publications 50, 119–141. https://doi.org/10.1144/gsl.sp.1990.050.01.07

Mohriak, W., Nemčok, M., Enciso, G., 2008. South Atlantic divergent margin evolution: rift-border uplift and salt tectonics in the basins of SE Brazil. Geological Society, London, Special Publications 294, 365–398. https://doi.org/10.1144/sp294.19

Mohriak, W.U., Szatmari, P., Anjos, S., 2012. Salt: geology and tectonics of selected Brazilian basins in their global context. Geological Society, London, Special Publications 363, 131–158. https://doi.org/10.1144/sp363.7

Oppo, D., Evans, S., Iacopini, D., Kabir, S.M.M., Maselli, V., Jackson, C.A. -L., 2021. Leaky salt: Pipe trails record the history of cross-evaporite fluid escape in the northern Levant Basin, Eastern Mediterranean. Basin Research. https://doi.org/10.1111/bre.12536

Peel, F.J., 2014. How do salt withdrawal minibasins form? Insights from forward modelling, and implications for hydrocarbon migration. Tectonophysics 630, 222–235. https://doi.org/10.1016/j.tecto.2014.05.027

Pichel, L.M., Peel, F., Jackson, C.A.-L., Huuse, M., 2018. Geometry and kinematics of salt-detached ramp syncline basins. Journal of Structural Geology 115, 208–230. https://doi.org/10.1016/j.jsg.2018.07.016

Pichel, L.M., Jackson, C.A.L., Peel, F., Dooley, T.P., 2019a. Base-salt relief controls salt-tectonic structural style, São Paulo Plateau, Santos Basin, Brazil. Basin Research 32, 453–484. https://doi.org/10.1111/bre.12375

Pichel, L.M., Finch, E., Gawthorpe, R.L., 2019b. The Impact of Pre-Salt Rift Topography on Salt Tectonics: A Discrete-Element Modeling Approach. Tectonics 38, 1466–1488. https://doi.org/10.1029/2018tc005174

Pichel, L.M., Jackson, C.A.-L., 2020. The enigma of the Albian Gap: spatial variability and the competition between salt expulsion and extension. Journal of the Geological Society 177, 1129–1148. https://doi.org/10.1144/jgs2020-055

Quirk, D.G., Hertle, M., Jeppesen, J.W., Raven, M., Mohriak, W.U., Kann, D.J., Nørgaard, M., Howe, M.J., Hsu, D., Coffey, B., Mendes, M.P., 2013. Rifting, subsidence and continental break-up above a mantle plume in the central South Atlantic. Geological Society, London, Special Publications 369, 185–214. https://doi.org/10.1144/sp369.20

Quirk, D.G., Schødt, N., Lassen, B., Ings, S.J., Hsu, D., Hirsch, K.K., Von Nicolai, C., 2012. Salt tectonics on passive margins: examples from Santos, Campos and Kwanza basins. Geological Society, London, Special Publications 363, 207–244. https://doi.org/10.1144/sp363.10

Rangel, H.D., Martins, F.A.L., Esteves, F.R., Feijó, F.J., 1994. Bacia de Campos. Boletim de Geociências da Petrobras 8 (1), 203–218.

Rowan, M.G., Peel, F.J., Vendeville B.C., 2004, Gravity-driven fold belts on passive margins. In McClay, K.K. (Eds.), Thrust tectonics and hydrocarbon systems: AAPG Memoir 82, 157–182.

Rowan, M.G., Ratliff, R.A., 2012. Cross-section restoration of salt-related deformation: Best practices and potential pitfalls. Journal of Structural Geology 41, 24–37. https://doi.org/10.1016/j.jsg.2011.12.012

Rowan, M.G., 2014. Passive-margin salt basins: hyperextension, evaporite deposition, and salt tectonics. Basin Research 26, 154–182. https://doi.org/10.1111/bre.12043

Rowan, M.G., Giles, K.A., Hearon IV, T.E., Fiduk, J.C., 2016. Megaflaps adjacent to salt diapirs. Bulletin 100, 1723–1747. https://doi.org/10.1306/05241616009

Sclater, J.G., Christie, P.A.F., 1980. Continental stretching: An explanation of the Post-Mid-Cretaceous subsidence of the central North Sea Basin. J. Geophys. Res. 85, 3711–3739. https://doi.org/10.1029/jb085ib07p03711

Szatmari, P., 2000. Habitat of petroleum along the South Atlantic margins. In: Mello, M.R., Katz, B.J. (Eds.), Petroleum Systems of South Atlantic Margins: AAPG Memoir 73, 69–75.

Trusheim, F., 1960. Mechanism of salt migration in northern Germany. AAPG Bulletin 44, 1519–1540.

Vendeville, B.C., Jackson, M.P.A., 1992 a. The rise of diapirs during thin-skinned extension. Marine and Petroleum Geology 9, 331–354. https://doi.org/10.1016/0264-8172(92)90047-i

Vendeville, B.C., Jackson, M.P.A., 1992 b. The fall of diapirs during thin-skinned extension. Marine and Petroleum Geology 9, 354–371. https://doi.org/10.1016/0264-8172(92)90048-j

Wescott, W.A., Hood, W.C., 1994. Hydrocarbon Generation and Migration Routes in the East Texas Basin. Bulletin 78. https://doi.org/10.1306/bdff908c-1718-11d7-8645000102c1865d

Winter, W.R., Jahnert, R.J., França, A.B., 2007. Bacia de Campos. Boletim de Geociências da Petrobras 15(2), 511–529.

10 Apêndices

Comprovação de publicação do Artigo 1 na revista Journal of South American Earth Sciences em 2020.

Journal of South American Earth Sciences 98 (2020) 102474

Contents lists available at ScienceDirect

Journal of South American Earth Sciences

journal homepage: www.elsevier.com/locate/jsames

Seismic tectono-stratigraphic analysis of the Aptian pre-salt marginal system of Espírito Santo Basin, Brazil

Francyne Bochi do Amarante[a,*], Juliano Kuchle[a], David Iacopini[b,c], Claiton Marlon dos Santos Scherer[a], Renata dos Santos Alvarenga[a], Patrycia Leipnitz Ene[a], André Basso Schilling[a]

[a] Instituto de Geociências, Universidade Federal Do Rio Grande Do Sul, 9500 Bento Gonçalves Avenue, Building 43137, Agronomia, 91501-970, Porto Alegre, RS, Brazil
[b] School of Geosciences, University of Aberdeen, United Kingdom
[c] Dipartimento di Scienze Della Terra, Dell'Ambiente e Delle Risorse (DiSTAR), Università Degli Studi di Napoli Federico II, Italy

DOI: https://doi.org/10.1016/j.jsames.2019.102474

Comprovação de publicação do Artigo 2 na revista Basins Research em julho de 2021.

RESEARCH ARTICLE

Pre-salt rift morphology controls salt tectonics in the Campos Basin, offshore SE Brazil

Francyne Bochi do Amarante ✉, Christopher Aiden-Lee Jackson, Leonardo Muniz Pichel, Claiton Marlon dos Santos Scherer, Juliano Kuchle

First published: 16 July 2021 | **https://doi.org/10.1111/bre.12588**

DOI: https://doi.org/10.1111/bre.12588

ANEXO I

Título da Dissertação/Tese:

IMPACTO DA TOPOGRAFIA RIFTE NA TECTÔNICA E SEDIMENTAÇÃO DOS ESTÁGIOS SAG E MARGEM PASSIVA – BACIAS DE CAMPOS E ESPÍRITO SANTO, SUDESTE DO BRASIL

Área de Concentração: **Estratigrafia**

Autor: **FRANCYNE BOCHI DO AMARANTE**

Orientador: **Prof. Dr. Claiton Marlon dos Santos Scherer**

Examinador: **Prof. Dr. Fernando Farias Vesely**

Data: 20/08/2021

Conceito: A

PARECER:

A tese apresentada é de altíssima qualidade e representa uma contribuição significativa para o conhecimento geológico das bacias estudadas e margens divergentes de maneira geral, sobretudo o artigo 2. A exposição oral da candidata foi clara, bem-organizada e com uso adequado do tempo. Durante as arguições, a candidata demonstrou nível de argumentação compatível com o título de doutora. Como sugestão geral de modificação, caso permitido pelo programa, seria interessante ilustrar melhor os dados que subsidiaram as interpretações estratigráficas e sedimentológicas apresentadas no artigo 1. Parabéns pelo belo trabalho. **Segue em anexo exemplar da tese com observações.**

Assinatura: Data: 20/08/2021

Ciente do Orientador:

Ciente do Aluno:

ANEXO I

Título da Dissertação/Tese:

IMPACTO DA TOPOGRAFIA RIFTE NA TECTÔNICA E SEDIMENTAÇÃO DOS ESTÁGIOS SAG E MARGEM PASSIVA – BACIAS DE CAMPOS E ESPÍRITO SANTO, SUDESTE DO BRASIL

Área de Concentração: **Estratigrafia**

Autor: **FRANCYNE BOCHI DO AMARANTE**

Orientador: **Prof. Dr. Claiton Marlon dos Santos Scherer**

Examinador: **Prof. Dr. Claudio Riccomini**

Data: 20/08/2021

Conceito: A, com louvor.

PARECER:

A candidata apresentou um trabalho voltado ao estudo da influência da topografia do estágio de “rift” no tectonismo e na sedimentação atuante durante os estágios de “sag” e margem passiva nas bacias do Espírito Santo e de Santos. Trata-se de tema inédito e relevante, com importância na compreensão da evolução dessas bacias e na prospecção de hidrocarbonetos. O trabalho está bem redigido, ilustrado e organizado. O documento apresentado compreende uma parte introdutória de fundamentação teórica, bem desenvolvida, com revisão bibliográfica atualizada dos principais temas de interesse à tese. Compreende também dois artigos publicados em periódicos internacionais (Journal of South American Earth Sciences e Basin Research), ambos conceituados na área de conhecimento. Nesses artigos são apresentados os principais resultados do estudo em cada uma das bacias, comprovando a hipótese de trabalho. A apresentação oral do trabalho foi muito clara e bem concatenada. Na arguição a candidata respondeu com propriedade às questões formuladas, demonstrando segurança e domínio do tema. Em conclusão, este avaliador considera o trabalho de excelente nível, fazendo jus ao conceito “A”, com louvor, ora atribuído.

Assinatura: 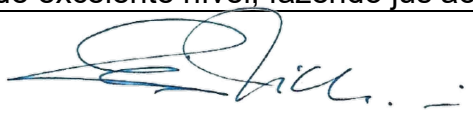 Data: 20/08/2021

Ciente do Orientador:

Ciente do Aluno:

ANEXO I

Título da Dissertação/Tese:

IMPACTO DA TOPOGRAFIA RIFTE NA TECTÔNICA E SEDIMENTAÇÃO DOS ESTÁGIOS SAG E MARGEM PASSIVA – BACIAS DE CAMPOS E ESPÍRITO SANTO, SUDESTE DO BRASIL

Área de Concentração: **Estratigrafia**

Autor: **FRANCYNE BOCHI DO AMARANTE**

Orientador: **Prof. Dr. Claiton Marlon dos Santos Scherer**

Examinador: **Profa. Dra. ARIANE DA SILVEIRA**

Data: 20/08/2021

Conceito: A, com louvor

PARECER:

O trabalho apresentou todos os quesitos para o grau de doutoramento.
Artigos muito bons, texto muito bem escrito. Apresentação muito clara e objetiva.

Visto que os 2 artigos já foram publicados, não cabe qualquer sugestão nesse sentido.
Ficam aqui apenas algumas sugestões, caso a pesquisa tenha continuidade, em alguns itens, quais sejam:

1. No capítulo Estado da Arte, acrescentar mais referências bibliográfica, deixando mais próximo dos artigos;
2. Na carta cronoestratigráfica (Figura 3.2), criar outra ao lado, especificando e/ou detalhando o que está no texto e não pode ser visto na carta crono apresentada;
3. No item 4. Dados e Métodos:
   3.1 Nas duas bacias é comentado sobre o volume 3D, no entanto não foi apresentada nenhuma imagem em 3D, o que ajudaria muito, principalmente tratando-se de falhas e se utilizado o atributo sísmico de coerência / variância;
   3.2 Nas figuras 4.1 e 4.2 de localização da base de dados indicar o nome dos poços, em especial o well 6, que foi descrito. Sugiro fazer uma legenda nas figuras;
4. Achei uma pena não terem sido separadas as imagens de volume nas diferentes frequências (10 Hz, 20 Hz e 40Hz). Ficou poluída a imagem;
5. Faltou o modelo de velocidade para gerar o volume em profundidade. Fica mais coerente para a correlação com os perfis. A depender da área, pode haver uma grande diferença na morfologia. Por outro lado, se o modelo de velocidade não for bom, poderá ficar pior do que não ter feito. De qualquer modo, a tentativa

devia ter sido feita.

6. Na tabela de fácies 8.1, Hyperpycnal trata-se de processo e não de associação de fácies;
7. Embora o foco do estudo não tenha sido em sedimentologia apenas, gostaria de ter visto uma tabela de Facies Box senão de todas, mas das principais fácies sedimentares descritas no testemunho.

Enfim, trabalho excelente, não tendo como deixar de levar em consideração que foi desenvolvido no prazo, os artigos foram publicados, e, em meio a uma pandemia, com todas as dificuldades que envolve.
Parabéns e muito sucesso!

Assinatura: Data: 20/08/2021

Ciente do Orientador:

Ciente do Aluno: